Spring 5-31-2021

Investigating the mechanism of the Escherichia coli ATP-binding cassette (ABC) transporter MetNI

Matthew Foronda
mforonda@dons.usfca.edu

Investigating the mechanism of the *Escherichia coli* ATP-binding cassette (ABC) transporter MetNI

A thesis presented to the faculty
of the Department of Chemistry
at the University of San Francisco
in partial fulfillment of the requirements for the degree of
Master of Science in Chemistry

Written By

Matthew Foronda
Bachelor of Science in Chemistry
University of Portland

05/24/2021

Investigating the mechanism of the *Escherichia coli* ATP-binding cassette (ABC) transporter MetNI

Thesis written by Matthew Foronda

This thesis is written under the guidance of the Faculty Advisory Committee, and approved by all its members, has been accepted in partial fulfillment of the requirements for the degree of

Master of Science
in Chemistry
at
the University of San Francisco

Thesis Committee:

Janet G. Yang, Ph.D.
Research Advisor

Lawrence Margerum, Ph.D.
Professor Emeritus

Osasere Evbuomwan, Ph.D.
Assistant Professor

Eileen Fung, Ph.D.
Interim Dean, College of Arts and Sciences

Acknowledgements

I would like to thank my research advisor Dr. Janet Yang for providing me with guidance, feedback, and mentorship throughout my time in her lab. She fostered a supportive environment that helped me develop the resilience needed to withstand the trial-and-error process of research while granting me the freedom to take ownership of this ongoing project. I would also like to thank my thesis committee members, Dr. Margerum and Dr. Evbuomwan for their support as well as their effort put towards challenging me to think more deeply about my research and how to move forward. I am very grateful for Dr. Agard and Dr. Narlikar at UCSF for allowing me to use their instruments and lab workspace. This project would not have the data it has now without their generosity. A big shout out goes to Emily Wong and Johnny Rodriguez for walking me through how to properly use each instrument, showing me where to store precious reagents, and answering my questions during our time together. I need to give a huge thank you to Jeff Oda and Matt Helm for fixing and monitoring the plethora of instruments at USF, as well as demonstrating how to use any tools or machinery I needed for my project. I also owe a note of gratitude for Deidre Shymanski and all that she does behind the scenes so that the chemistry department can function properly. I must also thank the friends I made at USF for all the great times we had doing all sorts of activities. I truly cherish the memories spent with you all. Finally, I would not have arrived to where I am today without the constant support of my family. Mom, Dad, Sarah, Diana, you are all there to both support and challenge me to be the best I can be. Being the baby of the Foronda family has been a privilege that has helped me accomplish much more than what I could have done alone.

Table of Contents

List of Figures

List of Table Captions

Abstract

Chemical homeostasis is a baseline requirement for any cell to survive. ATP-binding cassette (ABC) transporters play a vital role in homeostasis by importing nutrients and exporting toxins against their concentration gradients by utilizing the energy of ATP hydrolysis. Malfunctioning ABC transporters cause a variety of health problems, including cystic fibrosis, Stargardt's disease (vision loss), and the development of drug-resistant tumors. An important step in solving these medical issues is to first understand the structure and mechanism of ABC transporters. Various studies have made great strides in depicting the structure and details of different ABC transporters and their mechanisms, however, many of these details were discovered with transporters in highly artificial environments using X-ray crystallography. This project aims to further understand the mechanism of the *E. coli* methionine importer MetNI using functional studies.

A fluorescence anisotropy assay was developed as a functional study that would assess the dissociation constant between MetNI and its periplasmic binding protein MetQ. ATP-binding by MetNI was found to be a prerequisite for MetNI-Q complex formation. MetNI saw a slightly higher affinity for apo MetQ (K_d = 281 nM ± 36 nM) than L-Met bound MetQ (527 nM ± 107 nM). These similar binding affinities support the hypothesis that MetNI follows two different mechanisms originally proposed by Nguyen et. al.; one for the preferred L-Met substrate, and one for L-Met derivatives in situations of L-Met scarcity. Preliminary trials investigating the dissociation constant between the MetNI C2 domains and L-Met found a K_d dissociation constant between the MetNI C2 domains and L-Met of 484 nM. Moving forward, the ATP requirements for MetNI-Q complex formation will be investigated using MetNI transporters with nucleotide binding domain chimeras.

Chapter 1: Introduction

1.1: The Lipid Bilayer and Membrane Proteins

A crucial requirement for cell survival is maintaining an optimal internal chemical environment. The cell must consistently maintain homeostasis, which includes variables such as pH, ion and solute concentration, and redox state. To maintain the proper internal environment, the cell creates a semi-permeable membrane to separate its intracellular compartment from the extracellular space. The membrane consists of a lipid bilayer, arranged with hydrophobic tails facing inward and hydrophilic heads facing outward. The bilayer forms a flexible yet strong barrier, approximately 3-4 nm thick and with remarkable fluidity in the lateral plane.[1]

While small, nonpolar molecules such as oxygen and carbon dioxide gas move unassisted through the membrane, other molecules that are large or polar are unable to traverse the barrier by simple diffusion. To assist with molecular transport, cellular membranes contain a variety of integral membrane proteins that provide permeation pathways for the movement of specific substrates through the lipid bilayer. In general, integral membrane proteins are involved in a variety of tasks including intercellular adhesion, signal transduction pathways, enzymatic activity, and cell-to-cell recognition; however, substrate transport is the most vital activity in maintaining chemical homeostasis.[2] This project focuses on membrane proteins that drive substrate transport.

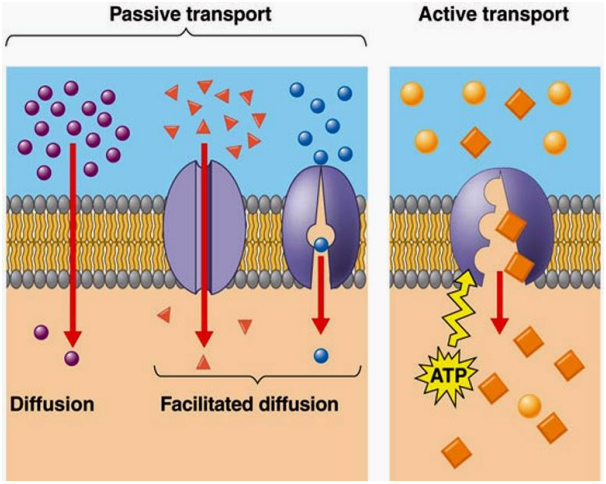

Figure 1-1: Passive and active transporters. Passive transporters are essential for facilitated diffusion while active transporters utilize ATP hydrolysis to import substrates against their concentration gradient. Image taken directly from (4).

Approximately 10% of the *E. coli* genome plays a role in transport processes, suggesting a similarly significant ratio of genomic data tied to transport in all cell species.[3] There are two main types of integral membrane proteins that support transport: passive and active transporters. Passive transporters, also referred to as channels, facilitate movement along concentration gradients by forming highly selective, regulated pathways through the membrane (Fig. 1-1).[4] In many cases, channels can be activated or "gated" in response to stimuli, including certain ligands, changes in membrane potential, and physical membrane distortion. In contrast, active transporters require energy to move substrates against a concentration gradient. These intermembrane "pumps" utilize the energy stored in multiple forms, including photons, a secondary chemical gradient, or more commonly, ATP. The focus of this thesis falls under the branch of ATP-driven transporters.

1.2: ATP-Driven Transport

At least 10% of the ATP requirements of bacterial and human cells are dedicated to substrate transport.[2] There are four types of ATP-driven pumps: P-class, V-class, F-class, and ATP-binding cassette (ABC) transporters (Fig. 1-1).[4] Each type of transporter is highly selective for particular substrates, and many of them are regulated in response to physiological needs and environmental availability. The divergence into four different types allows these ATP-driven pumps to perform a multitude of functions in various locations within the cell. ATP-driven pumps play diverse biological roles, including importing and exporting a variety of substrates, acidifying lysosomes that break down harmful antigens, generating the intracellular and extracellular ion concentrations crucial to neuron communication, and synthesizing ATP in the mitochondria.

P-class pumps, often referred to as P-type ATPases, are responsible for the transport of many types of ions (Na^+, K^+, Ca^{2+}, H^+) and phospholipid molecules. A prominent example of a P-type ATPase is the sodium-potassium pump, which maintains the electrochemical gradient necessary for transmission of nerve impulses. This class also includes several heavy metal pumps, which regulate metal homeostasis as well as metal resistance in several organisms.[5] With P-class pumps, the transporter itself is covalently modified via ATP phosphorylation. When substrate is bound to the transporter, phosphorylation at a conserved aspartate residue triggers a conformational change. This structural rearrangement translocates the substrate from one side of the membrane to the other.[4]

V-class and F-class ATPases are both responsible for proton transport and have similar structures. The most recognized example of the F-class ATPase is ATP synthase. In this transporter, energy is captured from the flow of H^+ down its concentration gradient via a rotary structure. This rotary structure converts kinetic rotational energy into potential energy in the form of ATP. Conformational changes in the transporter bring ADP and inorganic phosphate together in the proper arrangement to form ATP. These two classes of transporter are also responsible for pumping H^+ ions from the cytosol into lysosomes, acidifying and breaking down any contaminants the lysosome may hold.

Lastly, ABC transporters transport a wide variety of substrates, ranging from individual ions to large siderophore compounds. Each transporter serves its unique purpose and is highly specific for its substrate or set of substrates. These transporters exist in all kingdoms of life, and the ABC superfamily is larger and more diverse than any other type of ATP-driven pumps.[6] Hundreds of transporters have been found in organisms ranging from prokaryotes to humans [for a recent review, see (6)]. ABC transporters are divided into two main functional categories: importers and exporters. Importers, which are only found in prokaryotes, facilitate the uptake of molecules such as carbohydrates, amino acids, and vitamins against their concentration gradients. Exporters use the energy of ATP binding and hydrolysis to transfer

metabolites, toxins, and peptides out of the cell, likewise against their concentration gradients. Unlike the P-type pumps, not a single ABC transporter has been discovered that is both an importer and an exporter.[6]

1.3: ABC Transporter Malfunctions and Their Consequences

A total of 49 ABC transporters have been identified in the human body and several of these and several of these transporters are linked to various health conditions.[7] Mutations in ABC transporters lead to diseases such as cystic fibrosis, Stargardt's disease, and drug-resistant tumors[8,9,10]. Cystic fibrosis is caused by a malfunction of the cystic fibrosis transmembrane conductance regulator (CFTR) transporter. The CFTR transporter is present in epithelial cells lining the lungs and is the only known ABC transporter that serves as an ion channel. Interestingly, the ATPase functionality has been lost for CFTR, and thus it is sometimes referred to as a "broken" ABC transporter. The channel allows for proper anion flow between extracellular fluid and epithelial cells, which in turn mediates the amount of liquid that epithelial cells absorb. This process ensures the proper viscosity of mucus in the lungs. A mutation in the CFTR transporter leads to a decrease in anion flow, triggering epithelial cells to absorb water, but not anions, thereby thickening mucus in the lungs and decreasing its fluidity. Ultimately, this malfunctioning transporter results in a buildup of viscous mucus in the lungs that increases the risk of life-threatening bacterial infections.[8]

A mutation of ABC transporter ABCA4 can lead to Stargardt's disease, for which the main pathology is vision loss. The ABCA4 transporter exports harmful by-products of the visual cycle performed by cells within the retina. When the transporter malfunctions, these toxic by-products accumulate in the retina, ultimately causing cell death and a gradual loss in central vision.[9]

Some ABC exporters are promiscuous in terms of their substrate specificity. These exporters, including P-gp, MRP, and BCRP, transport large hydrophobic compounds, such as chemotherapeutics, in tumor cells.[10] This adaptation allows cancers cells to expel foreign, toxic molecules before they can accumulate at an effective intracellular concentration, a phenomenon termed "multi-drug resistance." This deleterious adaptation works against a variety of anti-cancer drugs, making cancerous tumors even more difficult to treat (Fig. 1-2).[11] If medicine is to ever cure the diseases caused by malfunctioning ABC transporters, researchers must first completely understand the structure and mechanisms of action of ABC transporters.

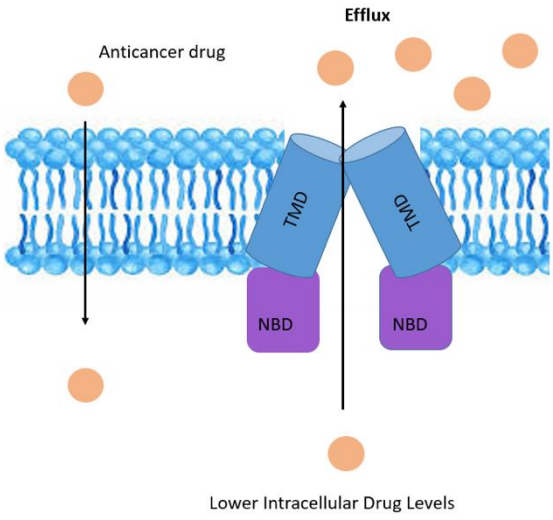

Figure 1-2: A model of a mutated ABC exporter removing anticancer drugs from a tumor cell. Image inspired by (10).

1.4: Structure and Function of ABC Transporter Components

1.4.1: General Structure

ABC transporters consist of a minimum of four domains: two transmembrane domains (TMDs) embedded in the lipid bilayer, and two nucleotide binding domains (NBDs) located on the cytoplasmic side of the membrane where ATP is available for binding and hydrolysis (Fig. 1-3).[6] Coupling helices connect the TMDs to the NBDs and are largely responsible for linking the conformational changes between each subunit.

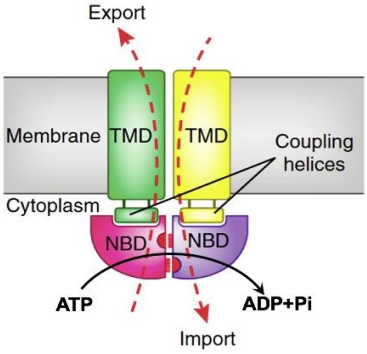

Figure 1-3: General structure of an ABC transporter. For every transporter there are two NBDs, two TMDs, and coupling helices at each NBD-TMD junction. Image taken directly from (6).

1.4.2: Nucleotide Binding Domains

The nucleotide binding domains (NBDs) are highly conserved regions of the transporter, meaning that the nucleic acid sequence in this region is nearly identical across the entire ABC transporter family. The NBD is responsible for ATP binding and hydrolysis. The two NBDs of an ABC transporter come together to form two ATP-binding pockets at the interface of the subunits (Fig. 1-4). Each NBD can be divided into two constituent domains: the RecA domain and the alpha-helical domain. ATP-binding sites are formed when the RecA domain of one NBD and the alpha-helical domain of the other NBD come together. Overall, this forms two ATP-binding sites in the NBD region of one transporter.

The RecA domain contains universally conserved regions such as the Walker A and B motifs, and H-motif. The Walker A motif, also known as the P-loop, binds the α and β-phosphates of ATP. The Walker B motif and the H-motif are recognized for their role in initiating ATP hydrolysis (Fig. 1-5). The glutamate side chain from the Walker B motif, and the histidine side chain from the H-motif are candidates for the general base that polarizes a nearby water molecule to enable nucleophilic attack, leading to hydrolysis of ATP.[12] This Walker B motif also anchors the Mg^{2+} that coordinates and positions the ATP molecule.[13]

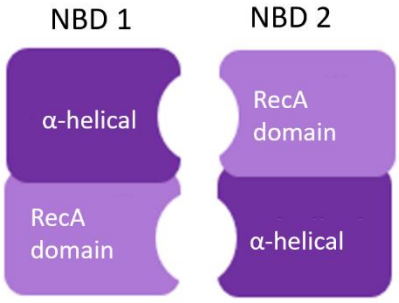

Figure 1-4: A simplified structure of the nucleotide binding domain (NBD). See text for description.

The alpha-helical domain is more diverse between ABC transporters; however, it contains three conserved regions: the ABC signature motif, the D-loop, and the Q-loop. The ABC signature motif (LSGGQ) plays a crucial role in ATP binding by forming hydrogen bonds to the γ-phosphate of the ATP molecule (Fig 1-5). The D-loop consists of the amino acid sequence EATSALD. The N-terminal glutamate (E) engages one active site while the C-terminal aspartate (D) engages the P-loop of the opposite active

site. With a connection to both active sites, researchers believe the D-loops play a crucial role in the communication between active sites.[14] The third conserved region is the Q-loop, which interacts with the ATP binding site and plays a large role in coupling ATP hydrolysis with the movement of the transmembrane domain. The Q-loop is highly flexible and can adopt different structural conformations in response to ATP binding and hydrolysis. The conformation of the Q-loop transmits information about the nucleotide state of the NBDs to the TMDs.[15]

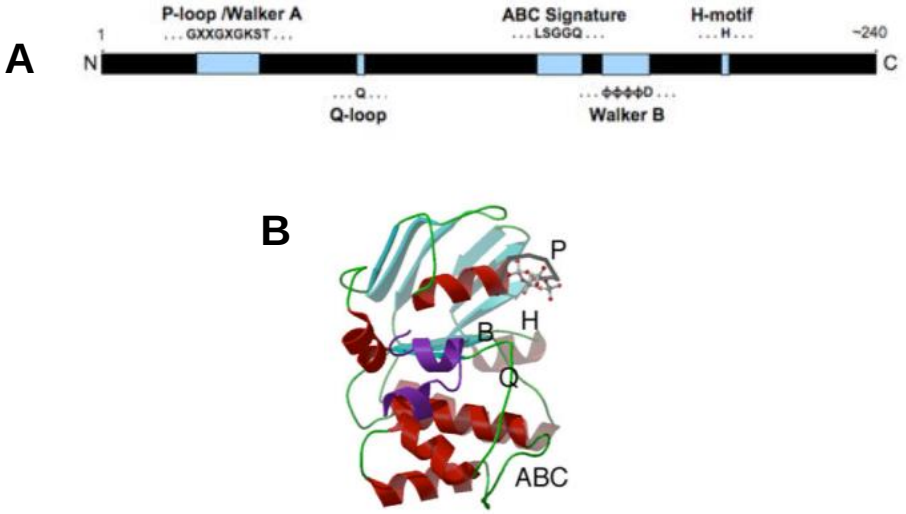

Figure 1-5: Location of various conserved regions of the NBD. (a) Location of the Walker A, Walker B, Q-loop, ABC signature motif, and H-motif in the NBD's primary structure. (b) Location of the Walker A (labeled as P), Walker B (B), H-motif (H), Q-loop (Q), and ABC signature motif (ABC) in a crystal structure of a vitamin B_{12} (BtuCD) transporter. Images taken directly from (6).

1.4.3: Transmembrane Domains

The transmembrane domains (TMDs) of the ABC transporter constitute the portion of the transporter that is embedded in the lipid bilayer and forms the permeation pathway for substrate transport. Alpha helices traverse the membrane several times, varying from 5 to 10 helices per TMD, for a total of 10-20 helices for a complete transporter. There is considerable variation in the structure of the TMDs across different ABC transporters, which reflects the diversity in substrate specificity. Variability in the architecture of the transmembrane helices is the basis for the classification system of ABC transporters (see Section 1.5 for a more detailed description).

A common feature of all TMDs is the interaction with the NBDs via "coupling helices." These relatively flexible structures contain a universal three amino acid motif, EAA. The helices form non-covalent interactions with the Q-loop of the NBDs and can thus reposition in response to structural changes in the NBDs. In effect, the nucleotide state and conformation of the TMDs are linked, or coupled, thereby capturing the energy in ATP to drive substrate transport.[16]

1.4.4: Substrate Binding Protein

A crucial component of ABC importers is their cognate substrate binding protein (SBP). The location of an SBP differs depending on the cell type in which it resides. SBPs in Gram-negative bacteria are untethered in the periplasmic space and bind to the transporter via non-covalent interactions. Substrate binding proteins in Gram-positive bacteria are either anchored to the lipid bilayer adjacent to the ABC transporter or are fused to the TMDs of the transporter itself.[17] SBPs have a bilobal architecture, and the two lobes are maneuverable to change conformation depending on substrate conditions. The lobes rotate on a hinge, coming together when substrate binds in-between them separating once the substrate has dissociated.[18] This conformational change is often referred to as the "Venus flytrap mechanism" for its similarity to the opening and closing of the carnivorous plant's leaf.[19] (Interestingly, integral membrane proteins related to ABC transporters translate the physical presence of an insect to an action potential that drives the closure of the leaf.)

The highly specific SBPs are thought to sequester substrates in the periplasm and deliver them to the membrane-embedded transporter (see Section 1.6 for a more detailed description). While this model is the most intuitive, work by some groups suggests that SBPs for certain transporters may play different roles. For example, work by the Duong group demonstrated that the SBP is less likely to complex with the maltose transporter when substrate concentrations are high.[20] This reduction in complex formation was proposed to serve as a method for limiting ATP hydrolysis when the cell has access to a sufficient amount of maltose in the periplasm. Whether or not the SBP has a similar responsibility in other ABC importer systems is an area of active research.

To aid in the handoff of a substrate between the SBP and transporter, "scoop loops," or short periplasmic helices covalently attached to the TMDs, binds substrates from the SBP (Figure 1-6). This interaction places the substrate in the transmembrane space of the transporter and moves the transport process forward. These scoop loops have been found in the maltose and vitamin B_{12} transporters, however, not all importers have these scoop loops as evidenced by the absence of a scoop-loop in the methionine importer.[21,22,23]

The presence of an SBP adds an extra component to consider when dissecting the intermediate states during a transport cycle. Understanding how and when the SBP binds to the transporter is crucial to understanding the transporter mechanism. Functional studies thus far have been focused on determining the

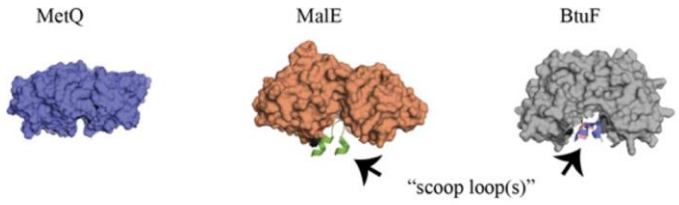

Figure 1-6: Structures of substrate binding proteins of type I ABC importers. MalE and BtuF have scoop loops while MetQ does not. Image taken directly from (22).

binding affinities of the SBP to its transporter using mutational analyses, different nucleotide states, and the presence and absence of substrate.[22,24,25]

1.4.5: Regulatory Domains

An additional component of some ABC importers are intracellular inhibitory domains. An ABC importer uses the energy from ATP binding and hydrolysis to pump substrates against the concentration gradient. If the cell has an adequate supply of a particular substrate, further import would waste cellular energy. To prevent unnecessary import, transporters including the methionine and molybdate systems have regulatory domains fused to the NBDs.[28] At high intracellular concentrations, a substrate binds to the regulatory domains and forces the transporter to adopt a conformation that prevents further ATP hydrolysis.[26,27] This phenomenon, termed transinhibition, acts as a regulatory mechanism that maintains ideal concentrations of certain substrates inside the cell.

1.4.6: Subunits Forming Complete Transporters

The formation of the transmembrane domains, nucleotide binding domains, and for importers, substrate binding proteins can require the production of five separate subunits: one subunit for each TMD and NBD, and one subunit to form the SBP. This is the case for the methionine, maltose, and vitamin B_{12} transporters. However, there is a broad diversity in the number of subunits necessary to create a transporter. For example, in some transporters, such as the $FhuBC_2D$ transporter (which transports several different siderophores), the two TMDs are contained within one polypeptide. Some transporters, such as the TAP1 transporter, consist of two polypeptides, each containing a TMD and NBD. Interestingly, the TMD subunits for the TAP1 transporter, which contribute to the process of exporting antigens in mammalian cells, are not identical.[28] Each TMD subunit is unique, making for an asymmetrical transmembrane domain. There are also transporters, such as the P-gp transporter in human cells, that are entirely made from one unit. In summary, despite the number of ways a transporter may be composed, ultimately, these transporters have a base structure of two TMDs and two NBDs that come together to endergonically transport a diversity of substrates: uniting them into one ABC superfamily.

1.5: ABC Transporter Types

There are three distinct groups of ABC transporters that are determined by the structural architecture of the transporter. The transporters within each group not only share a similar structure, but often times share similarities in finer mechanistic details. A study suggesting a mechanism for a transporter

often suggests that the mechanism may apply to all of the transporters in its group. The three types of ABC transporter are type I importers, type II importers, and ABC exporters which are defined by their transmembrane domain fold (Fig. 1-7).[6]

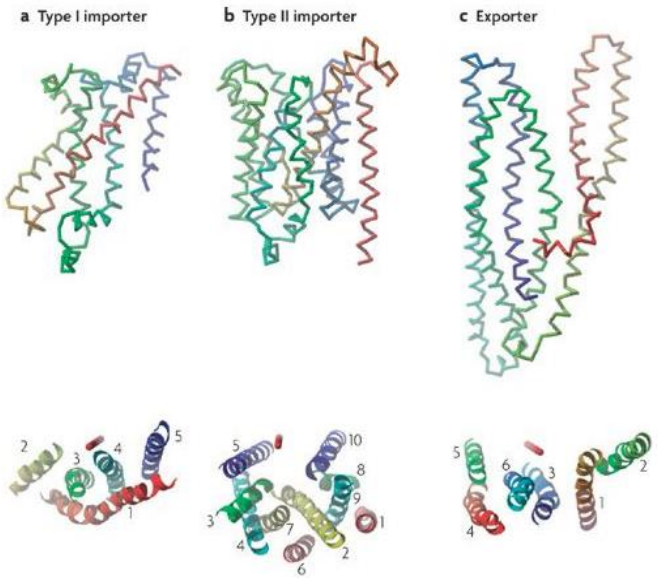

Figure 1-7: Model structures for type I importer, type II importer, and ABC exporters. Structure of transmembrane helices for Type I importer (MetI), Type II importer (BtuC), and exporter (Sav 1866) taken directly from (6).

1.5.1: Type I Importer

Type I ABC importers, such as the molybdate, maltose, and methionine systems (ModABC, MalFGK, and MetNIQ, respectively), contain 5-8 helices per domain. All but one of the helices are arranged perpendicular to the lipid bilayer. One transmembrane helix per domain lies more horizontally to the transmembrane cavity and wraps around the other helices, contacting each one. Type I importers tightly couple ATP usage with the transport of relatively small molecules, including sugars, amino acids, peptides, and compatible solutes.[29,30,31,32] The TMDs contain a low-affinity binding site for the substrate located approximately halfway through the membrane. The most well-studied type I importer is the maltose transporter, which has been captured in several intermediate conformations during the transport cycle. Crystal structures of this transporter reveal a distinct substrate binding site in the transmembrane space between the TMDs, where specific non-covalent contacts form between maltose and amino acid side chains within the permeation pathway.[33]

1.5.2: Type II Importer

Type II importers include the vitamin B_{12} transporter and various iron-containing transporters (BtuCDF, HI1470/1), where the substrates are much larger and hydrophobic than those of type I importers.[37] Type II ABC importers contain 10-12 transmembrane helices per domain, with all helices oriented parallel to the transmembrane cavity. TM helices 5 and 10 mainly constitute the interface between the two TMDs, which is responsible for forming the translocation pathway.[34] These importers transport substrates that are more scarce than type I importer substrates. This difference can explain why type II transporters have higher substrate transport affinities than type I importers, with dissociation constants in the nano- to picomolar range, while type I importers have dissociation constants in the micro- to nanomolar range.[35,36,37,38] In type II importers, the substrate is trapped in a non-specific hydrophobic cavity within the transmembrane

domains, in contrast to the specific binding interactions seen in type I transporters. The type II transmembrane domains form two gates that regulate access to the interior hydrophobic pocket, termed the cytoplasmic and periplasmic gates, based on their position within the lipid bilayer. These gates open and close in a coordinated manner during substrate transport. When the periplasmic gates are open, substrate can enter the transmembrane cavity from the outside of the cell. The periplasmic gates close before the cytoplasmic gates open and release the substrate into the cell interior, and this coordinated opening and closing ideally ensures unidirectional transport across the membrane (for a visual summary and further description, see Figure 1-9 in Section 1.7.2).

These transporters may be less efficient at energy usage than type I importers, as suggested by studies measuring the number of ATP molecules hydrolyzed per substrate transported. For example, for the type II vitamin B_{12} transporter BtuCD, ~100 ATP molecules were hydrolyzed per vitamin B_{12} molecule transported *in vitro*.[39] The authors proposed that this large type II transporter may require numerous rounds of ATP hydrolysis to enable conformational changes. Another hypothesis is that substrate can escape into the extracellular matrix instead of passing through to the cytoplasm.[40] With such a poor ATP to substrate ratio, previous researchers proposed that the substrate may be released on both the extracellular end of the transporter as well as the cytoplasmic end. This unproductive leakage may account for the high ATP requirements for some type II importers.

1.5.3: Exporters

The third group of ABC transporter are the ABC exporters. They consist of 6 TM helices per subunit or 12 helices per transporter which are arranged parallel to the transmembrane pathway. There is no binding protein for ABC exporters, leaving the responsibility of substrate specificity solely up to the substrate binding site within the TMDs. As with importers, the substrate forms noncovalent interactions with the α-helices that line the transmembrane cavity in ABC exporters. There are a number of residues that can interact with substrate allowing for several combinations of non-specific interactions in the TMDs. For this reason, ABC exporters are often promiscuous in the substrates they export. Numerous molecules can be identified as substrates for a single exporter since there are a multitude of residues that interact with the substrate, allowing for a more diverse pool of substrates.[41]

1.5.4: Further Classification of Human ABC Transporters

The human genome contains 49 ABC genes that have been separated into seven subfamilies, labeled A-G, based on their genomic data. These ABC genes can be alternatively spliced to form a variety of transporters. Human transporters are often named based on their subfamily classification. For example, the ABC transporter whose malfunction is linked to Tangier disease is called ABCA1 as it is a part of the

ABC subfamily A. Each subfamily contains a number of transporters that do not necessarily share similar functions. A few subfamilies of note are subfamily B, which consists partially of transporters responsible for multidrug resistance in cancer cells, and subfamily C, which contains the CFTR transporter whose malfunction causes cystic fibrosis.[42]

1.6: Prevailing Transport Mechanism: Alternating Access Model

Transporters transition through multiple conformations per transport cycle, and two distinct conformations provide a starting point for understanding ABC transport mechanism (Fig. 1-7).[43] In the inward-facing conformation, the TMDs are open to the cytoplasm, and the permeation pathway is inaccessible from the periplasmic side of the lipid bilayer. In contrast, in the outward-facing conformation, the TMDs are arranged with the permeation pathway open to the periplasm.

Observations of the inward-facing and outward-facing conformations can be incorporated into an intuitive model for transport: the widely-accepted alternating access model. In this model, conformational changes in the TMDs are driven by changes in the nucleotide state of the NBDs. In the absence of nucleotide, the NBDs are separated, and the TMDs are in the inward-facing conformation. Binding of ATP at the interface between the two NBDs triggers the rearrangement of the TMDs to the outward-facing conformation. The energy from ATP binding is thought to provide the energy necessary to stabilize this conformation. Upon ATP hydrolysis, the NBDs separate, which is coupled to a transition back to the inward-facing conformation.[43]

The alternating access model can be applied to both ABC importers and exporters. For an ABC importer, the SBP delivers the substrate to the transporter, driving formation of the ATP-bound outward-facing conformation. Docking of the SBP and release of the substrate into the permeation pathway triggers ATP hydrolysis, which in turn drives the rearrangement from the outward-facing to inward-facing conformation. The substrate can then exit to the cytoplasm. The NBDs must release ADP and inorganic phosphate before the next transport cycle can occur. For ABC exporters, the cytoplasmic substrate accesses the TMDs in the inward-facing conformation. Substrate is transported once ATP binds to the NBDs, driving a rearrangement to the outward-facing conformation. Following substrate exit, ATP is hydrolyzed and the NBDs separate. ADP and inorganic phosphate are released, and the transporter returns to its inward-facing conformation to repeat the cycle.[6]

In addition to the inward-facing and outward-facing conformations mentioned above, intermediate states have been isolated and characterized in crystallographic and solution-based studies of various ABC transporters. These intermediate conformations, include resting, pre-translocation, and post-hydrolysis states, have placed a spotlight on further understanding and elucidating the mechanisms for different ABC transporters.

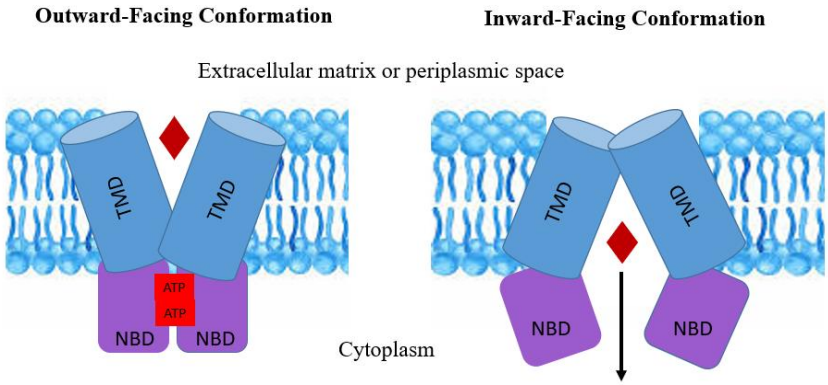

Figure 1-8: Alternating access model for ABC transport. ATP binding at the NBDs drives the outward-facing conformation (left). The inward facing conformation is open to the cytoplasm (right). Substrate (red diamond) is transported across the membrane upon changes in nucleotide state.

1.7: A Diversity of Mechanisms For ABC Transporters

While the alternating access model provides a starting point for understanding many ABC transporter mechanisms, the intermediate steps in between the inward-facing and outward-facing conformational states vary widely between transporters. Mechanisms can vary between different types of transporters, between transporters that share the same transporter type, and even for a single transporter that is studied in two different *in vitro* environments.

1.7.1: Proposed Mechanisms of a Type I Importer (Maltose Transporter $MalFGK_2$)

The maltose $MalFGK_2$ transporter is one of the most studied ABC transporters and is an example of an ABC transporter with more than one proposed mechanism. The mechanism depicted in Fig. 1-8a was proposed following studies with the transporter solubilized in the detergent n- dodecyl-β-D-maltoside. [46] In this model, the MalE SBP binds maltose with high affinity and specificity in the periplasm and delivers it to the membrane-embedded transporter. The SBP must bind maltose prior to binding to the transporter. Substrate-bound SBP then binds the transporter in its nucleotide-free state. Once substrate-loaded SBP forms a complex with the transporter, ATP binds to the NBDs and triggers the transition to the outward-facing conformation via the coupling helices.

This change in TMD conformation causes the SBP to pry open, and with the aid of the scoop loop, substrate is released to the transporter.[23] The maltose substrate then binds to a low affinity binding site within the TMDs. The transport of maltose is complete once ATP is hydrolyzed, causing the NBDs to separate. Therefore, nucleotide hydrolysis drives the transporter into its inward-facing conformation, allowing substrate to pass through into the cytoplasm of the cell. [23]

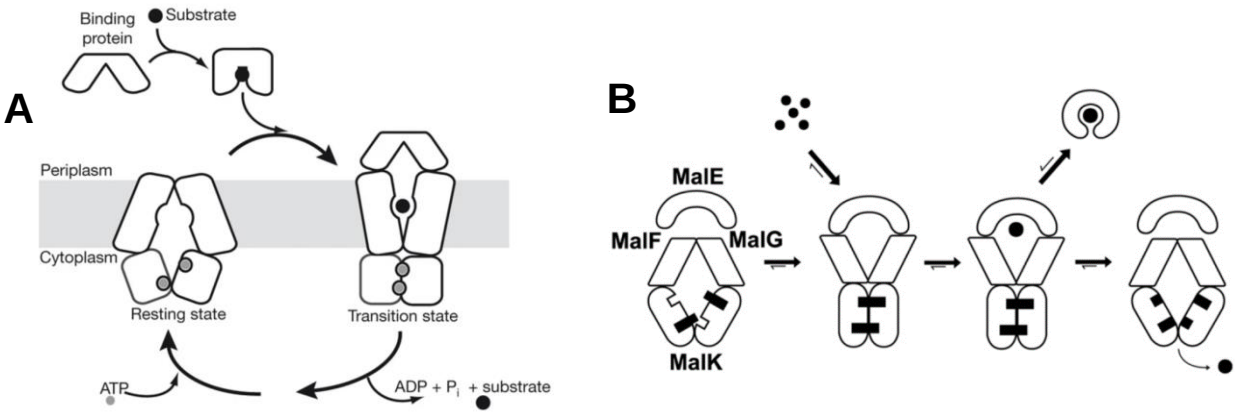

Figure 1-9. Possible mechanisms for maltose transport. (a) This mechanism was proposed based on structural studies of the transporter solubilized in detergent. The image was taken directly from (45). (b) A second possible maltose transporter mechanism based on functional studies of the transporter in lipid nanodiscs. The figure was taken directly from (46).

The original mechanism (Fig 1-8a)has been questioned as it was primarily based on structural studies performed with the transporter in detergent micelles. In these crystallography studies, lattice contacts and detergent effects may stabilize conformations that do not exist *in vivo*. Equilibrium studies of the maltose transporter in lipid nanodiscs, a more accurate mimic of the lipid bilayer, indicating a distinct mechanism for transport (Fig. 1-9b).[44] Using crosslinking and fluorescence quenching experiments, Bao and colleagues reported that ATP binding alone is enough to convert the transporter from the inward-facing to the outward-facing conformation. Additionally, MalE can bind the transporter without maltose in the binding pocket. Following complex formation, substrate binds to the complex and later crosses the membrane upon ATP hydrolysis. However, in the presence of excess substrate, MalE sequesters substrate and dissociates from the transporter, inhibiting further substrate transport.[45]

1.7.2: Proposed Mechanisms of a Type II Importer (Vitamin B_{12} Transporter BtuCD-F)

The vitamin B_{12} transporter is the most well-studied type II importer, playing a key role in understanding the differences between type I and type II importers. One model for BtuCD-F transport was based on structural studies of the transporter in detergent (Fig. 1-10).[46] Crystal structures of BtuCD in several intermediate states revealed three gates surrounding the hydrophobic cavity in the transmembrane region: two on the cytoplasmic side, labeled cyto gates 1 and 2 (Fig. 1-10), and one on the periplasmic side (peri gate). These gates block or allow substrate to pass through the transporter based on the nucleotide state and presence of substrate. In this proposed mechanism, substrate-bound SBP BtuF docks onto the transporter in its ATP-bound form (configuration 1 to 2). In this conformation, the cytoplasmic gates are closed but the periplasmic gates are open to allow substrate into the transmembrane cavity. Next, substrate is released from BtuF and trapped within the transmembrane cavity by cytoplasmic and periplasmic gates. ATP is subsequently hydrolyzed, opening the cytoplasmic gates and allowing the substrate to pass into the

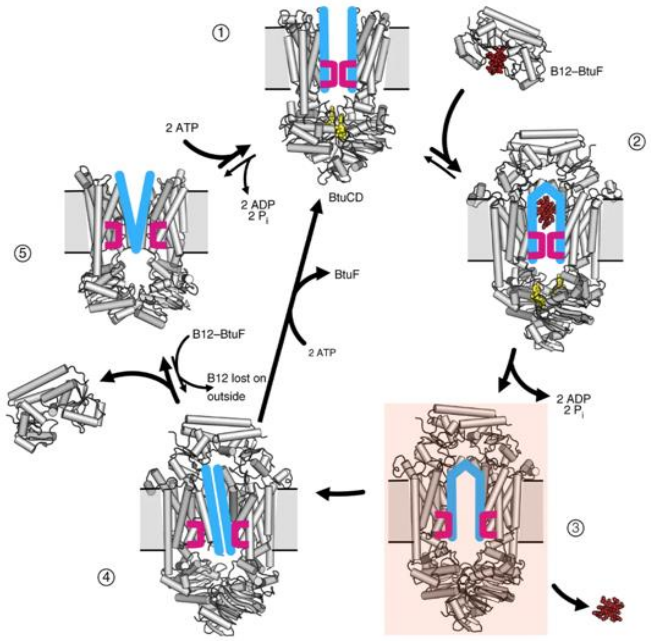

Figure 1-10: Proposed mechanism of the BtuCD-F importer based on structural studies. Yellow ball and stick represent nucleotides, red ball and stick depict vitamin B_{12}, blue lines depict TM helices 5 in each BtuC subunit, which form the gate and cytoplasmic gate I. Magenta brackets depict cytoplasmic gate II, which is formed by the loop between TM helices 2 and 3, in each BtuC subunit. Image taken directly from (47).

cytoplasm (configuration 2 to 3). BtuF dissociates from the complex and ATP binds to the transporter to restart the transport cycle (configuration 4 to 1).

In contrast, a separate study with the transporter in both detergent micelles and liposomes resulted in a different mechanism for BtuCD-F (Fig. 1-11).[47] In this model, substrate-bound BtuF is able to bind to BtuCD in its nucleotide-free state (configuration I). Upon binding to the transporter, the substrate is released from BtuF, and vitamin B_{12} passes through the transmembrane domains while BtuF is still bound to BtuCD (configuration II). ATP-binding and hydrolysis is necessary to dissociate the BtuCD-F complex and return the transporter to its outward-facing, nucleotide-free state (configuration III and IV).

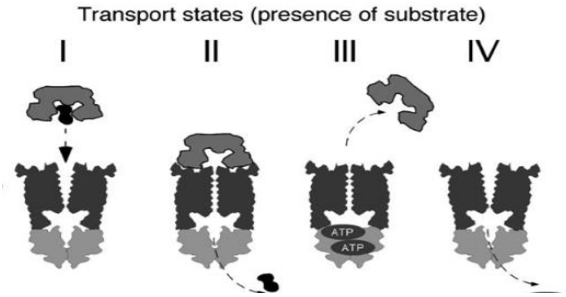

Figure 1-11: Proposed mechanism for the type II BtuCD-F importer from functional studies. The figure was taken directly from (48).

1.8: Transporter of Focus: Type I Methionine Importer MetNI

The focus of this thesis is to examine the mechanism of the Type I methionine importer MetNI, specifically under what nucleotide and substrate conditions MetQ complexes with MetNI (Fig. 1-11). Although the transporters linked to disease in humans are ABC exporters, ABC importers are seen as reliable models for exporter activity due to homology (25-30%) between the two classes of transporters, especially in the NBDs.[48] Here we utilized the methionine transport system from *Escherichia coli*, which was first studied by Kadner and Watson in 1974.[49]

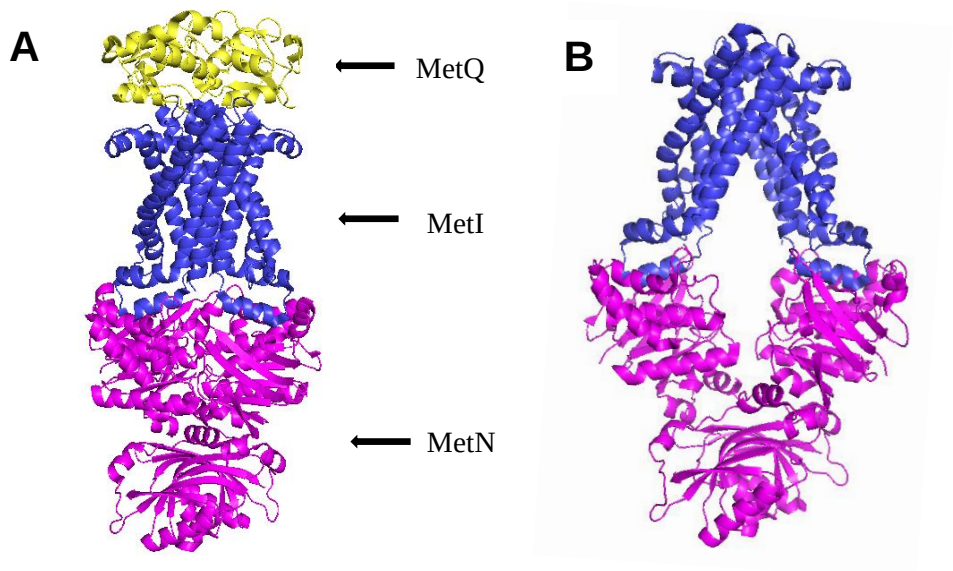

Figure 1-12: Crystal structures of the methionine importer MetNI. (a) The outward-facing conformation of MetNI in complex with the substrate-binding protein MetQ (22). MetQ is pictured in yellow, the TMDs are pictured in blue, and the NBD and C2 domains are pictured in purple. (b) The inward-facing, transinhibited conformation of MetNI(53).

1.8.1: MetN: The Nucleotide Binding Domain

The nucleotide binding domain of MetNI is referred to as MetN. These subunits are identical to each other, however each is a separate polypeptide. To form a complete nucleotide-binding domain, the two polypeptides come together, associating to form a homodimer. There are a number of amino acids within the NBDs that interact with ATP, and two crucial amino acids are a glutamate at position 166 (E166) and a lysine at position 44 (K44). E166 is part of the Walker B motif (introduced in Section 1.4.2) and is necessary for ATP hydrolysis. The glutamate acts as a general base and polarizes H_2O for nucleophilic attack of the γ-phosphate. As depicted in Figure 1-13c, substituting glutamate with a glutamine (E166Q) residue hinders the ability to hydrolyze ATP without diminishing the binding of ATP (Fig. 1-13).[50] Glutamine is chosen as a substitute due to its similar size and structure to glutamate. The K44 amino acid located within the Walker A motif of MetNI has been proposed to play a central role in ATP binding. Substituting alanine for the lysine residue in the Walker A motif of the MJ0796 transporter reduces ATP-

binding by 15-fold.[50] This NBD mutant is a key component in locking a MetNI transporter in its nucleotide-free state.

An additional structural detail for the ATP-bound, outward-facing conformation of the MetNI transporter is the inability of the alanine-299 residues at the intersection of the adjacent NBDs to hydrogen bond(Fig. 1-13b) The distance between these residues is too far, allowing the transporter to remain in the outward-facing conformation. Once these residues come in closer proximity to each other (3 Angstroms or less), they initiate a hydrogen bonding complex that forces the transporter in the inward-facing conformation (for further details and images, see Section 1.8.3 and Figure 1-14).

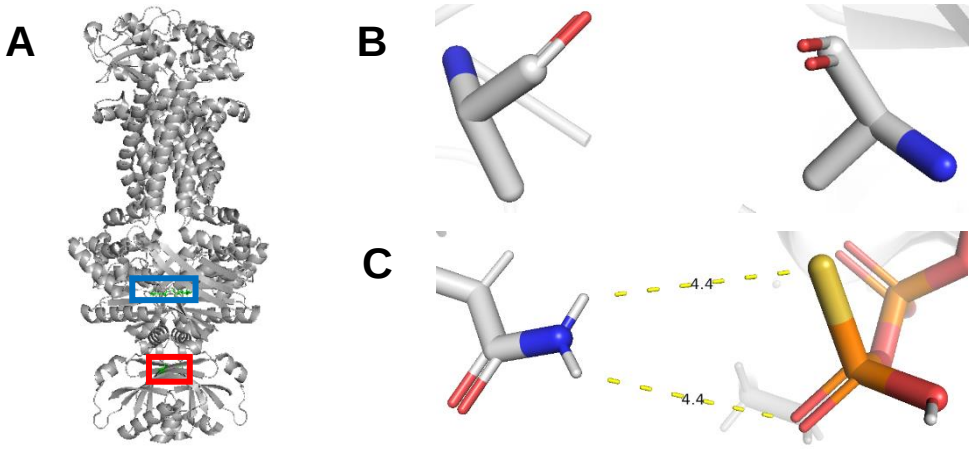

Figure 1-13: Uninhibited, outward-facing conformation of MetNI. (a) Crystal structure of ATP-bound MetNI in complex with apo MetQ. The approximate location of the alanine-299 residues and the E166Q mutation are boxed in red and blue, respectively (22). (b) Adjacent alanine-299 residues are unable to hydrogen bond in the outward-facing conformation. (c) ATPγS bound (right) bound to the E166Q residue (left) within the NBDs. All measurements are given in angstroms.

The ATP-binding pockets of MetN have a reported K_m of 330 ± 20 μM with ATP.[27] The K_m value is the concentration of substrate required for the transporter to achieve half of its V_{max} value. In the case of ATP, a transporter's V_{max} value is the maximum number of ATP the transporter hydrolyzes per minute. For this system, the lower the K_m value, the higher the affinity the transporter has for ATP. With typical intracellular ATP concentrations between 1-10 mM, MetNI's affinity for ATP is strong enough for the transporter to operate at its maximum capacity *in vivo*.[51] ATP-binding between the MetN subunits has been found to be cooperative (n = 1.7 ± 0.1) meaning that the affinity for ATP increases when one of the binding sites has bound ATP. This cooperativity suggests that the two ATP sites communicate with each other during the transport cycle.

1.8.2: MetI: The Transmembrane Domain

The two subunits that form the transmembrane region of MetNI are identical to each other (Fig. 1-11, blue). Each MetI subunit is composed of 5 helices. Unlike other ABC transporters, there are no MetNI

crystallographic structures with substrate bound within the TMD, however, there is a proposed binding site for L-methionine in the transmembrane region. The pathway through the membrane created by the interface between the two MetI subunits is thought to be selective for methionine derivatives.[22]

1.8.3: C2 domain: The Inhibitory Domain of MetNI

An added feature for many ABC importers is regulation of transporter activity. In the case of the MetNI transport, unregulated activity could lead to unnecessarily high levels of intracellular methionine and wasteful usage of ATP. Regulation of transport was first observed in *in vivo* studies by Kadner and Watson in 1975, in which a rapid decrease in methionine transport was observed as intracellular methionine increased.[52] Based on crystallography studies, a transinhibition mechanism was proposed, in which L-methionine binding traps MetNI in the inward-facing conformation. This regulatory strategy was further supported by *in vitro* biochemical studies in which L-methionine was shown to act as a non-competitive inhibitor of ATP.[53] The simplicity of this mechanism allows the cell to avoid more arduous regulatory processes, such as protein degradation and transcription regulation, which require longer response times and are energetically demanding processes. The presence of an allosteric regulatory mechanism prevents wasteful ATP hydrolysis and prevents the build-up of substrate inside of the cell.

An arginine residue at position 295 in the C2 regulatory domain of MetNI is crucial for transinhibition.[22] The side chain of arginine forms hydrogen bonds with the N-terminus of the L-methionine substrate (Fig. 1.14c), which in turn promotes a hydrogen bonding network between the peptide -NH and -

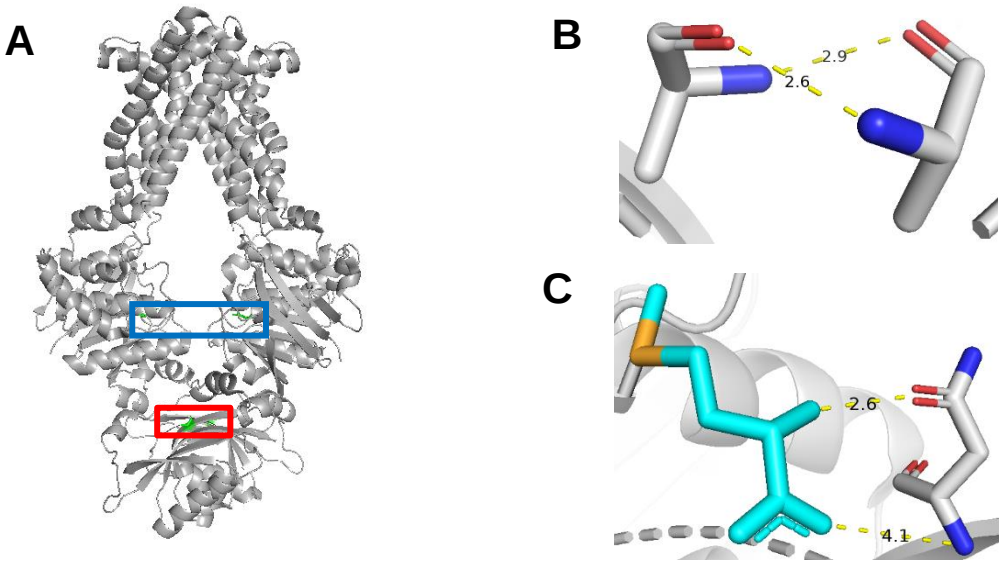

Figure 1-14: Transinhibited, inward-facing conformation of MetNI. (a) Crystal structure of MetNI with L-Met bound to its C2 domains(53). The approximate location of the N299 and Q166 residues are boxed in red and blue, respectively. (b) Adjacent alanine-299 residues that hydrogen bond in the transinhibited conformation. (c) The N295A side chain from one C2 domain (gray) forms hydrogen bonds with L-Met (cyan). All measurements are given in angstroms.

CO groups on the alanine amino acids located at position 299 in the adjacent NBDs (Fig. 1.14b). In comparison, when there is no L-Met bound to the C2 domains, the adjacent alanine amino acids at position 299 are too far to form a hydrogen bond (Fig 1-13, allowing the structure to more easily maneuver into the outward-facing conformation network locks the C2 domains together, preventing the NBDs from coming together to form the ATPase sites. A previously identified MetNI mutant N295A greatly reduces the binding affinity of L-Met for the C2 domains, nullifying the transinhibitory effect of intracellular methionine.[22]

1.8.4: MetQ: The Substrate Binding Protein of MetNI

The MetNI transporter can be found in Gram-negative bacteria, and thus the substrate-binding protein of the transporter, MetQ, resides in the periplasmic space. MetQ preferentially binds L-Met over related methionine derivatives. MetQ from *Neisseria meningitides* has a very high affinity for L-Met, with a K_d value of 0.2 nM. The equilibrium constant K_d is a constant that quanitifies the affinity between two molecules. The lower the K_d value, the stronger the affinity between two molecules. For example, MetQ has a much stronger affinity for L-Met (K_d of 0.2 nM) than it does for substrate D-Met with a K_d of 3.5 µM.[54] This preference for L-Met over D-Met is likely due to the cell's preference for L-oriented amino acids. All synthesized proteins are made with L- amino acids. Converting D-Met requires the presence of racemase enzymes that are not always present.

MetQ, like other SBPs, binds substrate in a Venus flytrap mechanism (Fig. 1-15a).[19,54] MetQ binds to MetNI in both its apo and its substrate-bound form, although the technique used in this published study is not widely accepted by the biochemistry community. Nonetheless, L-Met bound MetQ a ~40-fold weaker binding affinity to MetNI than apo MetQ.[55] The MetQ N229A mutant has a greatly reduced binding affinity to methionine derivatives and is often utilized as an easily producible apo MetQ substitute. MetQ N229A replaces the arginine amino acid at location 229 and replaces it with an alanine amino acid. The positively-charged side chain on arginine has strong ion-dipole interactions with the sulfur atom of the methionine

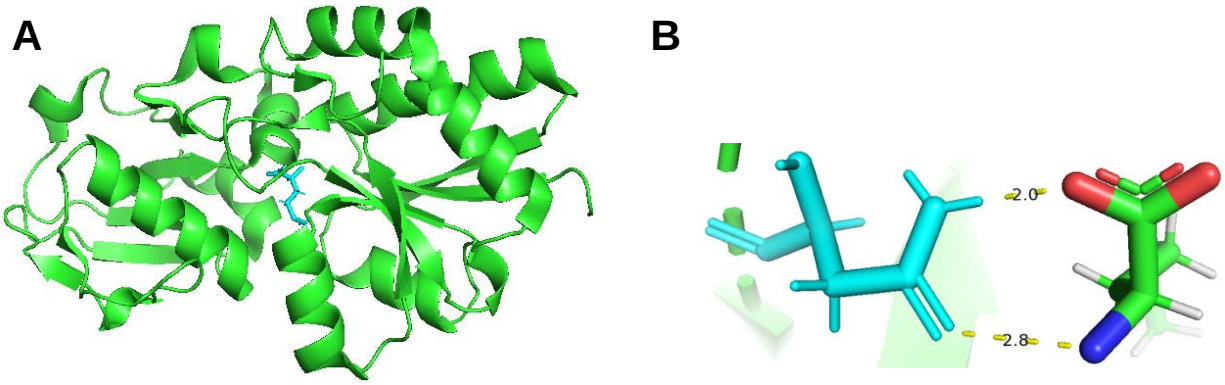

Figure 1-15: L-Met bound MetQ. (a) Crystal structure of L-Met bound MetQ (55) . (b) Image of the hydrogen bonding interactions between residue N229 and L-Met (cyan).

side chain (Fig. 1.15b). Replacing the arginine side chain with the alanine side chain causes the observed reduction in MetQ -methionine binding affinity.

1.9: Possible Mechanisms for Methionine Importer MetNI

Two different mechanisms have been proposed for MetNI transport, as described below. These mechanisms are very similar to the seemingly opposed mechanisms of the maltose transporter, and it is hypothesized that both mechanisms may be utilized for methionine import.

1.9.1: Canonical Model

Cellular proteins only utilize L-amino acids to construct proteins. For this reason, cells largely prefer to import L-amino acids to conserve energy rather than reconfigure amino acid stereocenters. In the canonical model, L-methionine is the preferred substrate for delivery into the cell. The transport cycle follows the original model proposed for the maltose transporter based on studies of the transporter in detergent. In this model, MetQ scavenges the periplasmic space until it binds L-Met. L-Met loaded MetQ then delivers the substrate to membrane-bound MetNI in its nucleotide-free state (Fig. 1-16). Following MetNI-Q complex formation, ATP binds to the NBDs, driving the transporter into its outward-facing conformation. This conformational change triggers L-Met release into the permeation pathway. ATP is then hydrolyzed, allowing the transporter to return to the inward-facing conformation, thereby transporting L-Met into the cell. Lastly, ADP dissociates from the NBDs and the transporter returns to the apo state, ready to engage in the next transport cycle.[24]

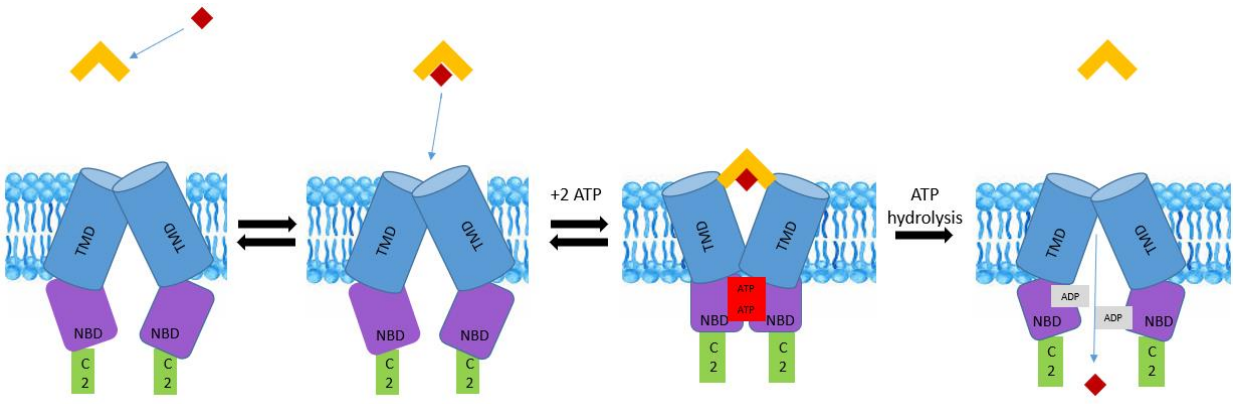

Figure 1-16: The canonical model for the MetNI transporter. In this model, MetNI-Q transports substrate L-Met.

1.9.2: Non-Canonical Model

A second possible mechanism involves the transport of methionine derivatives that have a lower binding affinity to MetQ, such as D-Met (Fig. 1-16). This mechanism, referred to as the non-canonical mechanism, is very similar to the mechanism proposed for the maltose transporter based on studies performed with the transporter in nanodiscs. The main difference between the canonical and non-canonical model is in steps 1 and 2. In the non-canonical model, apo MetQ binds to ATP-bound, MetNI before L-Met later binds to pre-complexed MetQ. D-Met arrives at the transporter-binding protein complex, where it is able to travel through a small pathway embedded in the MetQ protein. MetQ then twists 24° around an axis perpendicular to the interface between the two lobes of the protein. This twist creates an opening for D-Met to pass through MetQ, a mechanism not yet found in other ABC transporters, giving D-Met a path to the transmembrane cavity. From here, the mechanism behaves identically to the canonical mechanism in which ATP is hydrolyzed, driving the transporter to its inward-facing conformation and allowing substrate to travel into the cell.[22]

The proposed non-canonical mechanism is one that complements the classical mechanism and does not necessarily contradict it. Nguyen and colleagues propose that in situations of L-Met scarcity, the transporter will be biased towards the non-canonical mechanism and import less desirable methionine derivatives.[22] In this circumstance, the MetNI-apo MetQ complex is formed first and awaits arrival of a substrate molecule such as D-Met. Upon transport of D-Met, apo MetQ will dissociate from MetNI, rendering it available to roam the periplasm in search of more substrate. If L-Met becomes available, MetQ will bind to the substrate with high affinity and initiate the canonical mechanism. If L-Met is absent, apo MetQ will return to form a complex with MetNI, and pending L-Met derivative arrival, will begin the non-canonical mechanism. The combination of the canonical and non-canonical pathways would allow the

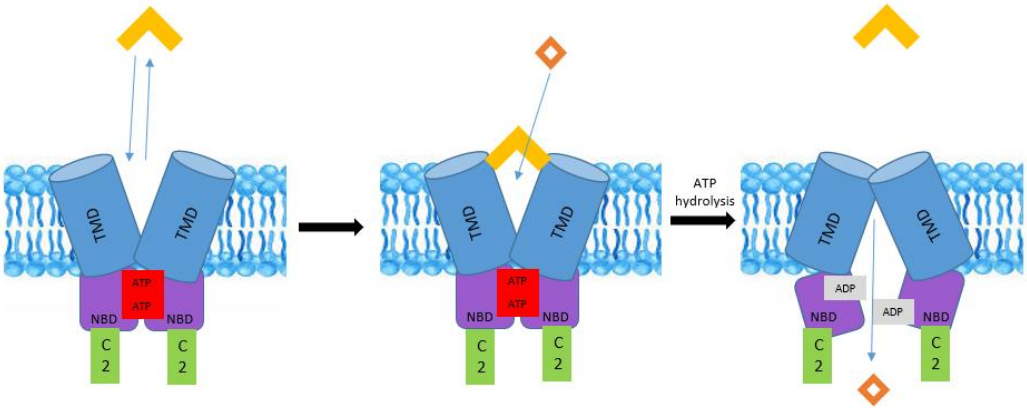

Figure 1-17: The non-canonical model of the MetNI transporter. This model is proposed to predominantly transport methionine derivatives such as D-Met (orange diamond).

MetNI transporter to rapidly adjust its substrate consumption, ensuring cell survival under different environmental conditions.[22]

1.10: Experimental Approach and Key Questions Addressed in This Work

Measuring binding affinities between an ABC transporter and its cognate binding protein is a key step in dissecting transport mechanisms. Our research efforts were focused on the requirements for the complex formation between the MetNI transporter and the MetQ substrate binding protein. We developed a solution-based technique to quantify the strength of this interaction under varying conditions, as detailed below.

The development of fluorescence anisotropy as a robust technique to study ABC transporter mechanism.

X-ray crystallography studies have been crucial in understanding ABC transporter function; however, these studies place the transporter in a highly artificial environment. Solution-based thermophoresis titrations assess ABC transporter binding affinities, however, the method has failed to reach widespread approval in the research community. Lastly, surface plasmon resonance has been utilized to assess binding affinities of other transporter complexes, but has failed to produce reliable data with the MetNI transporter.

Another commonly used method to study binding affinities in biochemistry is fluorescence anisotropy. Briefly, this method relies on the relationship between the size of a fluorescent molecule and its change in polarized light emission. When a stationary fluorescent molecule is excited, it emits a photon of light that travels on the same axis as the excitation photon. However, molecules in solution are not stationary. In the elapsed time between light absorption and emission (10^{-9} to 10^{-15} seconds) the molecule tumbles in solution. The light emitted is consequently depolarized due to this rotation. The smaller the dye molecule, the more it will rotate in solution and the more depolarized the emitted light.[56]

A fluorescence anisotropy study of the OppA ABC transporter system, which is responsible for the transport of the nine-amino-acid peptide bradykinin, had a series of precise binding affinities of two biomolecules in a variety of pH and temperature conditions. Following in their footsteps, our research aim was to measure the binding affinity between the MetNI transporter and the

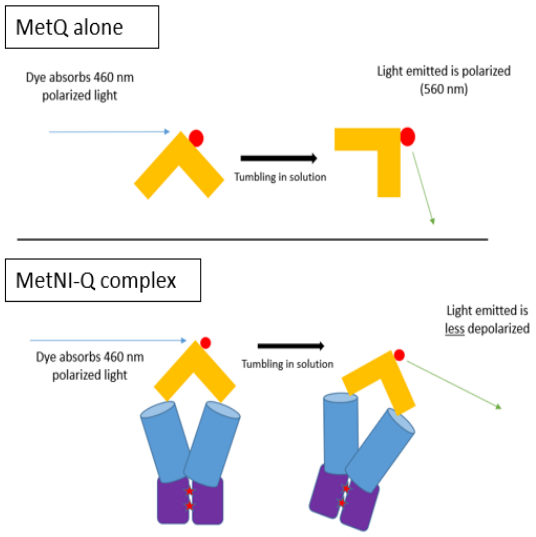

Figure 1-18: Schematic of anisotropy assay for the study of MetNI-Q complex formation.

MetQ SBP, (Fig. 1-17) using fluorescence anisotropy for the first time. We successfully measured the K_d of MetNI-Q complex formation under different conditions with a relatively small standard deviation in the results. Our results have suggested the presence of both the canonical and non-canonical model for methionine transport.

Which nucleotide states promote MetNI - Q complex formation?

In the proposed canonical mechanism for methionine import, MetQ binds to MetNI in its nucleotide-free state. This mechanism follows the original model for the maltose transporter, which was proposed based on studies performed in detergent. However, a crystal structure of the MetNI-Q complex in the apo nucleotide form has not been determined, and functional studies have not been able to support its possible existence. A more recent mechanism of the maltose transporter studied in lipid nanodiscs may provide more biologically relevant insight. In this mechanism, ATP-binding is a pre-requisite for the SBP to bind to the transporter.

To examine the role of nucleotide state in MetNI-Q complex formation, we measured the K_d value of the MetNI-Q complex in the presence of various nucleotides. Using our fluorescence anisotropy assay, we report a significant difference in K_d values based on the nucleotide state, with complex formation showing a strong preference for the ATP-bound state. This finding sheds light on the role of ATP binding in methionine transport.

Is MetQ bound to substrate prior to complex formation?

The canonical model for transport proposes that MetQ is bound to L-Met prior to forming a complex with MetNI. The affinity between MetQ and L-Met is extremely tight, with a K_d value of 0.2 nM[60], and the crystal structure of isolated MetQ bound to L-Met has been solved. However, the only existing crystal structure of the MetNI-Q complex was solved using a mutant form of MetQ that cannot bind substrate. Microscale thermophoresis experiments determined that this interaction was approximately 40 times stronger than with wild-type MetQ bound with L-Met (K_d = 27 ± 9 nM vs. 1100 ± 300 nM, respectively). While the discovery brought attention to the possibility of two different mechanisms for transport, the method used to determine the binding affinities has yet to be widely accepted, and thus these binding affinities are in question.

To examine the difference in binding affinities between apo and L-Met bound MetQ with MetNI in the presence of ATP, fluorescence anisotropy was utilized. We find a modest difference between the affinities of the two complexes, which can be incorporated into pre-existing models to explore the cellular preferences for L-methionine versus D-methionine.

Does binding of L-methionine to the C2 regulatory domains inhibit complex formation?

The elegant *in vivo* experiments conducted by Kadner demonstrated the transinhibition property of MetNI. Based on the crystal structure of MetNI, in conjunction with functional studies, it has been proposed that intracellular L-Met binds to the C2 domains of MetNI, forcing the complex into an inward-facing conformation. While the NBDs of the MetNI are separated in this conformation, it is unclear as to whether or not this arrangement precludes the binding of MetQ.

In this study, we are able to detect the dissociation of the MetNI-Q complex upon addition of excess L-methionine. While this result is very preliminary, it suggests that the intracellular level of substrate can prevent the binding of MetQ on the periplasmic side of the cell. This mechanism, in conjunction with the physical separation of the NBDs, could work to limit the intake of excessive L-methionine.

1.11: Summary

ABC transporters are crucial to cell homeostasis and cell viability in all kingdoms of life. Malfunctions in these transporters are linked to a number of conditions including cystic fibrosis, Stargardt's disease, and multi-drug resistance. In order to treat these ailments, scientists must first understand the mechanism of ABC transporters. A plethora of knowledge has already been discovered regarding ABC transporters, including their atomic structure, conformational states, and regulatory strategies. While the strides made to understand ABC transporters have been significant, there are details that have yet to be elucidated. To investigate these transporters, we address specific questions about the bacterial methionine importer MetNI. This importer contains the highly-conserved features found in human ABC exporters, and previous work has established robust expression and purification protocols. In this thesis, we specifically aim to determine the requirements for the formation of the transporter-substrate binding protein complex, MetNI-Q. Using a fluorescence anisotropy assay, we examine the nucleotide and substrate states that best promote complex formation and how the binding of L-Met to the C2 regulatory domains affects MetNI-Q stability. Our findings not only address these questions, but also offer more directions for future researchers to investigate.

References

1. Lewis B.A, Engelman D.M. Lipid bilayer thickness varies linearly with acyl chain length in fluid phosphatidylcholine vesicles". *J. Mol. Biol*. (1983). 166 (2): 211–7.
2. Yeagle P.L. The Membranes of Cells (Third Edition). *Elsevier*. (2016).
3. Busch W. Saier, M.J. The transporter classification (TC) system. *Crit. Rev. Biochem. Mol. Biol.* (2002). 27:287-337.
4. Campbell N., Reece J. Biology (Seventh Edition). *Pearson Education*. (2005).
5. Lee J.Y., Yang J.G., Zhitnitsky D., Lewinson O., Rees D.C. Structural basis for heavy metal detoxification by an Atm1-type ABC exporter. *Science*. (2014). 343(6175):1133-1136.
6. Rees D.C., Johnson E., Lewinson O. ABC transporters: the power to change. *Nature Reviews: Molecular Cell Biology*. (2009). 10:218-227
7. Vasiliou, V; Vasiliou, K; Nebert, DW (April 2009). "Human ATP-binding cassette (ABC) transporter family". *Human Genomics*. 3 (3): 281–90.
8. Gadsby D.C., Vergani P., Csanády L. The ABC protein turned chloride channel whose failure causes cystic fibrosis. *Nature.* (2006). 440(7083): 477-483.
9. Tsybovsky Y., Molday R.S., Palczewski K. The ATP-binding cassette transporter ABCA4: Structural and Functional Properties and role in Retinal Disease. *Adv Exp Med Biol.* (2010). 703: 105-125.
10. Choi C.H. ABC transporters as multidrug resistance mechanisms and the development of chemosensitizers for their reversal. *Cancer Cell Int.* (2005). 5:30.
11. Hamed A.R. Abdel-Azim N.S., Shams K.A., Hammouda F.M. Targeting multidrug resistance in cancer by natural chemosensitizers. *Bulletin of the National Research Centre*. (2019) 43:8.
12. Buchaklian A.H., Klug C.S. Characterization of the LSGGQ and H motifs from the Escherichia coli lipid A transporter MsbA. *Biochemistry*. (2006). 45(41):12539 – 12546.
13. Zhang X., Wigley D.B. The 'glutamate switch' provides a link between ATPase activity and ligand binding in AAA+ proteins. *Nat Struct Mol Biol.* (2008). 15(11):1223-1227.
14. Jones P.M., George A.M. Role of the D-loops in allosteric control of ATP hydrolysis in an ABC transporter. *J. Phys Chem A.* (2012). 116(11):3004-3013.
15. Jones P.M., George A.M. Mechanism of ABC transporters: A molecular dynamics simulation of a well characterized nucleotide binding subunit. *PNAS.* (2002). 99:12639-12644.
16. Orelle C., Alvarez F.J.D., Oldham M.L., Orelle A., Wiley T.E., Chen J., Davidson A.L. Dynamics of α-helical subdomain rotation in the intact maltose ATP-binding cassette transporter. *PNAS*. (2010). 107(47):20293-20298.
17. Bernttson R.P.A., Smits S.H.J., Schmitt L., Slotboom D.J., Poolman B. A structural classification of substrate-binding proteins. *Febs Letters.* (2010). 584(12):2606-2617.
18. Tang C., Schwieters C.D., Clore G.M. Open-to-closed transition in apo maltose-binding protein observed by paramagnetic NMR. *Nature*. (2007). 449(7165):1078-1082.
19. Mao B., Pear M.R., McCammon J.A., Quiocho F.A. Hinge-bending in L-arabinose-binding protein. The "Venus's-flytrap" model. *J Biol Chem.* (1982). 257(3):1131-1133.
20. Bao H., Duong F. ATP alone triggers the outward-facing conformation of the maltose ATP-binding cassette transporter. *J. Biol. Chem.* (2013). 288(5): 3439-3448.
21. Hvorup R.N., Goetz B.A., Niederer M., Hollenstein K., Perozo E. Locher K.P. Asymmetry in the structure of the ABC transporter-binding protein complex BtuCD-BtuF. *Science.* (2007). 317(5483):1387-1390.
22. Nguyen P.T., Lai J.Y., Lee A.T., Kaiser J.T., Rees D.C. Noncanonical role for the binding protein in substrate uptake by the MetNI methionine ATP Binding Cassette (ABC) transporter. *PNAS.* (2018). 115:45, E10596-E10604.
23. M.L. Oldham, Khare D., Quiocho F.A., Davidson A.L., Chen J. Crystal structure of a catalytic intermediate of the maltose transporter. *Nature*. (2007). 450:515-521.
24. Chen J. Molecular mechanism of the Escherichia coli maltose transporter. *Curr Opin Struct Biol.* (2013). 23(4): 492-498.
25. Lewinson O., Lee A.T., Locher K.P., Rees D.C. A distinct mechanism for the ABC transporter BtuCD-F revealed by the dynamics of complex formation. *Nat Struct Mol Biol*. (2010). 17(3): 332-338.

26. Gerber S., Comellas-Bigler M., Goetz B.A., Locher K.P. Structural basis of trans-inhibition in a molybdate/tungstate ABC transporter. *Science.* (2008). 321(5886): 246-250.
27. Yang. J.G., Rees D.C. The allosteric regulatory mechanism of the *Escherichia coli* MetNI methionine ATP binding cassette (ABC) transporter. *Journal of Biological Chemistry.* 2015. 290(14): 9135-9140.
28. Gaudet R., Wiley D.C. Structure of the ABC ATPase domain of human TAP1, the transporter associated with antigen processing. *EMBO J.* (2001). 20(17):4964-4972.
29. Van der Heide T., Poolman B. Osmoregulated ABC-transport system of *Lactococcus lactis* senses water stress via changes in the physical state of the membrane. *Proc. Natl. Acad. Sci.* (2000). 97:7102-7106.
30. Kerpolla R.E., Shyamala V.K., Klebba P., Ames G.F. The membrane-bound proteins of periplasmic permeases form a complex. Identification of the histidine permease HisQMP complex. *J. Biol. Chem.* (1991). 266(15):9857-9865.
31. Van der Heide T., Poolman B. Osmoregulated ABC-transport system of *Lactococcus lactis* senses water stress via changes in the physical state of the membrane. *Proc. Natl. Acad. Sci.* (2000). 97:7102-7106.
32. Bordignon E., Grote M., Schneider E. The maltose ATP-binding cassette transporter in the 21st century – towards a structural dynamic perspective on its mode of action. *Mol Microbiol.* (2010). 77(6): 1354-1366.
33. Oldham M.L., Chen S., Chen J. Structural basis for substrate specificity in the *Escherichia coli* maltose transport system. *PNAS.* (2013). 110(45):18132-18137.
34. Locher K.P., Lee A.T., Rees D.C. The E. coli BtuCD structure: a framework for ABC transporter architecture and mechanism. *Science.* (2002). 296:1091-1098.
35. Cadieux N., Bradbeer C. Reeger-Schneider E. Köster W. Mohanty A.K., Wiener M.C., Kadner R.J. Identification of the periplasmic cobalamin-binding protein BtuF of *Escherichia coli. J. Bacteriol.* (2002). 706-717.
36. Matle D., Zeltina A., Woo J.S., Goetz B.A., Locher K.P. Two stacked heme molecules in the binding protein BtuF of *Escherichia coli. J. Mol. Biol.* (2010). 404:220-231.
37. Klein, J.S. & Lewinson, O. Bacterial ATP-driven transporters of transition metals: physiological roles, mechanisms of action, and roles in bacterial virulence. *Metallomics.* (2011). 3:1098-1108.
38. Thulasiraman P., Newton S.M., Xu J., Raymond K.N., Mai C., Hall A., Montague M.A., Klebba P.E. Selectivity of ferric enterobactin binding and cooperativity of transport in gram-negative bacteria. *J. Bacteriol.* (1998). 180:6689-6696.
39. Patzlaff J.S., Van der Heide T., Poolman B. The ATP/Substrate Stoichiometry of the ATP-binding cassette (ABC) transporter OpuA. *JBC.* (2003). 278(32): 29546-29551.
40. Lewinson O., Lee A.T., Locher K.P., Rees D.C. A distinct mechanism for the ABC transporter BtuCD-F revealed by the dynamics of complex formation. *Nat Struct Mol Biol*. (2010). 17(3): 332-338.
41. Srikant S., Gaudet R., Murray A.W. Selecting for altered substrate specificity reveals the evolutionary flexibility of ATP-binding cassette transporters. *Curr Biol.* (2020). 30(9): 1689-1702.
42. Vasiliou V., Vasiliou K., Nebert D.W. Human ATP-binding cassette (ABC) transporter family. *Human Genomics*. (2009). 3(3):281-290.
43. Jardetzky, O. Simple allosteric model for membrane pumps. *Nature (London)*. (1966). 211:969-970.
44. Bao H., Duong F. ATP alone triggers the outward-facing conformation of the maltose ATP-binding cassette transporter. *J. Biol. Chem.* (2013). 288(5): 3439-3448.
45. Bao H., Duong F. Discovery of an auto-regulation mechanism for the maltose ABC transporter $MalFGK_2$. *PloS One.* (2012). 7(4):34836.
46. Korkhov, V.M., Mireku S.A., Locher K.P. Structure of AMP-PNP-bound vitamin B12 transporter BtuCD-F. *Nature*. (2012). 490:367-372.
47. Lewinson O., Lee A.T., Locher K.P., Rees D.C. A distinct mechanism for the ABC transporter BtuCD-F revealed by the dynamics of complex formation. *Nat Struct Mol Biol*. (2010). 17(3): 332-338.
48. Hyde S.C., Emsley P., Hartshorn M.J., Higgins C.F. Structural modeling of ATP-binding protein associated with cystic fibrosis, multidrug resistance and bacterial transport. *Nature.* (1990). 346: 362-365.
49. Kadner R.J., Watson W.J. Methionine transport in Escherichia coli: physiological and genetic evidence for two uptake systems. *J Bacteriol.* (1974). 119(2):401-409.
50. Zogbhi M.E., Altenberg G.A. ATP binding to two sites is necessary for dimerization of nucleotide-binding domains of ABC transporters.
51. Fuhrman B.P., Zimmerman J.J. Pediatric Critical Care. *Elsevier*. (2011). 1058-1072.

52. Kadner R.J. Regulation of methionine transport activity in Escherichia coli. *J. Bacteriol.* (1975). 122(1):110-119.
53. Johnson E., Nguyen P.T., Yeates T.O., Rees D.C. Inward facing conformations of the MetNI methionine ABC transporter: Implications for the mechanism of transinhibition. *Protein Science*. (2012). 21(1): 84-96.
54. Nguyen P.T., Lai J.Y., Kaiser J.T., Rees D.C. Structures of the *Neisseria meningitides* methionine-binding protein MetQ in substrate-free form and bound to L- and D-methionine isomers. *Protein Science.* (2019). 28(10): 1750-1757.
55. Nguyen P.T., Li Q.W., Kadaba N.S., Lai J.Y., Yang J.G., Rees D.C. The contribution of methionine to the stability of the Escherichia coli MetNIQ ABC transporter – substrate binding protein complex. *Biol. Chem.* (2015). 396(9-10): 1127-1134.
56. Huang X. Fluorescence polarization competition assay: the range of resolvable inhibitor potency is limited by the affinity of the fluorescent ligand. J Biomol Screen 2003, 8, 34–38.

Chapter 2: Methods

2.1: Expression of MetNI and MetQ Proteins

Previously published plasmids were gifts from Douglas Rees (Caltech) and were expressed in *E. coli* BL21-Gold DE3 cells (Agilent). MetNI and MetQ constructs were transformed by mixing 25 µL of cells with 1 µL of the respective plasmid (~100 ng/µL) and incubated 10 min on ice. The cells were heat shocked for 20 seconds in a 42°C bath and cooled for two min on ice. Two hundred µL of LB (Lysogeny Broth) media were added before shaking at 225 rpm at 37°C for 30 min. Two hundred µL of cells were grown on agar plates with 200 µg/mL ampicillin at 37°C overnight.

Five mL starter cultures were made with LB media inoculated with a single colony of the transformed cells. Starter cultures contained 200 µg/mL of ampicillin and were left to grow overnight at 37°C and 225 rpm. Starter cultures were added to Fernbach flasks containing 1L of Terrific Broth media (24g/L yeast extract, 12 g/L tryptone, 72 mM K_2HPO_4, 17 mM KH_2PO_4 and 0.5% glycerol, autoclaved) with 100 µg/mL of ampicillin to begin large-scale growth. Large-scale growth was performed at 37°C and 180 rpm. To check for growth, the optical density at 600 nm was monitored by checking the optical density of 1 mL samples. Once the optical density reached a value of 2, the cells were induced with a final concentration of 1 mM IPTG for 1 hour. Cultures were pelleted by centrifuging at 13,500 rpm at 4°C using a Beckman Avanti J-25 I floor centrifuge and a JLA 16.25 rotor. Pellets were stored at -80°C until protein purification was performed.

2.2: Transformation of MetNI Double Mutants (Lm N295AE166Q Lu N295A & Lm N295A Lu N295A)

The procedure for the expression of MetNI double mutants were identical to that above but with minor modification. One hundred µL of *E. coli* BL21-Gold DE3 cells were transformed with 2 µL of both the Lm and Lu plasmids (~100 ng/µL). The mixture was set on ice for 10 min before being heat shocked for 20 seconds in a 42°C bath. The cells were then cooled on ice for 2 min before addition of 1 mL of SOC (Super Optimal broth with Catabolite repression) media and incubation at 37°C and 225 rpm for 1 hour. Two hundred µL of cells were plated onto an agar plate containing 200 µg/mL of ampicillin and kanamycin and left to grow overnight at 37°C.

2.3: Purification of MetNI

All strains of the MetNI transporter, as well as the MetQ SBP, were purified using an ÄKTA Pure FPLC System (GE Healthcare). The entire procedure was kept on ice or performed at 4°C unless noted otherwise. Fifteen g of cells were homogenized in 150 mL of MetNI buffer {50 mM

[tris(hydroxymethyl)methylamino]propanesulfonic acid (TAPS) pH 8.5, 250 mM NaCl, and 1% n-Dodecyl β-D-maltoside detergent (DDM; Anatrace)}. Deoxyribonuclease (10 µg/mL) (Sigma-Aldrich), lysozyme from bovine pancreas (10 µg/mL; Sigma-Aldrich), and PMSF (1µM) were added once the cells were homogenized in buffer. DDM detergent was added to a 1% mass-to-volume ratio (1.5g in 150 mL), not including the DDM present in the MetNI buffer, to the cell lysate.

The lysate was stirred for 20 min before sonication with a flat tip sonicator (Branson Ultrasonics Sonifier), on ice, at 20% bursts of 50 kHz for 45 seconds followed by 90 seconds of cooling for 7 cycles, for a total of 5 min and 15 seconds of sonication. The solution was then centrifuged at 19,000 rpm for 20 min in a Beckman Avanti J-25 I centrifuge and a JLA-20 rotor. Imidazole was added to the supernatant to a final concentration of 25 mM. The mixture was loaded onto a Ni-NTA HisTrap 5mL HP column (GE Healthcare) using MetNI buffer containing 25 mM imidazole at 2 mL/min as the mobile phase. The column was washed with MetNI buffer with 25 mM imidazole until the UV reading reached the baseline level at 280 nm, and the same processes were repeated for with MetNI buffer containing 75 mM imidazole. Protein was eluted with MetNI buffer containing 350 mM imidazole. The eluent was injected onto a HiPrep 26/10 Desalting column (GE Healthcare). Collected peak fractions (10-12 mL) were pooled and frozen in liquid nitrogen before storing at -80°C overnight.

Sixteen hours later, the eluent was centrifuged in 5 min intervals at 3500 rpm and concentrated to 5 mL or less with an Amicon Ultra-15 centricon tube with a 100 kD cutoff (Millipore) in an Eppendorf Centrifuge 5804R. The concentrated eluent was injected onto a Superdex 200 pg 16/600 sizing column (GE Healthcare). Peak fractions, appearing around 60 mL elution volume, were collected and added to a new Amicon Ultra-15 centricon tube with a 100 kD cutoff. The protein was centrifuged at 3500 rpm at 4°C until the protein reached a concentration between 10-20 mg/mL which was measured at 280 nm using an Implen Nanodrop N50. The absorbance was divided by the extinction coefficient of MetNI (83365 M^{-1} cm^{-1}) and multiplied by its molar mass (122034.85 g/mol) to determine the concentration in mg/mL.

2.4: Purification of MetNI Chimeras

The initial purification of MetNI chimeras followed the previous procedure for MetNI purification up to elution from the desalt column. From there, the method diverges with the goal of removing non-FLAG tagged MetNI transporters from the final product.

The eluent from the desalting column was loaded onto a 20-mL FLAG affinity column (Sigma-Aldrich). Once the UV peak from contaminant protein had passed through the column, an additional 30 mL of buffer was flowed through the column before the protein was eluted with 10 µg/mL FLAG peptide in MetNI buffer. To remove the FLAG peptide, the peak elute fractions were collected and concentrated from the FLAG affinity column in an Amicon Ultra-15 centricon tube with a 100 kD cutoff to less than 5 mL

before injecting the solution onto a Superdex 200 pg 16/600 sizing column (GE Healthcare). The peak eluted fractions were collected, concentrated in a separate Amicon Ultra-15 centricon tube with a 100 kD cutoff to a concentration close to 10 mg/mL before being flash frozen in liquid nitrogen and stored at -80°C.

2.5: Purification of MetQ

Eighteen grams of pelleted BL21 cells were homogenized (by hand, with a spatula) in 10 mL of 40 % sucrose, 1 mM EDTA, and 10 mM Tris pH 7.5 and then stirred at room temperature for 1 hour. The cells were then shocked by adding 500 mL of ice-cold deionized water. After stirring for 10 min at 4°C, buffer components were added to a final concentration of 25 mM Tris pH 7.5, 150 mM NaCl, 5 mM BME, and 17 mM imidazole. The resulting suspension was centrifuged at 15,817 rpm (37,500 x g) for 30 min. The lysate was loaded onto a 5 mL Ni-NTA column equilibrated in MetQ buffer (25 mM Tris pH 7.5, 150 mM NaCl, 5 mM BME). The column was washed with 10 column volumes of MetQ buffer with 17 mM imidazole. The protein was eluted with MetQ buffer containing 400 mM imidazole. The pooled fractions were injected onto a HiPrep 26/10 Desalting column previously equilibrated with MetQ buffer. The peak fractions were pooled and frozen in liquid nitrogen and stored at -80°C overnight.

Sixteen hours later, the pooled fractions were concentrated in an Amicon Ultra-15 centricon tube with a 10 kD cutoff until the volume was at or below 5 mL. The concentrated protein solution was then injected onto a Superdex 200 pg 16/600 sizing column. Peak fractions were collected (elution volume ~9 mL) and concentrated in an Amicon Ultra-15 centricon tube with a 10 kD cutoff until the concentration was 10 mg/mL. To calculate protein concentration, the absorbance was recorded at 280 nm with an Implen Nanodrop N50. To convert the concentration into mg/mL, the absorbance was divided by the extinction coefficient for MetQ (20400 M^{-1} cm^{-1}) and multiplied by the molar mass (29431.65 g/mol).

2.6: SDS-PAGE of Purification Process

Samples collected throughout the MetQ and MetNI purification process were analyzed for their protein content via SDS-PAGE. The samples collected for the gel were the lysate, pellet, and supernatant before injection onto the Ni-NTA column plus the flow-through, wash, and eluent solutions from the Ni-NTA column and finally the desalt and sizing elutions. All samples prepared for the gel had a final volume of 24 μL, where 12 μL of each sample was 2x loading buffer (4% SDS, 100 mM Tris-HCl, 20% glycerol, 0.2% bromophenol blue, 200 mM dithiothreitol) and the other 12 μL of the gel sample contained different ratios of the collected sample with its corresponding buffer depending on the sample (MetNI buffer for a MetNI purification analysis, MetQ buffer for a MetQ purification analysis). For the lysate, pellet, and sizing eluent samples, one μL of the final sample volume was the eluent while the remaining 11 μL of the sample was buffer solution. For the supernatant, flow-through, wash, Ni-NTA, and desalt eluent samples, 12 μL of

each sample was added to each SDS-Page sample prep. After the preparation of each sample, the samples incubated at 95ºC for 5 min before loading.

Ten µL of every prepared sample and a protein ladder (Bio-Rad) were loaded into separate wells of a Mini-Protean TGX gel (Bio-Rad). The gel was placed into a gel box and filled with 1x SDS running buffer (1 g/L sodium-dodecyl-sulfate, 3 g/L Tris (hydroxymethyl) aminomethane, 14.4 g/L glycine). The gel was run at 200 volts for 30 min. The gel was then placed into a container with Coomassie Blue staining solution (40% methanol, 10% acetic acid, 1g/L brilliant Coomassie blue staining powder) for 30 min with agitation. The Coomassie stain was removed, and destaining solution was added (40% methanol, 10% acetic acid) before the gel was agitated for an hour. The gel was then removed from the destaining solution and imaged using a ChemiDoc MP (BioRad).

2.7: ATPase assays

To measure the rate of ATP hydrolysis, a commercially available coupled enzyme system was utilized (Enzchek Phosphate Assay Kit, Invitrogen). In the presence of free phosphate, the enzyme purine nucleoside (PNP) converts the substrate 2-amino-6-mercapto-7-methylpurine riboside (MESG) into free 2-amino-6-mercapto-7-methylpurine, which absorbs light at 360 nm.

To convert the measured absorbance to concentration of P_i, phosphate standard curves were generated. A phosphate standard curve was prepared with 100 µL wells containing P_i concentrations of 500 µM, 250 µM, 100 µM, 50 µM, 10 µM, and 0 µM. Each reaction contained 55 mM Tris pH 7.5, 5 mM TAPS pH 8.5, 0.055% DDM, 55 mM NaCl, 1 mM BME, 5 mM $MgCl_2$, 200 µM MESG, 300 nM MetNI and 1U per reaction of PNP. A best-fit line of the data provided a reliable constant to convert AU to concentration of P_i.

To measure the ATPase activity of MetNI, 90 µL reactions were prepared in a Greiner black-clear bottom 96-well plate for absorbance measurement in a Tecan Infinite 200 plate reader. Ten µL of 50 mM $MgCl_2$ was injected into each well to initiate the reaction, and the absorbance at 360 nm was recorded every 20 seconds for a total of 500 seconds. The final buffer condition for each sample was identical to samples of the phosphate standard assay. Plots of AU vs. time (seconds) were graphed and the region with the steadiest linear trend (usually from 300s-500s) were analyzed to find the change in AU/sec. This slope was converted to find k_{obs}, or ATP hydrolyzed/minute per transporter, using the equation

$$\frac{AU}{sec} * \frac{M\ Pi}{AU} * \frac{60\ sec}{1\ min} * \frac{1}{3*10^{-7}\ M\ Met\ NI} = \frac{P_i}{min*MetNI} \qquad \text{(Equation 1)}$$

where the M Pi/AU component of this equation is the slope from the phosphate standard curve.

Plots of k_{obs} versus the concentration of ATP were fit to the following equation

$$k_{obs} = \frac{k_{cat}*[ATP]^n}{K_m^n+[ATP]^n} \quad \text{(Equation 2)}$$

where k_{cat} is the catalytic rate constant for ATP hydrolysis, K_m is the concentration of ATP at which ATPase activity equals half of k_{cat}, and n is the Hill coefficient. In this system, K_m (or Michaelis constant) is a measure of the affinity of MetNI for ATP, and the Hill coefficient is a measure of the cooperativity of ATPase activity between the two nucleotide binding sites.

ATPase assays to determine the affinity of L-Met for the C2 inhibitory domains of MetNI were performed as above except ATP was kept constant at 5 mM ATP while L-Met varied from 0 mM to 5 mM. Data from ATPase assays were fit to the equation

$$k_{obs} = \frac{k_{cat}}{(1+\frac{[L-Met]^n}{K_i{}^n})} \quad \text{(Equation 3)}$$

where K_i (the inihibition constant) is the concentration of L-Met at which k_{obs} is half of k_{cat}, and n is the Hill coefficient for the cooperativity of L-Met binding. All data fitting was conducted using Prism Version 7 software.

2.8: MetQ Labeling

This procedure largely follows that offered by Thermo Fisher; the manufacturer of the fluorescent dye used in the procedure (fluorescein 5-maleimide). One mL of ~10 mg/mL purified MetQ was injected onto a 5-mL HP Desalting column equilibrated in labeling buffer (25 mM Tris pH 7.0, 150 mM NaCl, 5 mM EDTA, 10 mM TCEP). Peak fractions were pooled, and labeling buffer was added for a final concentration of MetQ between 30-40 µM. Solid fluorescein 5-maleimide (FW = 427 kD, Thermo Fisher) was added to a final concentration of 1 mM (25x the molar ratio of MetQ). The solution was continuously inverted at room temperature for 2 hours. The labeling reaction was then quenched by adding beta-mercaptoethanol to a final concentration of 100 mM (FW = 78 g/mol, Bio-Rad) and inverted at room temperature for an additional 15 min. Next, the solution was injected onto a TALON 2-mL disposable gravity column with 200 µL of Ni-NTA (Qiagen) beads that had been previously equilibrated with MetQ buffer. The column was washed with 10 mL of MetQ buffer before elution with MetQ buffer containing 400 mM imidazole. The eluted protein was injected onto a 5 mL HP Desalting column previously equilibrated with MetQ buffer. The peak fractions were collected and pooled together. The labeling efficiency was determined using the equation

$$\frac{A_{494}}{\varepsilon} * \frac{MW\ of\ protein}{\frac{mg\ protein}{mL}} = \frac{moles\ of\ dye}{moles\ of\ protein} \quad \text{(Equation 4)}$$

in which A_{494} is the absorbance of the solution at 494 nm (peak absorbance wavelength of fluorescein 5-maleimide), ε is the extinction coefficient of fluorescein 5-maleimide (90,000 M^{-1} cm^{-1}), MW is 29431.65 g/mol (molar mass of MetQ), and mg protein/mL is the measured concentration of MetQ.

2.9: Anisotropy to Determine K_d of MetQ - MetNI In the Presence of ATP

A detailed step-by-step procedure for this section can be found in the Appendix.

Purified MetNI and a 1:5 dilution of purified maleimide-labeled MetQ (diluted with MetQ buffer) were separately spun at 90,000 rpm for 20 min at 4°C using an Optima TLX Ultracentrifuge in a TLA-100 rotor to remove any aggregates (Beckman). Following centrifugation, the concentration of each protein was determined by measuring the absorbance at 280 nm. 25 µL solutions were prepared on ice with final concentrations of 3 mM ATP, 3 mM EDTA, 0.06% DDM, 150 mM NaCl, 57.5 mM Tris pH 7.5, and 10 mM TAPS pH 8.5.

For MetQ N229A – MetNI E166Q experiments, the final concentration of MetNI E166Q varied from 0 – 10 µM. For MetQ WT – MetNI E166Q experiments, final concentrations of MetNI E166Q varied from 0 – 20 µM.

Once reaction mixtures were prepared on ice, 20 µL of each solution were transferred to a black-clear bottom Greiner 384-well plate. The solutions were placed in the Spectramax Gemini plate reader preset to 37°C for 10 min. After incubation, fluorescence polarization (FP) values were recorded with the sensitivity of the sensor set to high.

FP values and their corresponding MetNI concentrations were plotted and analyzed using Prism. First, relative B_{min}, B_{max}, and K_d values were determined using the equation

$$FP = \frac{B_{max} * [MetNI]}{K_d + [MetNI]} + B_{min} \quad \text{(Equation 5)}$$

in which FP is the recorded fluorescence polarization value, B_{max} is the maximum FP asymptote, B_{min} is the minimum FP asymptote, and K_d is the MetNI concentration at which 50% of the maximum change in FP has been reached.

FP values were then converted to fraction bound using the equation

$$fraction\ bound = \frac{FP - B_{min}}{B_{max}} \quad \text{(Equation 6)}$$

Fraction bound values were then plotted as a function of MetNI concentration and fit to the equation

$$fraction\ bound = \frac{[MetNI]}{K_d + [MetNI]} \quad \text{(Equation 7)}$$

with fraction bound values produced by calculations using Equation 6, and K_d representing the concentration of MetNI at which fraction bound is equal to 50%.

2.10: Using Fluorescence Anisotropy to Determine K_d of L-Met to MetQ N229A - MetNI E166Q Complex

The procedure to determine the K_d of L-Met for the MetQ N229A – MetNI E166Q complex was nearly identical to determining the K_d of MetQ – MetNI in the presence of ATP with a few changes. Instead of varying the concentration of MetNI, each reaction contained 5 μM MetNI E166Q and 20 nM MetQ N229A. The concentration of L-Met varied from 0 – 20 μM. The equation to calculate B_{min}, K_d, and B_{max} was modified to

$$FP = B_{max} - \frac{B_{max} * [MetNI]}{K_d + [MetNI]} + B_{min} \quad \text{(Equation 8)}$$

The fraction bound equation changed as well. This equation follows Equation 7 with the exception that as MetNI increases, the fraction of bound MetQ decreases, resulting in Equation 9.

$$fraction\ bound = 1 - \frac{[MetNI]}{K_d + [MetNI]} \quad \text{(Equation 9)}$$

Chapter 3: Results

3.1: Protein Expression and Purification

In any biochemical project, significant quantities of protein must first be expressed and purified. While the results below were mainly generated using published protocols (see references 1-5), the complexity of the multi-day procedures warrant a detailed explanation and analysis, which is provided below.

3.1.1: MetNI Expression

The plasmids utilized for MetNI expression contained both the MetI and MetN genes, with a ten-histidine residue (10xHis) tag engineered at the N-terminus of the MetN. The 10xHis tag allowed for the purification of MetNI protein via immobilized nickel affinity chromatography. To express MetNI, BL21 *E. coli* cells, known for their ability to express large amounts of exogenous proteins, were transformed with plasmids via standard protocols. Large-scale growths in Terrific Broth (TB) media were induced with IPTG (isopropyl β-D-1-thiogalactopyranoside) and harvested for subsequent purification.

3.1.2: MetNI Purification

Routine purifications starting with 15 grams of BL21 cell pellets yielded 20-30 mg of purified MetNI protein on average. Multiple runs were performed to provide the amount of protein necessary for ATPase assays and anisotropy experiments.

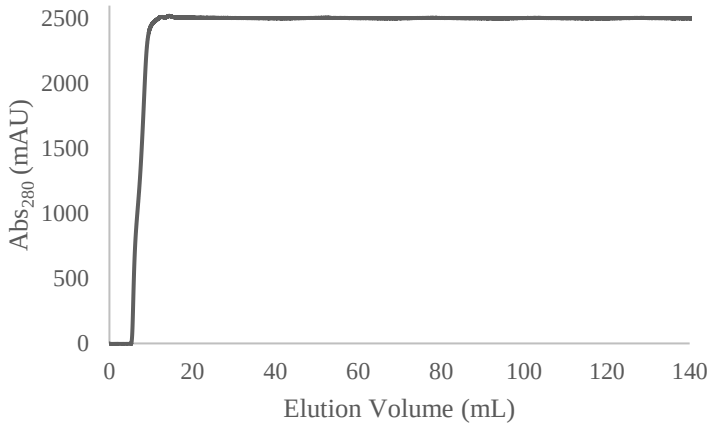

Figure 3-1: Loading of protein supernatant onto a nickel affinity column. Clarified cell lysate containing overexpressed MetNI was loaded onto a HisTrap HP 5-mL column.

Since MetNI is a membrane-embedded protein, detergent was necessary to extract the protein from the lipid environment. To solubilize MetNI, n-dodecyl β-D maltoside (DDM) was added to the MetNI buffer (50 mM[tris(hydroxymethyl)methylamino]propanesulfonic acid)

(TAPS) pH 8.5, 250 mM NaCl, and 0.05% n-Dodecyl β-D-maltoside (DDM) to a final concentration of 1% (w/v). Clarified cell lysate was applied to a HisTrap nickel affinity column to purify His-tagged MetNI (GE Healthcare). The eluent had a high absorbance (~2500 mAU), from non-His-tagged (Fig. 3-1). Next, buffer containing 25 mM imidazole was used to wash away non-specific proteins bound to the column, followed by a second wash using 75 mM imidazole. A small amount of non-specific contaminant protein was removed from the column in these wash steps, as seen in the spike in absorbance that occurs when the elution volume reaches ~90 mL in Fig. 3-2. Finally, MetNI was eluted from the resin using buffer containing 350 mM imidazole. The imidazole, present at high concentrations, competed with and displaced the 10xHis tag, thereby promoting the elution of MetNI. Imidazole, when present at high concentrations (250 mM or higher), outcompetes His-tagged protein for the nickel-resin beads, eluting the protein from the column.[6]

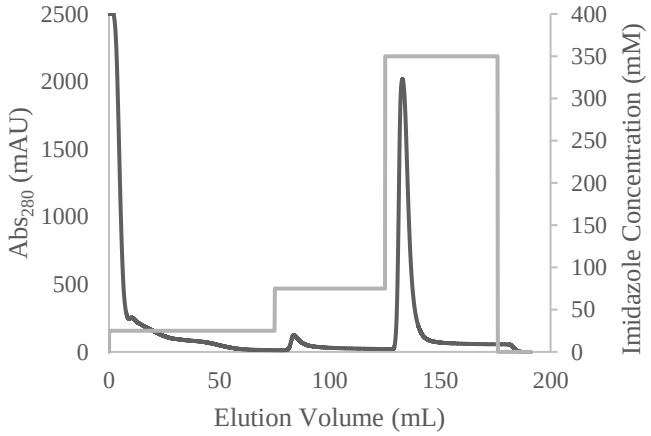

Figure 3-2: Washing and elution of MetNI protein from affinity column. The dark trace indicates the absorbance at 280 nm, and the light trace indicates the imidazole concentration.

The resulting eluent (consisting mostly of MetNI) was injected onto a desalting column (HiPrep 26/10, GE Healthcare) to remove imidazole from the buffer. This step was crucial, as excess imidazole can cause the protein to precipitate out of solution over time. Figure 3-3 plots the eluent's conductivity and absorbance at 280 nm versus the elution volume. In the figure, a dip in conductivity occurred as the protein eluted from the column, and later a sharp increase in conductivity occurred at approximately one column volume (52 mL) as the imidazole exited the column.

The final stage of purification involved injection of the eluent from the desalting column onto a size exclusion column (HiLoad 16/600 Superdex pg 200, GE Healthcare). In Figure 3-4, a small peak of aggregated protein appeared at the void volume,

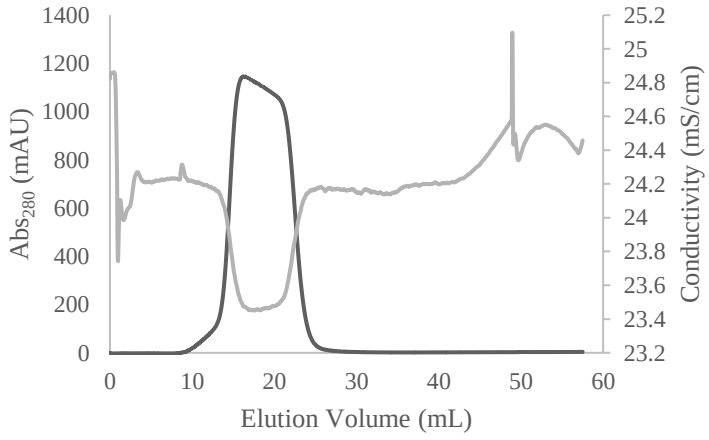

Figure 3-3: Removal of imidazole from MetNI eluent. The collected eluent from the 5-mL HP HisTrap column was injected onto a HiPrep 26/10 desalting column. The dark trace depicts the absorbance at 280 nm while the light trace indicates conductivity.

45 mL. The large monodisperse peak at 60 mL is the desired MetNI transporter with a molecular weight of 122 kD.

To analyze the purity of the final product, as well as analyze the efficacy of each step of the purification process, SDS-PAGE was performed. Figure 3-5 shows a gel containing different samples taken during the MetNI purification process. Lane 1 is a molecular weight standard ladder. Lane 2 is the cell lysate following homogenization of the cell pellet in MetNI buffer and 1% w/v DDM. Lane 3 is the pellet of insoluble cellular material obtained via centrifugation, and lane 4 is the supernatant which contained solubilized proteins. Lane 5 is the flow-through obtained from application of the supernatant over the HisTrap column. Lane 6 is the wash collected using MetNI buffer containing 25 mM imidazole, and lane 7 is the wash collected using MetNI buffer containing 75 mM imidazole. Lane 8 is the eluent collected when flowing buffer containing 350 mM imidazole through the HisTrap column. Lane 9 is the eluent collected following injection of the HisTrap eluent onto the HiPrep 26/10 desalting column. Lane 10 is the eluent following injection of the desalted eluent onto the HiLoad 16/600 Superdex pg 200 size exclusion column.

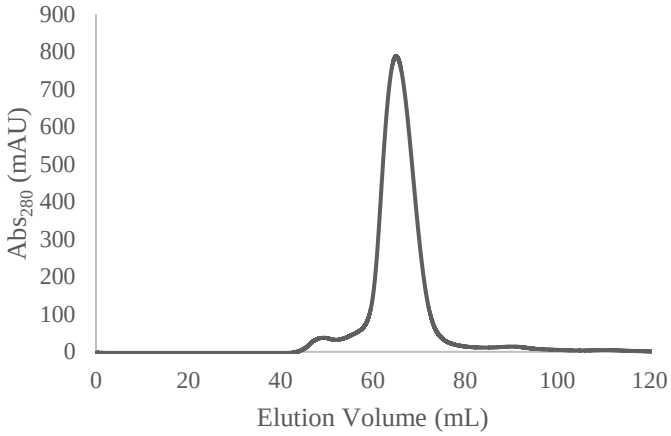

Figure 3-4: Size exclusion chromatography of MetNI. The collected eluent from the desalting column was concentrated to 5 mL before injection onto a HiLoad 16/600 Superdex pg 200 column.

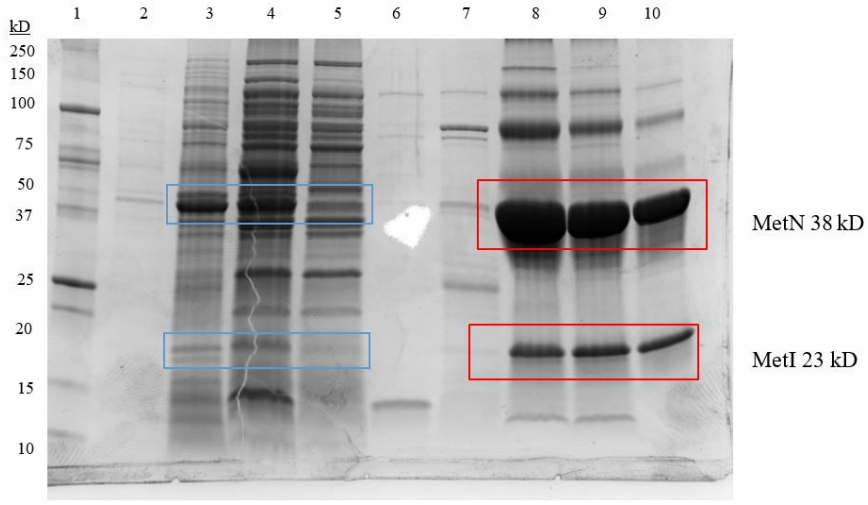

Lane 1: Standard ladder
Lane 2: Cell lysate
Lane 3: Insoluble cell pellet
Lane 4: Solubilized cell supernatant
Lane 5: His-Trap flow-through
Lane 6: 25 mM imidazole wash
Lane 7: 75 mM imidazole wash
Lane 8: 350 mM imidazole eluent
Lane 9: Desalt chromatography eluent
Lane 10: Sizing chromatography eluent

Figure 3-5: SDS-PAGE analysis of the MetNI purification procedure.

Outlined in blue boxes in Figure 3-5 are the dissociated MetN and the MetI portions of the transporter. In lanes 3 and 4 (samples of cell pellet and cell lysate, respectively) the MetN and MetI bands are enriched relative to other proteins, indicating a high level of expression. A considerable amount of MetNI is found in the pellet following centrifugation (Lane 4), indicating that some protein remained in the membrane. In lane 5 (HisTrap flow-through) the bands are noticeably lighter, indicating successful retention of MetNI on the nickel resin. In subsequent purification steps, the MetN and MetI bands outlined in red become more prominent, indicating a higher concentration of MetNI compared to contaminating proteins. While the intensity of the transporter bands remains consistent across lanes 8-10, the presence of contaminating proteins decreases as shown by the fading of the non-MetNI bands in each successive lane. The final purified MetNI sample shown in lane 10 contains minimal amounts of contaminants and is appropriate for use in subsequent assays.

3.1.3: MetQ Expression

The plasmids utilized for MetQ expression contained MetQ gene followed by a six-histidine residue (6xHis) tag engineered at the C-terminus. The 6xHis tag allowed for the purification of MetQ protein via immobilized nickel affinity chromatography. Similar to MetNI expression, BL21 *E. coli* cells were transformed with plasmids via standard protocols.[3]

The protocol for large-scale expression of the MetQ substrate binding protein was modified to increase yield. Previously, MetQ was expressed in autoinduction media, a method made popular due to its ease of use.[5] After numerous purification runs yielding low amounts of MetQ (1-3 mg per 18 g of cells), MetQ expression was tested in TB media. SDS-PAGE analysis revealed a significant difference in expression levels depending on growth media, as seen in Figure 3-6. Lane 1 is a molecular weight standard ladder. Lane 2 contains cellular lysate from cells grown in autoinduction media, while lanes 3 and 4 contain lysate from two separate growths using TB media. While less total cell lysate is loaded in lane 2, there is an unambiguous increase in MetQ expression relative to other proteins in lanes 3 and 4. As a result of this increased expression, subsequent purifications resulted in approximately 10-fold higher yield of MetQ, as described below.

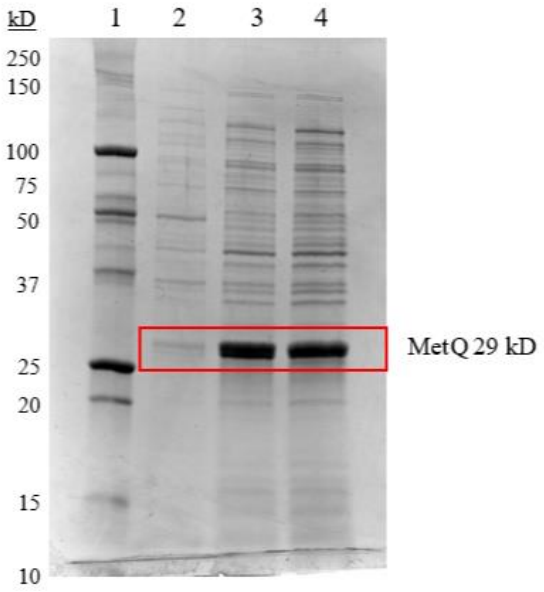

Lane 1: Standard ladder

Lane 2: MetQ expressed in autoinduction media

Lanes 3 & 4: MetQ expressed in TB broth

Figure 3-6: SDS-PAGE of cell lysate from different cell growth protocols.

3.1.4: MetQ Purification

Much of the MetQ purification procedure followed that of the MetNI purification procedure with a set of modifications. The chromatograms of the purification procedure (nickel-affinity chromatography, desalt chromatography, and size-exclusion chromatography can be viewed in Figures 3-7 to 3-10 with an SDS-PAGE analysis in Fig 3-11. Each chromatogram is described in greater detail throughout this section.

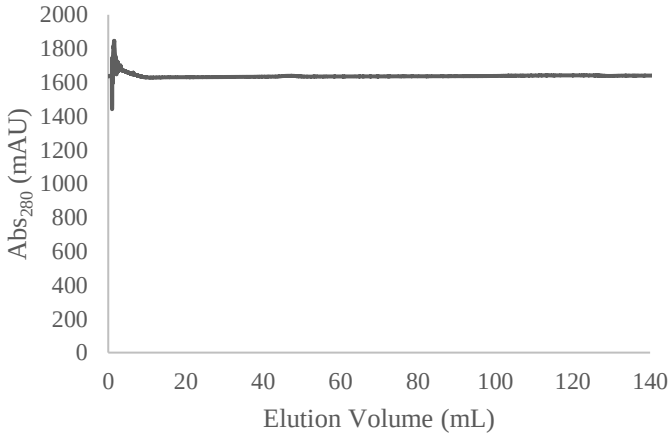

Figure 3-7: Loading of periplasmic extract onto nickel affinity column. Periplasmic extract containing overexpressed MetQ was loaded onto a 5-mL HisTrap HP column.

The purification of MetQ required different considerations than that of MetNI, because MetQ is a soluble protein, so detergent was not necessary, and MetQ contains a cysteine residue near the N-terminus that can lead to non-physiological, *in vitro* dimerization under non-reducing conditions. This concern pertains to MetQ in a purely artificial environment as cellular conditions are reducing and prevent *in vivo* dimerization from occurring. To prevent artificial dimerization, the reducing agent beta-mercaptoethanol (BME) was added to all buffers utilized in purification. Lastly, the periplasmic localization of MetQ necessitated a significant modification to the purification protocol. MetQ is produced by ribosomes in the cytoplasm of the cell. To target MetQ to the periplasm, a signal sequence on the nascent polypeptide chain is recognized by specialized cellular machinery. MetQ is then shuttled to the inner membrane of the bacteria and is eventually threaded through the membrane into the periplasmic space. Once inside the periplasm, the signal sequence is cleaved from MetQ. The signal-sequence-containing MetQ and cleaved MetQ are regarded as the immature and mature forms, respectively. As a consequence of over-expression, the targeting and cleavage machinery of the cell can be overwhelmed, leading to increased amounts of immature MetQ relative to mature MetQ. As mature MetQ is the species responsible for transport of L-methionine, it was important to isolate only mature MetQ for biochemical studies. To obtain mature MetQ, an osmotic shock procedure was employed to lyse only the outer membrane of the *E.coli* cells, as described below.

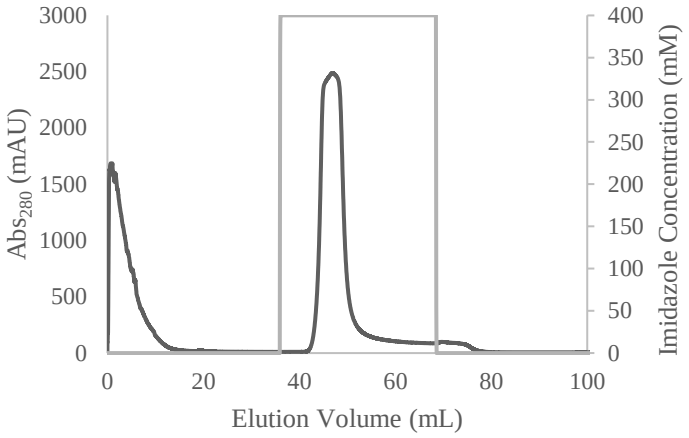

Figure 3-8: Washing and elution of MetQ protein from affinity column. The dark trace indicates the absorbance at 280 nm and the light trace depicts the imidazole concentration.

Cell pellets were first homogenized in a small volume of high concentration of sucrose (2 grams / mL). This slurry of cells was then mixed with 30 times the volume of deionized water, triggering lysis of the outer

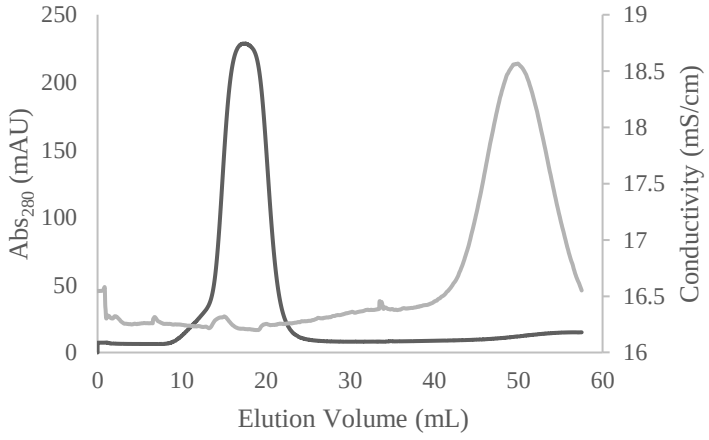

Figure 3-9: Removal of imidazole from MetQ eluent. The eluent collected from the 5-mL HisTrap column was loaded onto a HiPrep 26/10 desalting column. The dark trace indicates the absorbance at 280 nm, and the light trace indicates the conductivity.

membrane only. This was followed by the addition of Tris (50 mM final pH 7.5), sodium chloride (150 mM final), and BME (5 mM final). Following osmotic shock, much of the MetQ purification procedure using chromatography was similar to that of MetNI (Figs. 3-6 through 3-10). The osmotic shock solution was centrifuged to separate non-periplasmic components from the periplasmic lysate (lanes 3 and 4). The periplasmic lysate was loaded onto a HisTrap column, and the flow-through was collected (Fig. 3-7 and Fig. 3-11, lane 5). Due to the lower affinity of 6xHis-MetQ for the nickel-resin beads, the multiple wash steps used in MetNI purification were omitted (Fig. 3-8). Bypassing these washes resulted in a significant amount of contaminating proteins in the HisTrap eluent, as seen in lane 7 of Figure 3-11. Size exclusion chromatography of the desalted eluent, shown in Fig 3-10, revealed the presence of two different MetQ populations at 55 mL and 90 mL elution volumes. Based on the molecular weight of MetQ, the peak at 90 mL corresponds with a monomer of MetQ, whereas the peak at 55 mL was unexpected. To investigate the composition of the peak at 55 mL, SDS-PAGE was performed using samples from both peaks (Fig. 3-11). Lane 1 is a protein ladder, lane 2 is the cellular preparation following osmotic shock, lane 3 is the cell pellet following centrifugation. Lane 4 is the periplasmic extract, and Lane 5 is a sample of the flow-through from the 5-mL HisTrap HP column. Lane 6 is a sample of the following wash with MetQ buffer with 0 mM imidazole. Lane 7 is a sample of the eluted protein collected when flowing MetQ buffer with 400 mM imidazole. Lane 8 contains sample that overflowed from Lane 7. Lane 9 is a sample of the eluted protein following injection to the desalting column. Lane 10 is a sample of the first peak (55 mL) eluted from the sizing column. Lane 11 is the second peak (90 mL) eluted from the sizing column.

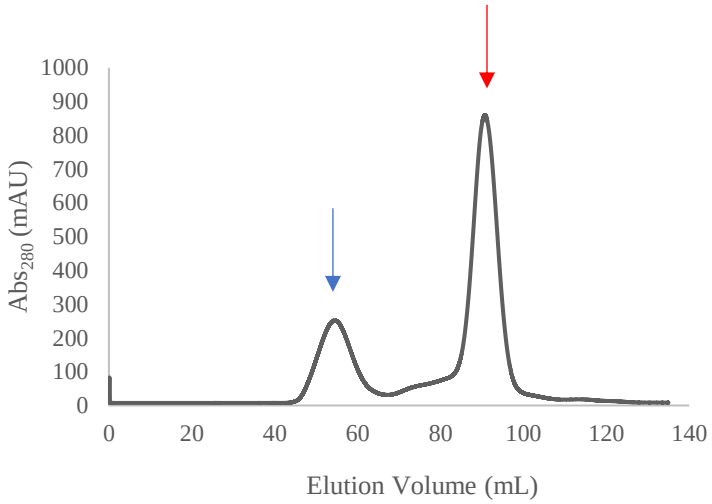

Figure 3-10: Size-exclusion chromatography of MetQ. The eluent collected from the desalt column was concentrated to 5 mL before injection onto a HiLoad 16/600 Superdex pg 200 column. The peak indicated by the blue arrow is immature MetQ. The peak indicated by the red arrow is mature MetQ.

The conclusion from SDS-PAGE analysis was that the protein in the 55 mL peak was slightly larger than the protein in the 90 mL MetQ (Fig. 3-11, blue and red arrows, respectively). One explanation for the is that the 55 mL peak contained immature MetQ, which is slightly larger than mature MetQ due to its uncleaved signal sequence. The hydrophobic nature of the signal sequence in immature MetQ may have caused aggregation of this species, resulting in a distinct peak at 55 mL that is noticeably smaller than that of the mature MetQ peak at 90 mL. This observation suggests that some of the inner membrane may have

lysed despite the osmotic shock procedure. Eighteen g of BL21 cells gave a final sample of reasonable purity and yielded 20-30 mg of purified MetQ protein.

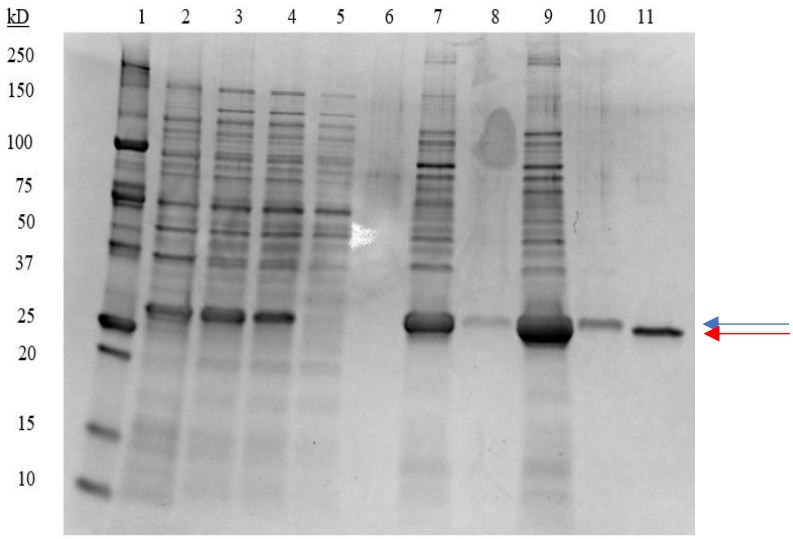

Lane 1: Standard ladder
Lane 2: Cell lysate following osmotic shock
Lane 3: Insoluble cell pellet
Lane 4: Solubilized periplasmic extract
Lane 5: His-Trap flow-through
Lane 6: 0 mM imidazole wash
Lane 7: 400 mM imidazole eluent
Lane 8: Overflow from Lane 7
Lane 9: Desalt chromatography eluent
Lane 10: Sizing chromatography peak 1 (immature MetQ)
Lane 11: Sizing chromatography peak 2 (mature MetQ)

Figure 3-11: SDS-PAGE analysis of MetQ purification procedure. The blue and red arrows identify immature and mature MetQ, respectively.

3.2: Effect of Single Amino Acid Substitutions in MetNI

In this work, we utilized a well-established ATPase assay to verify the activity of wild-type MetNI and to analyze the effect of single amino acid mutations in MetNI. This solution-based, real-time assay is commonly utilized to accurately determine the ATP hydrolysis rate of an enzyme. The protocol was modified to a plate reader format, and 10-12 individual reaction conditions could be tested simultaneously. Briefly, in this coupled enzyme system, purine nucleoside phosphorylase (PNP) catalyzes a reaction between inorganic phosphate and 2-amino-6-mercapto-7-methyl purine riboside (MESG) (Fig. 3-12).[7] A standard curve (see Fig 3-13) was generated by measuring the amount of product, 2-amino-6-mercapto-7-methyl purine, which has a 1:1 ratio with inorganic phosphate (reaction depicted in Fig. 3-12). 2-amino-6-mercapto-7-methyl purine absorbs light at 360 nm, and thus the absorbance at 360 nm is used as a measure of inorganic phosphate concentration, directly quantifying the amount of ATP hydrolysis in a solution.

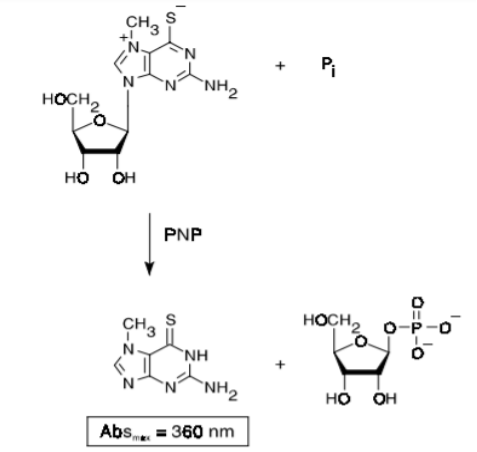

Figure 3-12: Schematic of the coupled-enzyme reaction for the Enzchek Phosphate Assay kit. Image taken directly from ThermoFisher.[6]

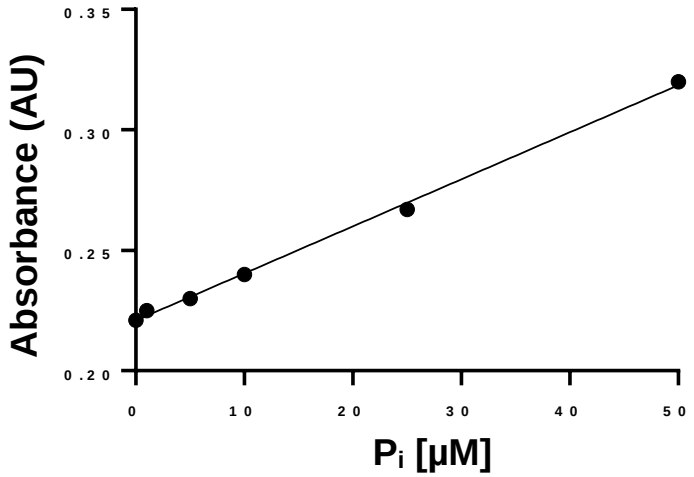

Figure 3-13: Standard curve for conversion of absorbance to concentration of inorganic phosphate. The equation for the best-fit line was y = 0.00195x + 0.2209 with an R^2 value of 0.9956.

The raw data from a representative experiment is shown in Figure 3-14. In this particular assay, the concentration of ATP was varied, and thus the absorbance at t = 0 varied between samples. ATP hydrolysis requires the presence of Mg^{2+} ion, and a final concentration of 5.5 mM $MgCl_2$ was injected into each sample at t = 120 seconds to start the reaction. 27 To determine the rate of ATP hydrolysis, the time points from 300-500 seconds were fit to a straight line. This time range provided the most reproducible data, as earlier and later time points often showed non-linear trends or leveling off of the absorbance value, respectively. The slope from the raw data was then converted into the observed rate constant (k_{obs}) using the conversion factor provided from the standard curve. Using this assay, the basic kinetic parameters, including $k_{cat,}$ K_m, and the Hill coefficient (n), were determined for MetNI.

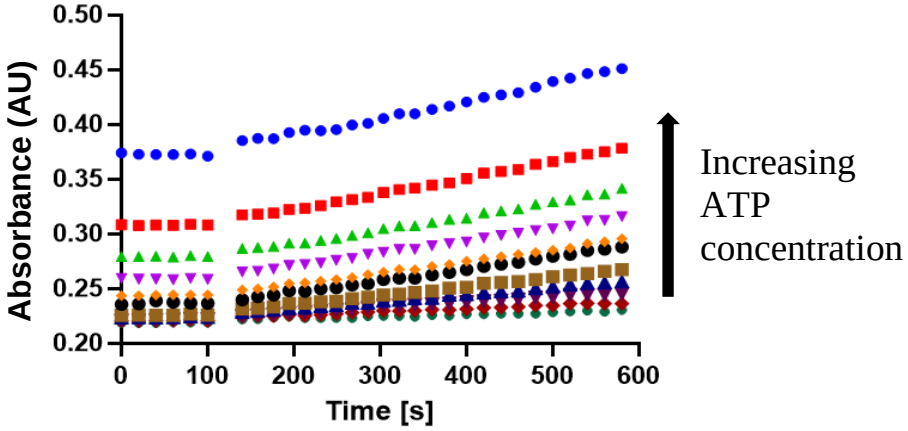

Figure 3-14: Raw data of MetNI ATPase assay with varying concentrations of ATP. Final concentrations of ATP varied from 0 – 5 mM ATP. A final concentration of 5.5 mM Mg^{2+} was injected at time = 120 seconds, allowing ATP hydrolysis to begin.

3.2.1 ATPase Activity of Wild-Type MetNI

First, to verify the quality of the protein resulting from the purification process, experiments using wild-type MetNI with varying ATP concentrations were performed and compared to published data (Fig. 3-15). Data were fit to a modified Michaelis-Menten equation:

$$k_{obs} = \frac{k_{cat} * [ATP]^n}{K_m + [ATP]^n}$$

where k_{obs} is the observed rate constant, k_{cat}, is the catalytic rate constant, n is the Hill coefficient, and K_m is the Michaelis-Menten constant.

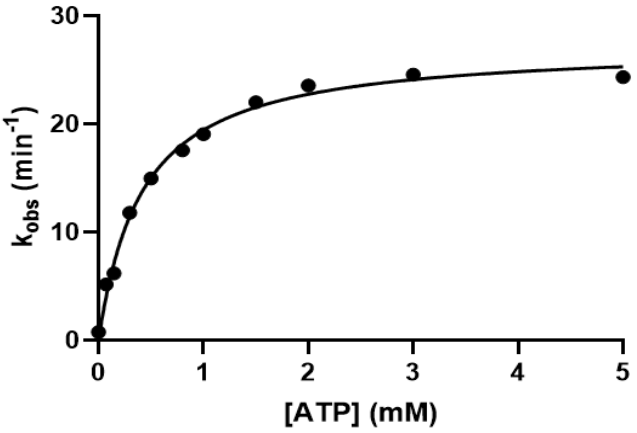

Figure 3-15: ATPase assay of wild-type MetNI in varying ATP concentrations. Best-fit parameters are k_{cat} = 30 ± 3 min^{-1}, K_mATP = 320 ± 120 µM , n = 0.9 ± 0.2.

As expected, ATP hydrolysis increased as a function of ATP concentration. The best-fit K_mATP value was 320 ± 120 µM, which is in good agreement with previously published work in which K_m = 330 ± 20 µM. In published work, experiments were performed at 33°C, while these assays were conducted at 37°C.[8] This could explain the significant difference between the catalytic rate constant determined here, k_{cat} = 30 ± 3 min^{-1} and the published k_{cat} value of 17 ± 1 min^{-1}. Surprisingly, our results little cooperativity based upon the Hill coefficient of 0.9 ± 0.2, while published data report that n = 1.7 ± 0.1. As a guiding principle, a Hill coefficient of 0 signifies negative cooperativity between the two ATP binding sites, a coefficient of 1 indicates no cooperativity, and a cooperativity of 2 signals positive cooperativity between the binding sites. To confirm these preliminary results, further experimentation with lower concentrations of ATP should be performed. Given the consistent values for k_{cat} and K_m, we concluded that the protein purification process yielded MetNI with sufficient specific activity.

Next, to verify the transinhibitory regulation of MetNI, ATPase activity was measured as a function of L-methionine concentration. As expected, the hydrolysis rate decreased as concentrations of L-methionine increased (Fig. 3-16). In this assay, at saturating concentrations of ATP, the ATPase activity decreases and approaches zero. The K_i(L-Met) value was 41 ± 13 μM, in good agreement with previous studies (41 ± 2 μM).[7] This corresponds with the elegant *in vivo* observations from nearly 50 years ago, which showed that high cellular concentrations of L-methionine inhibit further import. Thus, L-methionine acts as both a substrate and inhibitor.

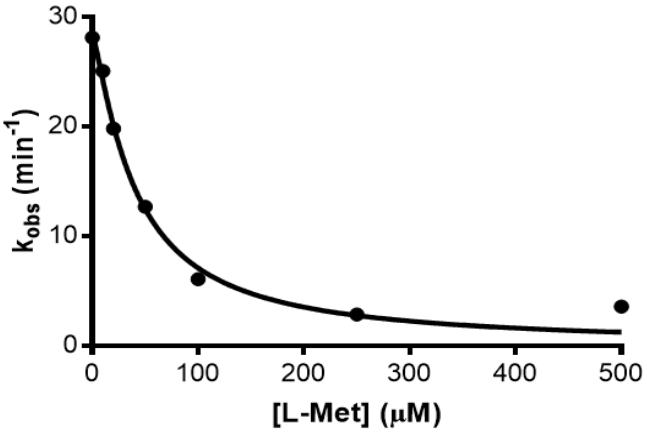

Figure 3-16: L-Met inhibits MetNI wild-type ATPase activity. Best fit parameters are K_i = 41 ± 13 μM, n = 1.2 ± 0.2, and k_{cat} = 28.5 ± 2.5 min^{-1}.

3.2.2 Confirmation of the Loss of ATP Hydrolysis in MetNI E166Q Mutant

To trap an intermediate ATP-bound state of MetNI, a canonical single amino acid substitution was employed. A glutamate to glutamine substitution in the Walker B motif of the NBDs allows the binding of ATP but impairs hydrolysis. By eliminating the negative charge on the side chain, the residue no longer acts as a general base, thereby reducing polarization of the water molecule involved in ATP hydrolysis. Kadaba et. al. first introduced this mutant and demonstrated that E166Q MetNI was unable to hydrolyze ATP.[3] Similarly, our experiments showed a complete loss of activity for E166Q MetNI (Fig. 3-17, red). These results, along with the crystallization of the E166Q transporter in the ATP-bound form, supports the use of this mutant as a tool to examine the MetNI transporter trapped in its ATP-bound form.

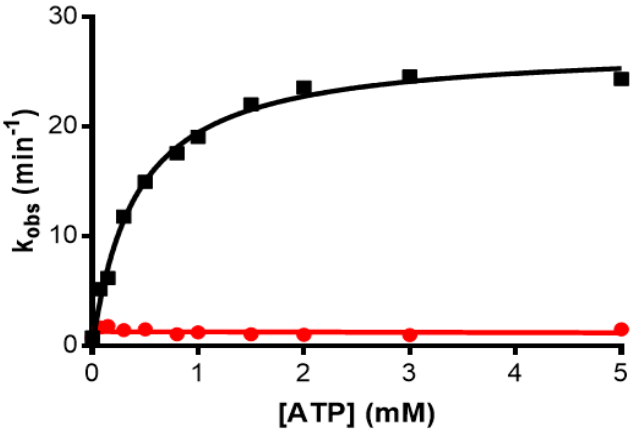

Figure 3-17: E166Q mutation eliminates MetNI ATPase activity. ATPase activity as a function of ATP concentration was measured using ATPase assays of MetNI wild-type (black) and MetNI E166Q (red).

3.2.3 MetNI N295A Mutant

To generate a version of MetNI that cannot be inhibited, a previously described N295A mutant was purified and tested.[2] This mutant dramatically decreased the binding affinity between L-Met and the C2 domain using structural studies, however kinetic studies were absent. To ensure that the N295A mutation solely affects transinhibition, but does not hinder ATP binding and hydrolysis, two ATPase assays were conducted. First, we measured the ability of L-methionine to inhibit ATPase activity. As expected, the rate of ATP hydrolysis by wild-type MetNI decreased as L-methionine concentrations increased (Fig. 3-18). The K_i(L-Met) value of 41 ± 13 μM for wild-type MetNI was in agreement with the published data (K_i(L-Met) = 41 ± 2 μM). In contrast, using the same series of L-methionine concentrations, the MetNI N295A

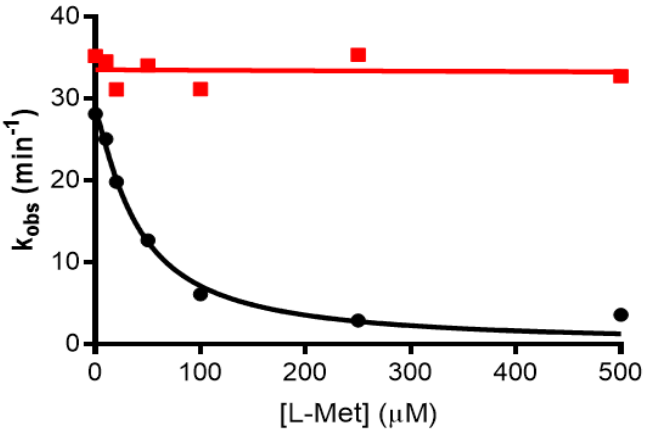

Figure 3-18: High L-Met concentrations do not inhibit MetNI N295A ATPase activity. ATPase activity as a function of L-Met concentration was measured using MetNI wild-type (black) and MetNI N295A (red).

mutant did not show any decrease in ATPase activity (Fig. 3-18, red). This data suggest that the N295A mutation eliminates the transinhibition phenomenon of MetNI.

Next, the ATP concentration was varied to determine the k_{cat} and K_mATP of the mutant (Fig. 3-19). The comparison of wild-type and N295A MetNI showed similar results, with k_{cat} values of 30 ± 3 min^{-1} and 34 ± 4 min^{-1}, respectively. Additionally, K_mATP values were within error, with values of 320 ± 120 μM for wild-type and 365 ± 200 μM for N295A. These results demonstrate that the effect of the N295A mutation is limited to the C2 regulatory domain and does not alter ATP binding and hydrolysis.

Together, the results from ATPase assays of wild-type, E166Q, and N295A versions of MetNI establish that these mutations indeed serve their intended purpose. With this confirmation in hand, we moved forward to determine the requirements for MetNI-Q complex formation.

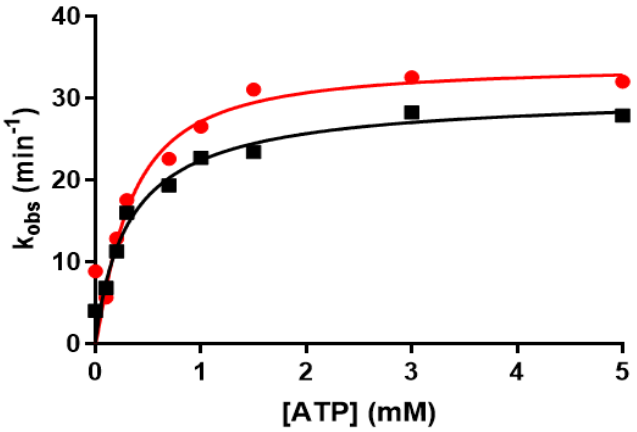

Figure 3-19: N295A mutation does not alter MetNI ATPase activity. ATPase activities of MetNI N295A (red) and MetNI wild-type (black) as a function of varying ATP concentration.

3.3 Development of Fluorescence Anisotropy Assay to Measure MetNI-MetQ Complex Formation

Fluorescence anisotropy is a widely accepted technique to measure the binding affinities between biomolecules. The results from the assay give a broader range of K_d values than the frequently utilized isothermal calorimetry (ITC) method.[9] While surface plasmon resonance (SPR) has been successfully employed to measure binding affinities between the BtuCD transporter and its cognate binding protein, reliable results were not achievable with the MetNI transporter.[10] The development of an anisotropy assay to quantify the binding affinity of the MetNI-Q complex will be a valuable tool in establishing the nucleotide and substrate requirements for association of the transporter and substrate binding protein. The identification of intermediates in the reaction cycle will allow us to build a comprehensive model for methionine transport.

3.3.1: Labeling Substrate-Binding Protein MetQ with Fluorescein 5-Maleimide

In anisotropy experiments, one member of a binding interaction must be fluorescently labeled. Ideally, the labeled protein alone and the protein complex are significantly different in size, with the smaller protein being labeled. In this arrangement, the rotational lifetime of the labeled protein alone varies greatly from that of the protein complex. For anisotropy experiments with the methionine transport system, the substrate-binding protein MetQ (29 kD) was labeled. Given the 1:1 ratio of MetNI to MetQ per functional transporter unit, the MetNI-MetQ complex has a molecular weight of 151 kD.

For these studies, activated fluorescein 5-maleimide dye was chosen because of its high quantum yield (0.79), ideal fluorescence lifetime (~4 nanoseconds), and low anisotropy if the dye is unconjugated (r = 0.021) versus attached to MetQ (r ~ 0.09).[11,12] Fluorescein 5-maleimide was covalently conjugated via maleimide chemistry to the single cysteine residue at amino acid position 23, near the N-terminus of MetQ. This amino acid is not featured in the crystal structure of MetQ because it is unstructured, suggesting that it is not critical for interaction between the two proteins.[11]

A brief summary of the MetQ labeling process is described here. More detailed procedures are provided in the Methods section. First, the reducing agent in the buffer was exchanged from BME to TCEP, as BME contains a thiol group that would react with the maleimide group on the dye. As recommended by the manufacturer, fluorescein 5-maleimide was dissolved in DMSO to 100 mM final concentration. The dissolved dye was added to a final concentration that was 5% DMSO (v/v) and 10-fold dye concentration to that of MetQ (~50 µM MetQ). The mixture was incubated for two hours, and the labeling reaction was quenched by addition of BME. The solution was then injected onto a 5-mL desalting column as a first step in removing excess dye. To further wash the labeled MetQ, the protein was then added to nickel resin beads in a standard 1.5-mL microcentrifuge tube. The 6xHis tag on MetQ allowed the capture of the labeled protein on the nickel beads. The sample was centrifuged at 10,000 rpm for one minute, thereby separating the beads and protein in the pellet and unconjugated dye in the supernatant. The supernatant was removed, and fresh buffer was added to the beads. This batch wash procedure repeated three times or until a constant absorbance at 492 nm was observed. The protein was eluted from the beads by addition of imidazole, and imidazole was subsequently removed via buffer exchange. The absorbance at 280 nm and 492 nm was measured for the samples (Table 3-1), which corresponds to the absorption maxima for protein and fluorescein, respectively. This early labeling procedure was problematic and required significant troubleshooting and optimization.

First, the amount of recovered protein following labeling was extremely low, with yields calculated around 5%. Second, of the protein that was recovered, only ~3% of MetQ was labeled. Lastly, it was suspected that a significant amount of unreacted dye remained in the final sample. The anisotropy value of the labeled MetQ (r = 0.052) was not much higher than the recorded anisotropy value of the unconjugated

maleimide dye (r = 0.032). This suspicion was raised after observing that latter batches of labeled MetQ were measured to have anisotropy values near r = 0.09. It was important to remove as much unconjugated dye as possible, as this contaminant would reduce the ability to detect changes in anisotropy.

Ideally, each potential issue would have been separately tested and analyzed to determine their effect on labeling. However, to preserve time and resources, the labeling protocol was concurrently modified in three ways. First, solid fluorescein dye was directly solubilized in MetQ buffer rather than addition via a high concentration DMSO stock of the dye. This modification may be responsible for the improved protein recovery (Table 3-1), as high concentrations of DMSO may have led to unfolding and precipitation of protein. DMSO has been shown to trigger protein unfolding in concentrations as low as 4% w/v.[13] Second, the molar ratio of dye: protein was increased from 10:1 to 25:1. While expensive, the investment in additional dye paid off, resulting in an ~33% increase in labeling (Table 3-1).

Lastly, to improve the efficiency of washing, the batch washing method was replaced with the use of a gravity column. In a gravity washing method, nickel resin beads are packed into a gravity column. The labeling reaction was added to the beads, and the protein was captured on this stationary phase. The beads were then washed with a total of five mL of buffer instead of three mL administered in batch washing. This gravity washing method effectively removed the unreacted dye, as suggested by the difference in anisotropy values between the labeled MetQ produced from the batch method and the labeled MetQ from the modified protocol (Table 3-3).

Table 3-1: Comparison of original and modified MetQ labeling protocols

	Original Protocol		**Modified Protocol**	
	Abs 280 nm	**Abs 492 nm**	**Abs 280 nm**	**Abs 492 nm**
Flow-Thru	0.976	1.369	9.34	22.5
Wash #1	0.050	0.058	0.316	0.915
Wash #2	0.024	0.035	0.023	0.025
Wash #3	0.000	0.002	0.001	0.018
Eluent	0.000	0.179	3.157	4.406
Desalt	0.000	0.036	0.691	0.968
	% Labeling (Original Protocol)		**% Labeling (Modified Protocol)**	
Final	2.9%		35.7%	
	% Recovered		**% Recovered**	
	2%		20%	

Together, these modifications led to the reproducible labeling of MetQ with increased recovery and labeling efficiency. Both protocols started with 6 mg of unlabeled protein, but the original protocol recovered 1.7% of protein while the modified protocol resulted in 10-fold more recovery (17%). Furthermore, the percent of MetQ that was labeled increased from 2.9% to 35.7%, as calculated using the absorbance values at 280 nm and 492 nm and Equation 1 (see Methods). MetQ contains only one cysteine amino acid, which ensures that a 1:1 ratio of protein: dye is the maximum that can be attained. In summary, the optimization of the labeling protocol yielded suitable amounts of labeled MetQ for subsequent anisotropy studies.

3.3.2: Anisotropy Control Measurements

As there was no recent precedent for anisotropy experiments at USF, a positive control was developed to ensure proper operation of the in-house fluorimeter. First, solubilized dye was added to varying concentrations of glycerol, and the anisotropy was measured. It was expected that increasing amounts of glycerol, being much more viscous than water (1.412 Pa·s vs. $8.90 * 10^{-4}$ Pa·s, respectively), would reduce the rotation of the dye, thereby increasing the anisotropy value. As predicted, the anisotropy value increased as the percent volume of glycerol increased (Table 3-2). This trend provided initial confidence in the procedure and in the settings employed on the Fluoromax (Horiba).

Table 3-2: Anisotropy values of solutions of fluorescein 5-maleimide in glycerol

% volume glycerol	Anisotropy
0	0.03160
5	0.04498
10	0.04641
20	0.05697
40	0.07413
60	0.11578
80	0.25341

To further assess the efficiency of the optimized protein labeling protocol, the anisotropy of free fluorescein 5-maleimide dye was compared to that of labeled MetQ protein (Table 3-3). In this case, the dye was resuspended in the same buffer as that of MetQ. The polarization value for labeled MetQ was 0.0902 ± 0.003, three times higher than the polarization value of free dye (r = 0.037 ± 0.004) and almost

twice as high as the labeled MetQ produced from the initial batch protocol (r = 0.057 ± 0.003). These data suggest that MetQ was successfully labeled during the labeling procedure and that minimal free dye remains in solution.

Table 3-3: Comparison of anisotropy values of free fluorescein 5-maleimide dye versus maleimide-labeled MetQ.

	Anisotropy	**Relative Standard Deviation (%)**
Unconjugated Dye	0.03681	10.5247
Labeled MetQ (Batch Protocol)	0.0567	6.0914
Labeled MetQ (Modified Protocol)	0.09019	3.6818

A series of preliminary experiments were conducted to determine the optimal experimental conditions for measuring MetNI-Q interactions using a Fluoromax-4 Spectrofluorometer (Horiba). First, the ideal concentration of labeled MetQ was determined through a series of serial dilutions.

Table 3-4: Concentration of fluorescein maleimide dye vs. average counts per second (CPS)

Concentration of fluorescein maleimide dye (M)	Avg CPS @ 535 nm
$1.00 * 10^{-6}$	$3.83 * 10^{6}$
$5.00 * 10^{-7}$	$2.14 * 10^{6}$
$2.00 * 10^{-7}$	$9.64 * 10^{5}$
$1.00 * 10^{-7}$	$7.84 * 10^{5}$
$2.00 * 10^{-8}$	$2.84 * 10^{5}$
$1.00 * 10^{-9}$	$2.07 * 10^{5}$

The optimal zone for emission was between 1×10^5 to 2×10^6 counts per second (CPS) as per the fluorometer user manual (Horiba). With MetQ labeled with at 20-30% on average, the optimal amount of MetQ to use in each anisotropy trial was determined to be 20 nM. This concentration of MetQ was ideal, as it produced sufficient signal for fluorescence anisotropy measurements while being far enough below the anticipated K_d to provide maximal change in anisotropy.

Second, the buffer conditions from the ATPase assay did not interfere with fluorescence readings, and thus the same conditions were used for anisotropy experiments. Lastly, the anisotropy was recorded

over time with high concentrations of protein, to ensure that neither the buffer conditions nor the incubation time required for equilibration resulted in aggregation.

3.4: Anisotropy Assays: Determining the K_d of the MetNI-Q Complex in Different Nucleotide and Substrate Environments

3.4.1. Initial Anisotropy Assays using ATP

With successfully labeled MetQ and appropriate settings for the in-house fluorimeter, anisotropy experiments to assess MetNI-Q complex binding affinities were ready to move forward. As a starting point, the MetNI-Q complex formation was assessed in the ATP-bound state, as this was the conformation isolated in crystallography studies.[2,26] A double mutant E166Q/N295A MetNI was utilized. The E166Q mutation prevented ATP hydrolysis, thereby allowing the trapping of ATP-bound states. As an extra precaution against ATP hydrolysis, 3 mM EDTA was added in conjunction with 3 mM ATP to ensure removal of any trace Mg^{2+} ions that would hydrolyze bound ATP. The N295A mutation hindered L-Met binding at the C2 domains, thereby eliminating any effect from transinhibition.

Using the in-house fluorimeter (Fluoromax-4 Spectrofluorometer), an experiment comparing the binding affinities of L-Met bound MetQ (MetQ wild-type) and apo MetQ (MetQ N229A) with ATP-bound MetNI was performed (Figure 3-20). The K_d value of apo MetQ with ATP-bound MetNI was determined to be 83 nM after a single trial while the K_d value of L-Met bound MetQ with ATP-bound MetNI was determined to be 2.7 µM. Previously published microscale thermophoresis studies found a similar trend with apo MetQ having a higher binding affinity than wild-type MetQ.[25]

While these initial assays were a success, it became apparent that the labor and reagent requirements of the experiment were unsustainable. A single experiment would take approximately 4-6 hours to

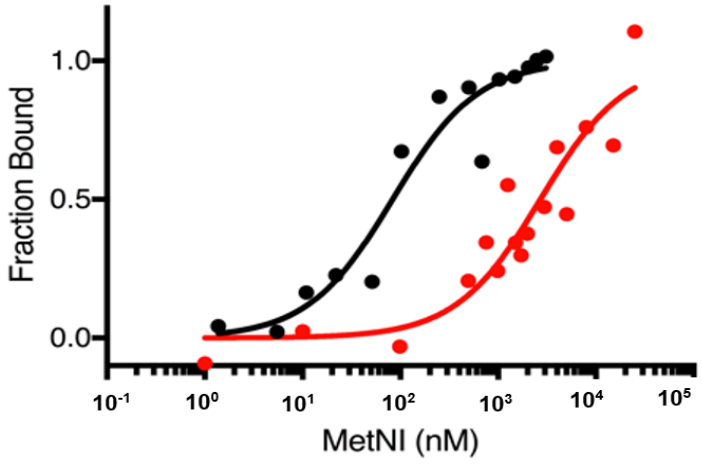

Figure 3-20: Initial anisotropy assays assessing MetNI-Q binding affinities in the presence of ATP. The black and red curves are two separate assays performed with 20 nM MetQ N229A and MetQ wild-type, respectively.

complete, as the in-house fluorimeter relied on a cuvette that holds only one 100 µl sample at a time. Additionally, the concentration of MetNI necessary to saturate MetQ exceeded 10 µM, and at 100 µl per sample, the total amount of MetNI was very substantial. Given the number of variables we planned to examine, a more efficient method would be very beneficial, if not essential. For this reason, we explored the possibility of using a spectrofluorimeter plate reader at UCSF. In this format, a single experiment could be conducted in only 30-60 minutes and each well used only 20 µl. After weeks of troubleshooting the procedure and equipment, anisotropy experiments were exclusively performed using a SpectraMax Gemini XS Microplate Spectrofluorometer (Molecular Devices).

3.4.2: Complex Formation as a Function of MetNI Nucleotide State: Apo, ATP-Bound, and ADP-Bound

The first variable assessed was the nucleotide state of the MetNI transporter. During the reaction cycle, possible nucleotide states include empty (or apo), ATP-bound, the ATP transition state, a post-hydrolysis state, and ADP-bound. As a starting point, we chose to test three nucleotide states: apo, ADP-bound, and ATP-bound. In structural studies, the MetNI-Q complex was crystallized in the ATP-bound state, while MetNI alone was crystallized with ADP bound to its NBDs.[2,26] While these structures provide strong evidence of the nucleotide requirements for complex formation, the possibility of artifacts due to crystal packing demands independent confirmation using a solution-based method. Discrepancy between functional and structural studies have been debated regarding other ABC transporters. For example, the original mechanisms for both the maltose (type I) and the vitamin B_{12} (type II) importers proposed based on crystallography studies did not align with mechanisms proposed for the transporters based on functional studies.[13-18]

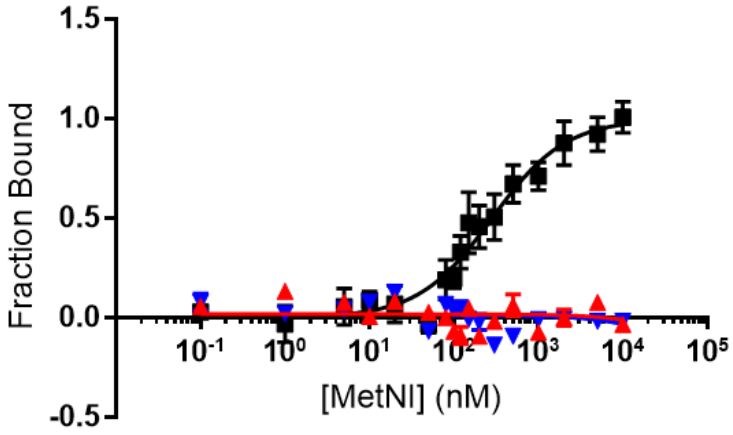

Figure 3-21: MetNI-Q complex formation requires ATP. Association of MetQ wild-type and MetNI E166Q/N295A was measured in the presence of ATP/EDTA (black), ADP (blue), or no nucleotide (red).

To test the effect of MetNI nucleotide state on complex formation, the double mutant E166Q/N295A MetNI was utilized, as described above. In these assays, 20 nM of wild-type MetQ was held constant while the concentration of E166Q/N295A MetNI was varied from 0 - 20 μM. Either ATP and EDTA, ADP, or no nucleotide was included in each reaction. While there was no detectable change in anisotropy in either the ADP or apo state, a reproducible, robust change was measured in the presence of ATP (Fig. 3-21). The data was best fit to a 1:1 binding curve with a K_d of 527 nM ± 107 nM. The formation of the complex in the ATP-bound state is in agreement with previous crystallography studies,[11] and is the first measured K_d value for an ABC transporter using fluorescence anisotropy.

3.4.3 Role of MetQ Substrate-State in MetNI-Q Complex Formation: Apo (MetQ N229A) or L-Met Bound (MetQ wild-type)

The second variable tested was the presence or absence of substrate bound to MetQ. In crystallography studies, apo MetQ has been crystallized in complex with MetNI in its ATP-bound state, however, attempts to capture an intermediate with substrate present were unsuccessful.[2] This intermediate has been trapped in both the maltose and molybdate transporters.[20,21] We hypothesize, however, that L-methionine must interact with MetQ at some point during the reaction cycle, as *in vivo* evidence suggests that transport cannot occur if the MetQ gene is deleted.[22] The same observation was made in both the maltose and vitamin B_{12} transporters, where transport was not detected in the absence of the SBP *in vivo* and *in vitro*, respectively.[23,24]

Due to its tight binding affinity, it is widely accepted that the substrate binding protein of ABC transporters commonly co-purifies with its cognate substrate.[25] To isolate substrate binding protein without substrate (apo), a common technique is to unfold the protein in the presence of urea. Urea is a chaotrope which disrupts the hydrogen bonding network of a solution or substrates. Following unfolding, MetQ is refolded to its original shape via the slow removal of the chaotrope. To circumvent this time-consuming and low-yielding process, Nguyen et al. introduced a single amino acid substitution (N238A) in *Neisseria meningitides* MetQ that drastically increased the K_d nearly 400-fold (0.2 nM for wild-type to 78 μM for mutant).[26] Based on crystallography studies, this asparagine forms key hydrogen bonds with both the α-amino and the α-carboxyl groups of the methionine substrate. By mutating this asparagine to alanine, a mimic for apo MetQ was created, allowing for an alternative to the extensive unfolding-refolding process. Apo MetQ could now be purified directly from cells overexpressing this mutant form of MetQ.

This strategy was implemented for use with *E. coli* MetQ. A mutation in the homologous site (amino acid position 229) in *E. coli* allowed for the direct isolation of apoMetQ from *E. coli* cells. The use of MetQ wild-type and MetQ N229A serves as equivalents for substrate-bound and apo MetQ, respectively. The anisotropy assay described above was then performed using MetQ N229A. As with wild-type MetQ,

no binding was detected for either ADP-bound or apo E166Q/N295A MetNI. Binding of MetQ N229A to E166Q/N295A MetNI was observed in the presence of ATP, however the K_d was approximately 2-fold lower than with wild-type MetQ (281 nM ± 36 nM vs 527 nM ± 107 nM, respectively) (Fig 3-22).

Table 3-5: Comparison of MetNI-Q complex binding affinities with substrate-bound MetQ vs. apo MetQ

	L-Met bound MetQ (wild-type) + ATP-bound N295A MetNI	**Apo MetQ (N229A mutant) + ATP-bound N295A MetNI**
K_d	527 nM ± 107 nM	281 nM ± 36 nM

While apo MetQ (MetQ N229A) showed a two-fold higher affinity for ATP-bound MetNI than L-Met bound MetQ (MetQ wild-type), this difference is relatively minor in a physiological setting. The similarity in binding affinities suggests the possibility that both complexes may be involved in methionine transport.

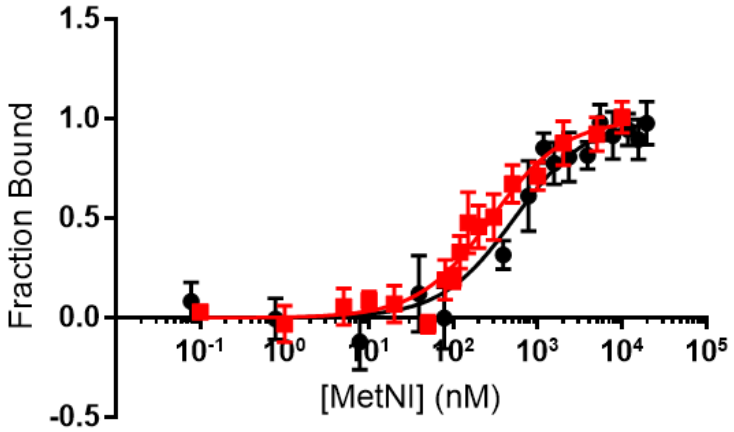

Figure 3-22: Binding affinity for ATP-bound MetNI. Complex formation was measured using MetNI E166Q/N295A and MetQ N229A (red) and MetQ wild-type (black)

3.4.4: L-Met as an Inhibitor of MetNI-Q Complex Formation

The third variable assayed was the presence or absence of L-Met at the regulatory C2 domains. Previous studies found that the ATPase activity of the MetNI transporter decreased with increasing concentrations of L-Met, which is consistent with the transinhibition model first proposed by Kadner.[27] In crystallographic studies, MetNI containing L-Met bound to the C2 domains was trapped in its inward-facing conformation, uncomplexed to MetQ.[28] This transinhibitory mechanism has only been observed in the methionine and molybdate transporters.[29] However, the maltose and vitamin B_{12} transporters were captured in an inward-facing conformation without their respective SBP.[30] Furthermore, Chen et al. proposed that

the maltose transporter in its IWF conformation complexed with its SBP (MalE) is an unstable, high energy structure that quickly dissociated.[31] While it is commonly accepted that binding of L-Met at the C2 domains prevents association of the NBDs, it is unclear as to whether MetQ can bind MetNI in this inhibited state. We hypothesize that transinhibition will sterically induce MetQ dissociation from MetNI.

To test if binding of L-Met to the C2 domains triggers the dissociation of the MetNI-Q complex, the experimental procedure was designed to ensure that all MetQ molecules were in a complex with MetNI. This experiment was performed by saturating 20 nM maleimide-labeled MetQ N229A with 1 μM MetNI E166Q and 3 mM ATP/EDTA. These concentrations were informed by previous anisotropy experiments (Section 3.4.2), where nearly 100% of MetQ N229A was in complex under these conditions. To ensure that the total concentration of L-Met was controlled in each reaction, these anisotropy trials utilized apo MetQ (MetQ N229A). This also ensured that L-Met was available to bind the C2 domains and not MetQ.

In a single preliminary trial, increasing concentrations of L-Met dissociated the MetNI E166Q - MetQ N229A complex. The K_d for MetNI-Q complex dissociation by addition of L-Met was determined to be 484 nM (Fig 3-23, see Methods for details of data fitting). Published ATPase measurements report a K_I of 41 ± 2 μM for L-Met to MetNI, which can be interpreted as synonymous to the K_d in this case. Though the binding affinity measurement in this anisotropy assay differs from that of previous kinetic studies on MetNI, this is the first evidence that L-Met binding to the C2 domain would inhibit MetQ association. Due to COVID-19 pandemic, only one trial was completed for this experiment. Going forward in this project, it will be crucial to repeat these experiments to determine the K_d. Experiments using higher concentrations of L-Met will be important to obtain a reliable binding curve.

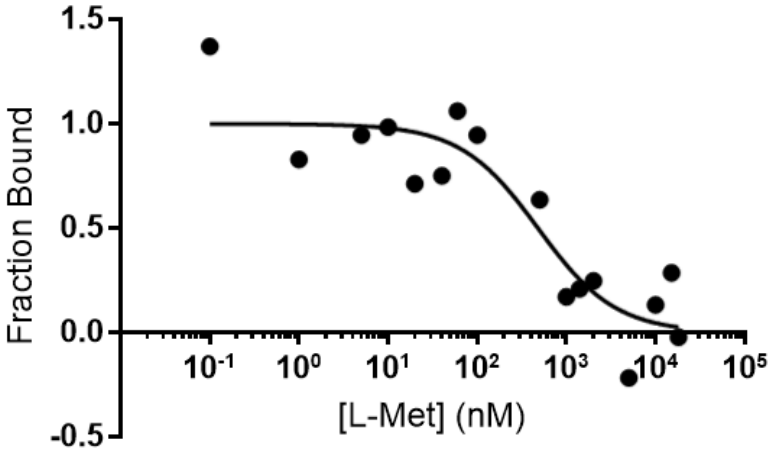

Figure 3-23: Preliminary anisotropy trial to determine K_d of L-Met - MetNI. Each reaction contained 20 nM MetQ N229A, 1 μM MetNI E166Q, 3 mM ATP/EDTA, and varying concentrations of L-methionine. The K_d of L-methionine to the C2 domain was 484 nM.

References

1. Kadner R.J., Watson W.J. Methionine transport in Escherichia coli: Physiological and genetic evidence for two uptake systems. *J. Bacteriol.* (1974). 119(2):401-409.
2. Nguyen P.T., Lai J.Y., Lee A.T., Kaiser J.T., Rees D.C. Noncanonical role for the binding protein in substrate uptake by the MetNI methionine ATP Binding Cassette (ABC) transporter. *PNAS.* (2018). 115:45, E10596-E10604
3. Kadaba NS, Kaiser JT, Johnson E, Lee A, Rees DC. The high-affinity *E. coli* methionine ABC transporter: structure and allosteric regulation. *Science.* (2008). 321: 250–253.
4. Locher K.P., Lee A.T., Rees D.C. The *E. coli* BtuCD structure: A framework for ABC transporter architecture and mechanism. *Science.* (2002). 296:1091-1098.
5. Studier F.W. Protein production by auto-induction in high-density shaking cultures. *Protein Expression and Purification.* (2005). 41:207-234.
6. Hefti M.H., Van Vjugt-Van der Toorn C.J.G., Dixon R., Vervoort J.A novel purification method for histidine-tagged proteins containing a thrombin cleavage site. *Anal Biochem.*
7. Enzchek Phosphate Assay Kit. *Thermo Fisher Scientific.* (2002).
8. Yang. J.G., Rees D.C. The allosteric regulatory mechanism of the *Escherichia coli* MetNI methionine ATP binding cassette (ABC) transporter. *Journal of Biological Chemistry.* 2015. 290(14): 9135-9140.
9. Norcross S., Sunderraj A., Tantama M. pH- and temperature-dependent peptide binding to the Lactococcus lactis oligopeptide-binding protein A measured with a fluorescence anisotropy assay. *ACS Omega.* (2019). 4(2): 2812-2822.
10. Lewinson O., Lee A.T., Locher K.P., Rees D.C. A distinct mechanism for the ABC transporter BtuCD-F revealed by the dynamics of complex formation. *Nat Struct Mol Biol*. (2010). 17(3): 332-338.
11. Moerke N.J. Fluorescence polarization (FP) for monitoring peptide-protein or nucleic acid-protein binding. *Current Protocols.* (2009). 1(1):1-15.
12. Zhang H., Wu Q., Berezin M.Y. Fluorescence anisotropy (polarization): from drug screening to precision medicine. *Expert Opin Drug Discov.* (2015). 10(11):1145-1161.
13. Chan D.S.H., Kavanagh M.E., McLean K.J., Munro A.W., Mitak-Vinkovic D., Coyne A.G., Abell C. Effect of DMSO on protein structure and interactions assessed by collision-induced dissociation and unfolding. *ACS Analytical Chemistry.* (2017). 89(18):9976-9983.
14. M.L. Oldham, Khare D., Quiocho F.A., Davidson A.L., Chen J. Crystal structure of a catalytic intermediate of the maltose transporter. *Nature*. (2007). 450:515-521.
15. Oldham M.L. Chen J. Crystal structure of the maltose transporter in a pretranslocation intermediate state. *Science.* (2011). 332:6034:1202-1205.
16. Bao H., Duong F. ATP alone triggers the outward-facing conformation of the maltose ATP-binding cassette transporter. *J. Biol. Chem.* (2013). 288(5): 3439-3448.
17. Lewinson O., Lee A.T., Locher K.P., Rees D.C. A distinct mechanism for the ABC transporter BtuCD-F revealed by the dynamics of complex formation. *Nat Struct Mol Biol*. (2010). 17(3): 332-338.
18. Korkhov, V.M., Mireku S.A., Locher K.P. Structure of AMP-PNP-bound vitamin B_{12} transporter BtuCD-F. *Nature*. (2012). 490:367-372.
19. Bao H., Duong F. Discovery of an auto-regulation mechanism for the maltose ABC transporter $MalFGK_2$. *PloS One.* (2012). 7(4):34836.
20. Oldham ML, Chen J. Crystal structure of the maltose transporter in a pretranslocation intermediate state. *Science.* (2011). 332:1202–1205.
21. Hollenstein K, Frei DC, Locher KP. Structure of an ABC transporter in complex with its binding protein. *Nature.* (2007). 446:213–216.
22. Merlin C., Gardiner G., Durand S., Masters M. The Escherichia coli metD locus encodes an ABC transporter which includes Abc (MetN), YaeE (MetI), and YaeC (MetQ). *J. Bacteriol.* (2002). 184(19): 5513-5517.
23. Shuman H.A. Active transport of maltose in Escherichia coli K12. Role of the periplasmic maltose-binding protein and evidence for a substrate recognition site in the cytoplasmic membrane. *J. Biol. Chem.* (1982). 257:5455-5461.

24. Borths E.L., Poolman B., Hvorup R.N., Locher K.P., Rees D.C. In vitro functional characterization of BtuCD-F, the Escherichia coli ABC transporter for vitamin B_{12} uptake. *Biochemistry.* (2005). 44:16301-16309.
25. Williams W.A., Zhang R.G., Zhou M., Joachimiak G., Gornicki P., Missiakas D., Joachimiak A. The membrane-associated lipoprotein-9 GmpC from Staphylococcus aureus binds the dipeptide GlyMet via side chain interactions. *Biochemistry.* (2004). 43(51):16193-202.
26. Nguyen P.T., Lai J.Y., Kaiser J.T., Rees D.C. Structures of the *Neisseria meningitides* methionine-binding protein MetQ in substrate-free form and bound to L- and D-methionine isomers. *Protein Science.* (2019). 28(10): 1750-1757.
27. Kadner R.J., Watson W.J. Methionine transport in Escherichia coli: Physiological and genetic evidence for two uptake systems. *J Bacteriol.* (1974). 119(2):401-409.
28. Johnson E., Nguyen P.T., Yeates T.O., Rees D.C. Inward facing conformations of the MetNI methionine ABC transporter: Implications for the mechanism of transinhibition. *Protein Science.* (2011). 21(1): 84-96.
29. Gerber S., Comellas-Bigler M., Goetz B.A., Locher K.P. Structural basis of trans-inhibition in a molybdate/tungstate ABC transporter. *Science*. (2008). 321(5886): 246-250.
30. Orelle C, Ayvaz T, Everly RM, Klug CS, Davidson AL. Both maltose-binding protein and ATP are required for nucleotide-binding domain closure in the intact maltose ABC transporter. *PNAS.* (2008). 105:12837–12842.
31. Chen J. Molecular mechanism of the Escherichia coli maltose transporter. *Curr Opin Struct Biol.* (2014). 23(4): 492-498.

Chapter 4: Discussion

This thesis addresses fundamental questions regarding the mechanism of the MetNI methionine importer. Crucial technical advancements in this project include a modified protein purification protocol with increased yield, an optimized MetQ labeling procedure, and the development of a reliable binding affinity assay using fluorescence anisotropy. The techniques developed here and the resulting data have allowed us to address key unknowns, such as the requirements necessary for MetNI - MetQ complex formation and the details of the transinhibition phenomenon. This work not only presents insights into MetNI transport but gives rise to further questions for both methionine import and ABC transporters in general.

4.1: Optimization of MetQ Protein Purification and Fluorescent Labeling Protocols

One of the main limitations in many biochemical studies is the availability of pure protein. Improvements in purification are a crucial first step necessary to ensure the feasibility of subsequent experiments. Before optimization, MetQ expression and purification were inconsistent and yielded low amounts of purified protein. The switch from autoinduction media to Terrific Broth media was a pivotal discovery.

An excess amount of glucose in the autoinduction media may have led to the low protein yields. If lactose is not completely digested then the *lac* operon would not be activated.[1] Another explanation for the low yield under these conditions is a decrease in O_2 solubility at higher temperatures leading to less breakdown of lactose and decreased protein expression.[2] The use of Terrific Broth media, where protein expression is induced by addition of a lactose analog, IPTG, produced a 5-fold increase in yield.

The second technical improvement was the optimized MetQ labeling procedure. Initial procedures resulted in 1-2% protein labeling, which did not provide enough fluorescent signal for anisotropy assays. Furthermore, the sample contained a high level of unconjugated dye, which masked changes in anisotropy. Modified labeling methods, including altering the protein:dye ratio and buffer components, increased the percentage of protein labeled. The use of a gravity column for washing efficiently removed unreacted fluorescein 5-maleimide dye. Ultimately the modified labeling protocol saw 12 times more fluorescently labeled MetQ, a crucial improvement for subsequent assays.

4.2 Development of Fluorescence Anisotropy Assay to Detect MetNI-Q Complex Formation

Previous attempts to measure the binding between MetNI and MetQ were difficult and unreliable. Surface plasmon resonance (SPR) was successfully employed to measure binding for the BtuCD-F vitamin B_{12} transporter however, adhesion of MetNI to the surface of the sensor chip was variable.[3] Microscale

thermophoresis was used to gather evidence of MetNI binding to MetQ however, this technique is relatively novel and is not commonly-accepted in the field.[4] Isothermal titration calorimetry is a standard technique to measure binding affinities that may be considered for measuring MetNI-Q binding, however, producing the amount of purified protein necessary for these experiments would be exceptionally difficult for the methionine transport system. Upon considering the challenges with the procedures mentioned, we developed a new system to fully address questions regarding MetNI - Q complex formation.

Fluorescence anisotropy is a widely accepted technique to measure binding affinities. This method measures solution-based equilibrium and requires standard instrumentation. Iterative experiments determined the ideal conditions to measure the MetNI-Q interaction. Variables in the experiments included the proper amounts of labeled MetQ for appropriate signal to noise ratios, ideal MetNI concentration ranges, removal of aggregate protein, buffer conditions, and temperature. Preliminary experiments were conducted using a standard cuvette-based fluorescence spectrophotometer. The protocol was subsequently adapted for use in a 384-well plate reader format, which decreased the amount of purified protein required by 5-fold per experiment. The modification to the plate reader format decreased the time required for each experiment from six hours to only one hour of experimentation. The detailed procedure appears in the appendix of this thesis for use in future projects.

4.3: ATP-Binding is a Prerequisite for MetNI-Q Complex Formation

One of the highly debated questions regarding ABC transporter mechanism is which nucleotide state(s) promote(s) transporter-SBP complex formation. According to the anisotropy experiments we performed, when MetNI was either nucleotide-free or trapped in an ADP-bound state, there was no detectable change in anisotropy when added to labeled MetQ. These measurements were conducted with both apo MetQ and L-Met-loaded MetQ. A lower bound for the K_d is approximately 20 μM, indicating that the MetNI-Q complex does not form with MetNI in its nucleotide-free or ADP-bound states.

The K_d of ATP-bound MetNI with MetQ, whether it was apo MetQ or L-Met bound MetQ, was much lower than results recovered with MetNI in the apo or ADP-bound nucleotide states (K_d values ranged from 200- 600 nM), suggesting that ATP-binding by MetNI is a prerequisite for the MetNI-Q complex to form. These findings are consistent with studies of the type I maltose importer in lipid nanodiscs and the type II vitamin B_{12} transporter in detergent, which also reported ATP-binding as a prerequisite for transporter-SBP complex formation.[3,5] Additionally, crystallization of the MetNI-Q complex has only been successful with the transporter in its ATP-bound state.[6] This is likely the most common configuration of the transporter as the normal ratio of intracellular ATP:ADP is 1000:1.[7] With the anisotropy data mentioned above, we conclude that MetNI requires ATP-binding as a prerequisite for MetNI-Q complex formation.

4.3.1: The Presence of L-Met as a Substrate Does Not Significantly Alter Complex Formation

An unexpected discovery in this work, was the similar binding affinity between apo MetQ and ATP-bound MetNI versus L-Met loaded MetQ and ATP-bound MetNI. The results from fluorescence anisotropy experiments (Fig 3.14) in the presence of 3 mM ATP show that apo MetQ has a stronger affinity for ATP-bound MetNI than L-Met loaded MetQ ((K_d = 281 ± 36 nM for MetQ N229A –MetNI E166Q/N295A, K_d = 527 ± 107 nM for MetQ wild-type – MetNI E166Q/N295A), see Fig 3-22). Under physiological conditions, this difference is not considered to be significant. While our results demonstrate an approximate two-fold difference in affinity, previously published thermophoresis titration curves suggest a 40-fold difference (K_d = 27 ± 9 nM for MetQ N229A – MetNI E166Q, K_d = 1100 ± 300 nM for MetQ wild-type- MetNI E166Q).[4] These previously published data were conducted under different *in vitro* reaction conditions. Nguyen et. al completed the reaction in 1 mM ATP, 1 mM EDTA, 20 mM TAPS pH 8.5, 100 mM NaCl, and 0.3 % Cymal-5 while we performed our assays in 3 mM ATP, 3 mM EDTA, 0.06% DDM, 150 mM NaCl, 57.5 mM Tris pH 7.5, and 10 mM TAPS pH 8.5. In addition, Nguyen et. al used a novel technique, microscale thermophoresis, that has not been widely accepted by the scientific community (personal communication with J. Yang). Further experimentation should be conducted to explore these disparate results. The generation of meaningful binding curves validate the use of fluorescence anisotropy to determine ABC transporter complex dissociation constants. Since fluorescence anisotropy can be adapted to different protein complexes this advancement opens the door for future ABC transporter mechanism research through the study of complex dissociation constants.

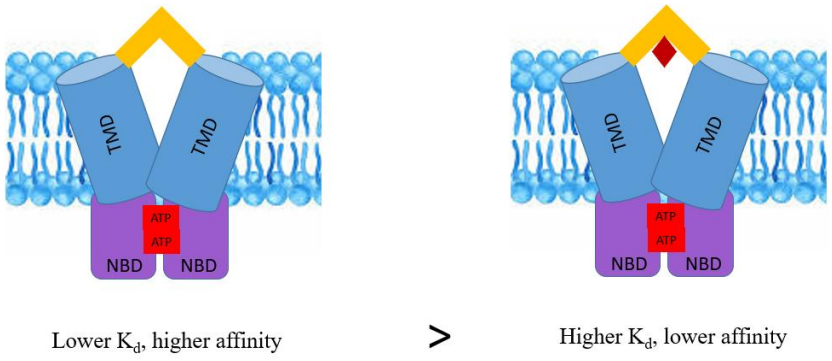

Figure 4-1: Visual representation of MetNIQ complex binding affinities. MetQ is shown in yellow, and L-Met is represented by the maroon diamond. In the presence of 3 mM ATP, apo MetQ was found to have slightly higher affinity for ATP-bound MetNI than L-Met bound MetQ. The K_d of MetQ N229A – MetNI N295A/E166Q is 281 ± 36 nM, and the K_d of MetQ wild-type – MetNI N295A/E166Q is 527 ± 107 nM,

4.3.2: Evidence for Both Classical and Non-Canonical Mechanisms of Methionine Transport

The data presented in this thesis provide evidence in support of both the classical and noncanonical models of methionine transport. In the classical model, MetQ first captures L-Met in the periplasmic space and then shuttles the substrate to the membrane-bound transporter. Based on the results shown here, we propose that ATP binding is a prerequisite for interaction between L-Met bound MetQ and MetNI. Anisotropy data demonstrate that MetQ and MetNI do not interact in the absence of ATP, and thus the "resting state" complex found in the maltose and vitamin B_{12} transporters may not exist for the methionine transporter. Once substrate-loaded MetQ binds to MetNI in its OWF conformation, L-Met is released into the transmembrane cavity, initiating ATP hydrolysis and triggering rearrangement to the IWF conformation (Fig. 4-2).

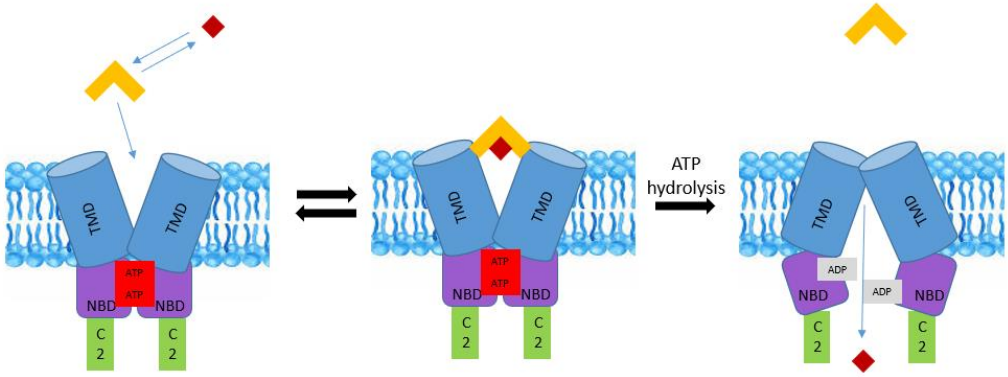

Figure 4-2: A classical mechanism for methionine transport. When extracellular L-Met is present (red diamond), periplasmic MetQ captures the substrate and delivers it to the transporter.

In the non-canonical model, apo MetQ binds to MetNI in its OWF, ATP-bound conformation. The periplasmic substrate can then interact with the preformed complex, passing through MetQ to the transmembrane cavity (Fig. 4-3). Our results show that apo MetQ interacts with MetNI only in the ATP nucleotide state, and that neither ADP nor the apo nucleotide state support complex association.

The presence of two mechanisms may seem unnecessary for a transporter, however, some researchers hypothesize each mechanism transports a unique substrate. Nguyen et al. proposed that the preference for a particular mechanism may be triggered in response to environmental conditions.[8] When extracellular L-Met concentrations are low, the cell can transition from importing L-Met via the classical model to importing L-Met derivatives using the non-canonical model. They developed this hypothesis upon depicting the structure of the MetNI-apo MetQ complex that had been solved by x-ray crystallography. However, while this finding has opened the door to discovering a new mechanism, crystallography studies place transporters in highly artificial environments and are best interpreted in conjunction with functional studies. Our measurement of a relatively strong binding affinity for the apo

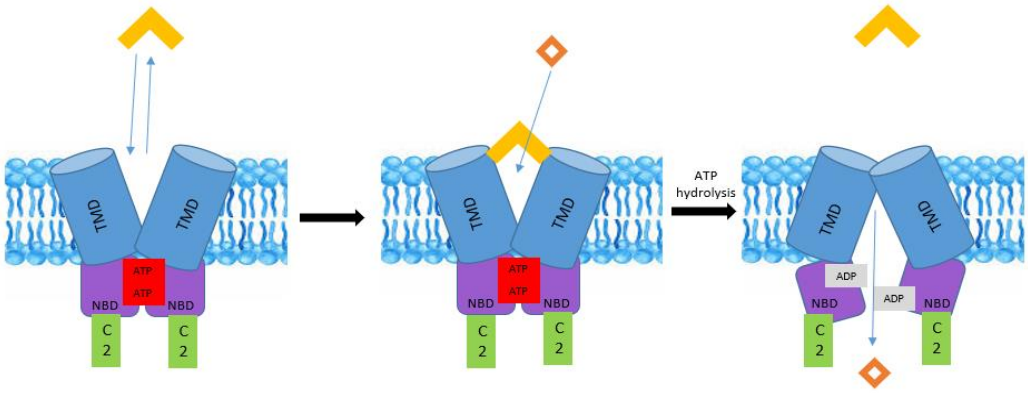

Figure 4-3: A non-canonical mechanism for methionine transport. In this model, if L-Met is unavailable, MetQ will dissociate from and rebind MetNI. A methionine derivative (red diamond) can access the translocation pathway if MetQ is bound to the transporter. The substrate can then enter the transmembrane pathway and be transported across the membrane upon ATP hydrolysis.

MetQ - MetNI complex strongly supports the existence of the non-canonical model. While MetQ N229A has a higher affinity for ATP-bound MetNI (K_d = 281 nM $\pm$ 36 nM), L-Met-bound MetQ was also able to bind to MetNI with a reasonably strong affinity (K_d = 527 $\pm$ 107 nM). The similarity in binding affinity between L-Met bound and apo MetQ is a further indicator of the presence of the classical and non-canonical mechanisms. Previous studies propose that there may be a substrate binding site in the translocation pathway that is selective for the sulfur atom in L-Met derivatives[8]. This binding site would attract L-Met derivatives to the MetNI-apo MetQ complex to initiate the non-canonical model. The possibility of a substrate binding site in the transmembrane domains, combined with our functional data showing similar binding affinities for both L-Met bound and apo MetQ - MetNI complexes, indicate that MetNI utilizes both mechanisms for transport. Through these distinct pathways, the cell maintains sufficient amounts of L-Met or L-Met precursors to maintain cellular function.

4.4: Transinhibition Mechanism of MetNI

In 1976, Kadner performed *in vivo* experiments in which the import of L-Met and D-Met decreased as intracellular L-Met concentrations increased[9]. This transinhibition mechanism was observed when high intracellular concentrations of methionine were present. This mechanism is thought to pause MetNI activity, conserving ATP and preventing the import of a substrate that is already in excess. This process is activated when intracellular L-Met binds to the C2 regulatory domains of MetNI, as based on both crystallography and functional studies. Figure 4-4 depicts the proposed conformational changes that occur upon L-Met binding to the C2 domains. Once L-Met binds to the C2 domains, the transporter is shifted to its inward-facing conformation.[8]

To build upon this observation, we sought to provide solution-based evidence that L-Met binding to the C2 domains can drive the dissociation of MetQ from MetNI. Using the fluorescence anisotropy assay

developed here, the MetNI-Q complex appeared to dissociate upon addition of increasing concentrations of L-Met. Using maleimide-labeled MetQ, the anisotropy value decreased when L-Met was added to a preformed MetNI-Q complex, presumably due to L-Met binding at the C2 domains. By plotting the anisotropy value as a function of L-Met concentration, the K_d value of L-Met to the C2 domains can be determined. In a single preliminary anisotropy assay, the K_d of L-Met to the C2 domains was 484 nM (Fig. 3-15). The data comes from a single trial, and while more results are required to report a reliable K_d value, this data provides a starting point in designing future assays. It will be crucial to perform this experiment using the N295A mutation to test that this effect is due to binding at the C2 domains. Overall, this preliminary result provides further detail to the transinhibition model (Fig. 4-4).

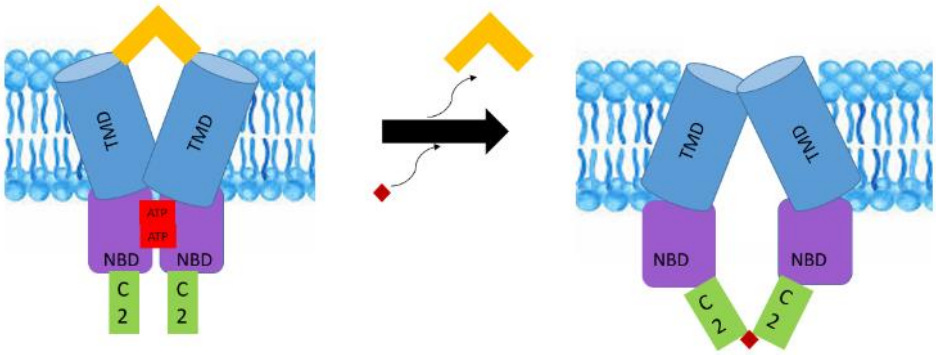

Figure 4-4: Binding of L-Met to the C2 domains of the transporter dissociates the MetNI-Q complex.

4.5: Future Experiments: Comparison of MetQ N229A and Apo MetQ Wild-Type

Given the tight affinity for L-Met, wild-type MetQ naturally co-purifies with L-Met expressed in *E. coli*. To obtain apo MetQ, a laborious unfolding-refolding protocol has been developed (see Fig. 4-5). The chaotrope guanidine hydrochloride is added to purified protein, disrupting the hydrogen bonds that hold together a protein's structure, triggering protein unfolding and the release of L-methionine. Guanidine hydrochloride is then slowly removed, driving refolding of MetQ into an apo form. In this work, however, we employed a mutant form of MetQ to reduce the time and resources necessary for experiments. This mutant, N229A, was utilized in previously studies as a mimic for apo MetQ. While isothermal titration

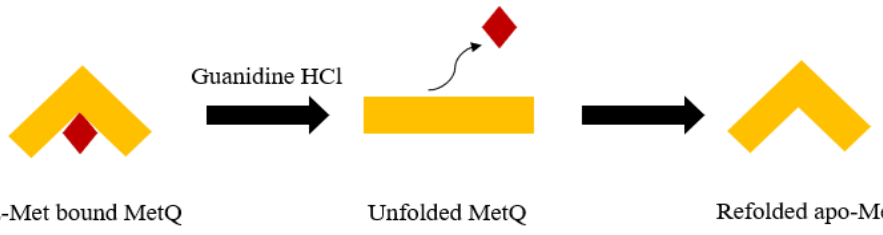

Figure 4-5: The unfolding-refolding process of wild-type MetQ. Addition and slow removal of guanidine hydrochloride removes the L-Met that co-purifies with wild-type MetQ.

calorimetry experiments have shown that a similar mutation in *Neisseria meningitides* negates L-Met binding, data regarding the *E.coli* MetQ N229A mutant is limited.[10] Further evidence must be obtained to confirm the use of this mutant as an appropriate substitute for apo wild-type MetQ.

The anisotropy assay developed in this work can be used to address this need. Specifically, the binding affinities of unfolded-refolded apo wild-type MetQ for ATP-bound MetNI can be compared to that of MetQ N229A. Similar K_d values would suggest that MetQ N229A binds to MetNI in a manner similar to that of apo WT MetQ, and that this mutant is appropriate for future studies.

4.6: Chimeric MetNI Transporter to Study Role of Two ATPase Sites

Both structural and functional studies show similar outcomes that suggest the two NBDs of a single transporter must come together during a reaction cycle. While there are two ATP-binding sites formed at the interface of the NBDs, it remains unknown if both sites must bind and hydrolyze ATP. For example, can MetNI function with a single bound ATP? Can MetNI function with two NBDs that bind ATP but only one that is able to hydrolyze ATP?

To address these types of questions, future experiments will involve heterodimeric, or chimera, transporters. In a chimera transporter, the TMDs would be identical but the NBDs would be different. Using mutations in the NBDs, chimera transporters can be trapped in asymmetric nucleotide states. For example, the mutant K44A involves a substitution in the Rec-A portion of the NBD. The loss of the lysine side chain prevents binding of ATP in the active site. In contrast, the mutant E166Q allows the NBD to bind but not hydrolyze ATP. Creating different pairings of wild-type, K44A, and E166Q mutations in the nucleotide binding regions will provide insight into the mechanism of methionine transport. Clues as to the ATP requirement for MetQ binding could be addressed using anisotropy assays. If there is no change in anisotropy in experiments with rising heterodimeric MetNI concentrations in solutions of fluorescently labeled MetQ, then that would reject the idea that that heterodimeric MetNI may successfully complex with MetQ.

In order to generate MetNI chimeras, a different purification strategy must be employed. A pilot protein purification using this strategy was successful, but was not pursued further due to time limitations. To create a chimera, a His-tag is attached to one NBD with a specific mutation and a FLAG-tag is attached to the other NBD with a different mutation. Since both mutations are expressed simultaneously in *E. coli*, three different versions of transporters are produced. Specifically, the transporters have either two His-tags, two FLAG-tags, or the chimera His-FLAG tags. To capture the desired chimera transporters, cell lysates are purified using a Ni-NTA resin column followed by an anti-FLAG antibody column. Through this tandem purification procedure, only chimera transporters with both the His-tag and the FLAG-tag would be collected.

Next, assays will be carried out to ensure that chimera transporters show activity that are consistent with that of homodimers. For example, His-FLAG chimeras which have two wild-type NBDs should show the same ATPase activity as His wild-type homodimers. Similarly, His-FLAG chimeras which have two E166Q NBDs should behave as did the His-E166Q homodimers measured in the anisotropy assays (Fig. 4-6). If K_d values and kinetic parameters for chimera transporters are comparable to those of homodimers, then the project can move forward with evidence suggesting the addition of multiple tags will not interfere with transporter activity.

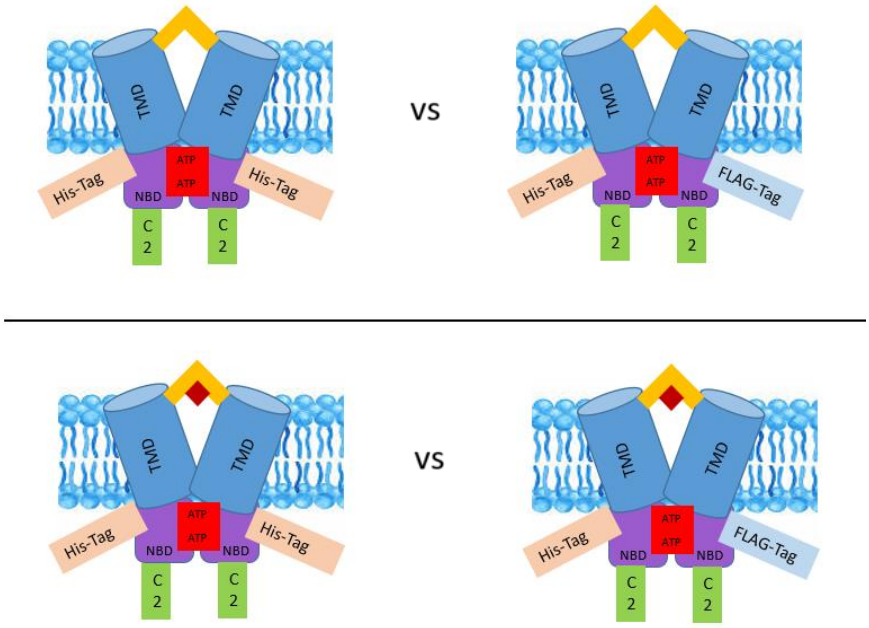

Figure 4-6: Initial control assays using MetNI chimeras. MetNI transporters containing E166Q NBDs with different tags will first be compared to singly-tagged E166Q NBDs. The binding affinities must be measured to ensure that any changes in subsequent data are due to mutations in the ATP site and not an artifact of the tag.

4.7: Investigating the Number of ATP Required for MetNI-Q Complex Formation

Building upon our finding that ATP is required for MetNI-Q complex formation, the next question is whether one or two ATP molecules are necessary for complex formation. Crystal structures of MetNI in its ATP-bound state have shown two ATP molecules bound to the transporter NBDs.[11] The ATPase activity between the two NBDs exhibit positive cooperativity, meaning that the binding of one ATP molecule increases the affinity for a second ATP molecule.[12] This project aims to further understand ATP usage by identifying the number of ATP molecules needed for complex formation. Anisotropy assays using chimeras in which one nucleotide binding domain can bind but not hydrolyze ATP and another that is unable to bind ATP would identify whether or not two functional ATP binding sites are required to form the MetNI-Q complex. As briefly noted in Section 4.6, if there is no change in anisotropy in experiments with rising

heterodimeric MetNI concentrations in solutions of fluorescently labeled MetQ, then that would reject the idea that that heterodimeric MetNI may successfully complex with MetQ.

According to crystallography studies, MetNI in its apo nucleotide state resides in an inward-facing conformation, which inhibits MetNI-Q complex formation. In the previously proposed model, the transporter switches to its outward-facing conformation when two ATP molecules bind to the NBD region.[8] The question that future work will address is whether one ATP binding at the NBD region provides sufficient energy for the transporter to switch to an outward-facing conformation. In this outward-facing conformation, it will be of great interest to determine if the transporter discriminates between apo and L-Met bound MetQ (Fig. 4-7). Studies of other ABC transporters have shown different results when it comes to the necessity of each ATP site. The type II importer BtuCD has been found to perform 5% of its maximum transport with only one functioning ATP site.[13] Previous studies have revealed positive cooperativity for MetNI (n = 1.7), meaning that the two ATP binding sites cooperate with one another. Meanwhile, His permease shows ~50% ATP hydrolysis activity with only one competent ATPase site.[14] The type I maltose transporter has also demonstrated positive cooperativity (n = 1.9 at pH 5), suggesting that two ATP binding are necessary for a change in conformation.[15]

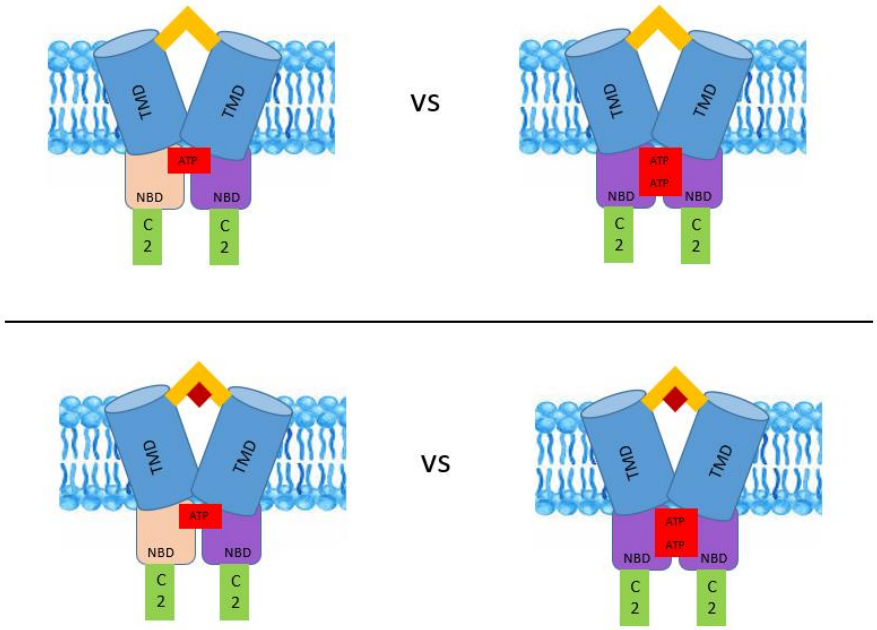

Figure 4-7: Investigation into the number of ATP required for MetNI-Q complex formation. The binding affinity between MetQ and MetNI chimeras will be examined to see if binding of only one ATP to the NBDs affects the dissociation constant of the MetNI-Q complex. The binding affinity of both apo MetQ (top) and L-Met bound MetQ (bottom) to MetNI chimeras (pictured with one wild-type NBD (purple) and one degenerate NBD (salmon)) will be determined and compared to the binding affinities of those complexes with two wild-type NBDs.

In order to investigate the effects of one degenerate ATP binding site, a mimic for MetNI with only one competent ATP-binding site must be purified. To mimic the binding of a single ATP molecule to the NBD region, future research will focus on the purification and experimentation of MetNI chimeras with one NBD that locks itself into the ATP-bound state (E166Q mutant) and one NBD that is unable to bind ATP (K44A mutant). This chimera, named MetNI E166Q – K44A, will be able to bind only one ATP molecule. Anisotropy assays of apo MetQ and L-Met bound MetQ will be performed with varying concentrations of the MetNI E166Q – K44A chimera. The K_d will provide key insight into whether the binding of only one ATP molecule is sufficient for MetNI-Q complex formation. If determined K_d values for these MetNI (E166Q – K44A) – MetQ complexes are much higher than previously determined K_d values (281 nM for the MetNI – apo MetQ complex and 527 nM for the MetNI – L-Met bound MetQ complex) then there would be evidence to suggest the binding of two ATP is necessary for the MetNI-Q complex to form.

A similar but distinct question about the MetNI transporter is whether or not one functioning ATPase site is sufficient for ATP hydrolysis to occur in the NBD region. In other words, if two ATP can bind to the NBDs but only one ATPase site can hydrolyze ATP, will the functioning ATPase site hydrolyze ATP or does the transporter require two functioning ATPase sites for hydrolysis to occur? To examine this question, a different MetNI chimera must be purified. This MetNI chimera must have one NBD that is able to bind and hydrolyze ATP (wild-type) and one NBD that is able to bind but not hydrolyze ATP (E166Q mutant). This MetNI chimera, named MetNI WT – E166Q will be utilized in ATPase assays to assess whether or not one functional ATPase site is sufficient for ATP hydrolysis to occur. Furthermore, if ATP hydrolysis can occur, it will be of interest to see if the rate of hydrolysis is similar or reduced in comparison to that of wild-type MetNI.

A few of the possible outcomes of these experiments are depicted in Fig. 4.8. Shown in (A) is a WT-E166Q MetNI chimera in which two ATP molecules are present and apo MetQ is in complex with the transporter. If MetNI is capable of hydrolyzing only one ATP at a time, this could result in the transition from (A) to (B), where apo MetQ remains bound to the OWF conformation of MetNI. In this case, the energy from binding one ATP would be sufficient to hold together the NBD dimer, suggesting that hydrolysis must occur at both ATP sites to drive transport. Alternatively, if the hydrolysis of one ATP may destabilize the NBD dimer, shown as (A) to (C), the transporter could rearrange to the IWF conformation, thereby driving dissociation of MetQ. This result would be consistent with a model in which only one ATP is hydrolyzed during the transport cycle. In another scenario, shown in (D), MetNI may not be able to hydrolyze any ATP, despite the fact that one NBD is functional. From this result, one could hypothesize

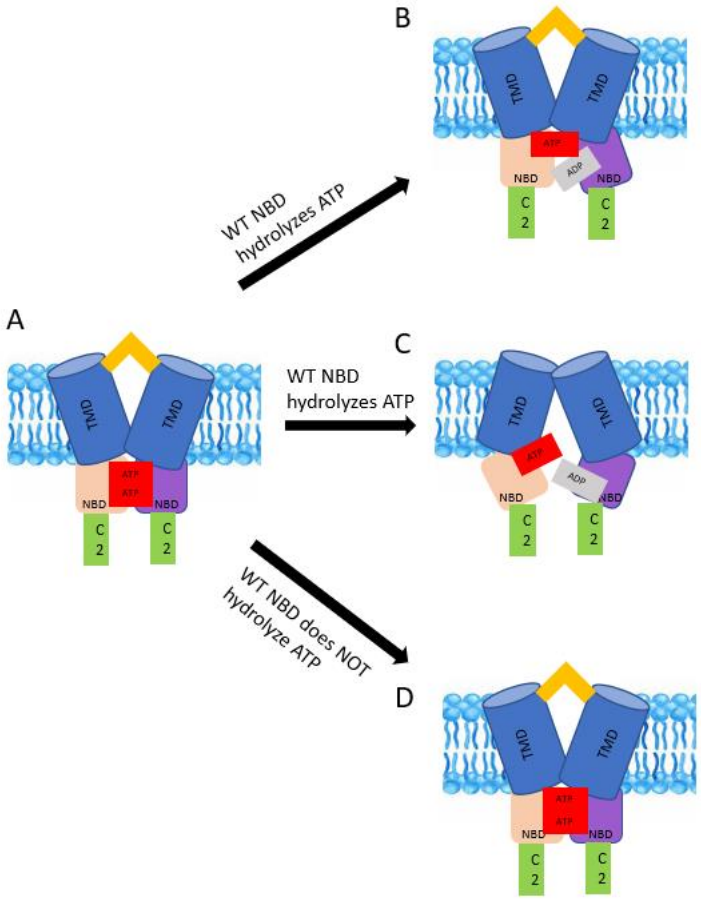

Figure 4-8: Possible conformational changes to a MetNI-Q complex with a single active ATPase site. (a) With one wild-type NBD (purple) and one E166Q mutant NBD (light pink), the transporter can bind two ATP molecules, triggering the outward-facing conformation and allowing binding of MetQ. (b) One possibility is that the transporter can then hydrolyze only one ATP, and that this may not be sufficient enough to drive rearrangement to the inward-facing conformation. (c) A similar but different possibility is that the transporter hydrolyzes one ATP, and that this is sufficient to drive rearrangement to the inward-facing conformation. (d) A third possibility is that both ATP sites must be functional in order for any hydrolysis to occur.

that two molecules of ATP are simultaneously hydrolyzed to trigger the switch from the OWF to the IWF conformation.

The possibilities outlined above are a starting point for consideration, and this list of outcomes is by no means comprehensive. The combination of ATPase and anisotropy assays developed in this thesis will provide the tools necessary to dissect the role of the two ATP sites and their influence on complex formation with MetQ. This would be a significant step forward to developing a complete understanding of the MetNI transporter mechanism.

4.8: Lipid Environment of the Transporter: DDM vs. Nanodisc

All of the experiments performed with MetNI thus far have been conducted with the transporter solubilized in the detergent n-dodecyl-β-D-maltoside (DDM). This detergent serves to extract the transporter from the bilayer and to interact with the hydrophobic portions of the TMDs, thereby solubilizing

the transporter. These experimental conditions are the most straightforward, as it only requires the addition of detergent to buffers. All x-ray crystallography studies of MetNI have been solved in the presence of detergent. However, MetNI may behave differently in a lipid bilayer in comparison to a detergent micelle. For example, the maltose transporter has been observed to hydrolyze ATP in the absence of substrate and SBP at a similar rate to when maltose and SBP are present, a phenomenon known as uncoupling.[16] Uncoupling of a transporter's ATPase activity is not uncommon, especially with the protein *in vitro*. This phenomenon is most prominent when the transporter is in lipid detergent. In the absence of maltose and SBP, the maltose transporter recorded an ATPase activity of ~900 nmol/min/mg in detergent micelles. The ATPase activity only slightly increases to ~1,000 nmol/min/mg (~11% increase) with maltose and SBP both present in solution. With the transporter in lipid nanodisc, the ATPase activity increased from ~700 nmol/min/mg ~1500 nmol/min/mg (~110% increase) in the absence and presence of maltose and SBP, respectively.[16] Researchers from the Bao group observed that the lipid environment of a nanodisc places more of a conformational constraint on the transporter, making the transporter more stable and less likely to freely switch between the inward and outward facing conformations that hydrolyze ATP in the process.[17] Due to the high level of uncoupled ATPase activity with transporter in detergent, many efforts have been focused on the reconstitution of ABC transporters into lipid nanodiscs (Fig. 4-9).[18]

In light of these observations in related transporters, it will be important to measure MetNI-Q complex formation using the transporter embedded in a nanodisc. These measurements will help to determine whether the results observed in detergent faithfully replicate *in vivo* behavior. While ATPase activity was mentioned to be affected by lipid activity, complex formation studied by Lewinson et. al. in 2010 found thermodynamic measurements for complex formation of the BtuCD-F transporter to be similar whether the transporter was in proteoliposomes or in detergent.[3]

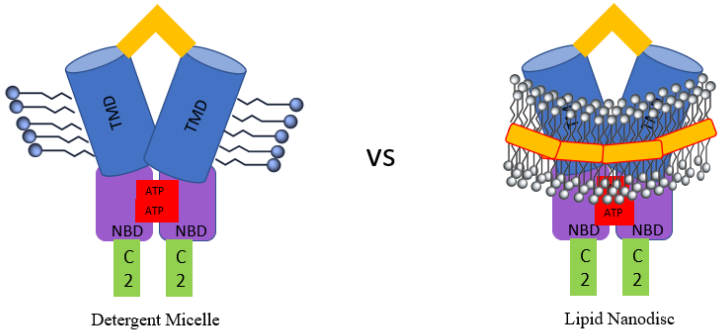

Figure 4-9: Lipid reconstitution of an ABC transporter. Reconstitution of MetNI into lipid nanodiscs may provide additional insight into the mechanism of methionine transport. Figure inspired by (18).

The results from assays performed in detergent will guide the following set of questions about transporter mechanism, developing the assays, and introducing new experiments to examine how different variables affect complex formation and transport mechanism.

4.9: Summary

This thesis presents multiple findings that reveal details of methionine transport. Through adapting an anisotropy assay for an ABC transporter system, we show that ATP binding by MetNI is a requirement for complex formation between the transporter and its periplasmic binding protein. Anisotropy data suggests that MetNI has a slightly higher affinity for apo MetQ than L-Met bound MetQ, an intriguing finding that suggests the further complexity of this transporter. Furthermore, we present preliminary data that suggest that L-Met binding to the C2 regulatory domains of the transporter dissociates the MetNI-Q complex, thereby preventing transport. Going forward, this project will continue to uncover features of the MetNI mechanism. Yet to be discovered details include the number of ATP molecules required per transport cycle and the intermediate states involved in transport of different methionine derivatives. The elucidation of the MetNI mechanism will aid in understanding how ABC transporters function in general, thereby enhancing our knowledge of related ABC transporters involved in human diseases.

References

1. Studier F.W. Protein production by auto-induction in high-density shaking cultures. *Protein Expression and Purification.* (2005). 41: 207-234.
2. Tromans D. Temperature and pressure dependent solubility of oxygen in water: a thermodynamic analysis. *Hydrometallurgy*. (1998). 48(3): 327-342.
3. Lewinson O., Lee A.T., Locher K.P., Rees D.C. A distinct mechanism for the ABC transporter BtuCD-F revealed by the dynamics of complex formation. *Nat Struct Mol Biol*. (2010). 17(3): 332-338.
4. Nguyen P.T., Li Q.W., Kadaba N.S., Lai J.Y., Yang J.G., Rees D.C. The contribution of methionine to the stability of the Escherichia coli MetNIQ ABC transporter – substrate binding protein complex. *Biol. Chem.* (2015). 396(9-10): 1127-1134.
5. Bao H., Duong F. ATP alone triggers the outward-facing conformation of the maltose ATP-binding cassette transporter. *J. Biol. Chem.* (2013). 288(5): 3439-3448.
6. Oldham M.L. Chen J. Snapshots of the maltose transporter during ATP hydrolysis. *PNAS.* (2011). 108(37): 15152-15156.
7. Fuhrman B.P., Zimmerman J.J. Pediatric Critical Care. *Elsevier*. (2011). 1058-1072.
8. Nguyen P.T., Lai J.Y., Lee A.T., Kaiser J.T., Rees D.C. Noncanonical role for the binding protein in substrate uptake by the MetnI methionine ATP Binding Cassette (ABC) transporter. *PNAS.* (2018). 115:45, E10596-E10604
9. Kadner R.J. Transport and utilization of D-methionine and other methionine sources in Escherichia coli. *J. Bacteriol.* (1977). 129(1): 207-216.
10. Nguyen P.T., Lai J.Y., Kaiser J.T., Rees D.C. Structures of the Neisseria meningitides methionine-binding protein MetQ in substrate-free form and bound to L- and D- methionine isomers. *Protein Science.* (2019). 28(10): 1750-1757.
11. Kadaba NS, Kaiser JT, Johnson E, Lee A, Rees DC. The high-affinity *E. coli* methionine ABC transporter: structure and allosteric regulation. *Science.* (2008). 321:250–253.
12. Yang J.G., Rees D.C. The allosteric regulatory mechanism of the Escherichia coli MetNI methionine ATP binding cassette (ABC) transporter. *J. Biol. Chem* (2015). 290(14):9135-9140.
13. Tal N., Ovcharenko E., Lewinson O. A single intact ATPase site of the ABC transporter BtuCD drives 5% transport activity yet supports full in vivo vitamin B_{12} utilization. *PNAS*. (2013). 110(14): 5434-5439.
14. Liu C.E., Liu P.Q., Ames G.F. Characterization of the adenosine triphosphatase activity of the periplasmic histidine permease, a traffic ATPase (ABC transporter). *J. Biol. Chem*. (1997). 272(21): 883-891.
15. Davidson A.L., Laghaeian S.S., Mannering D.E. The maltose transport system of *Escherichia coli* displays positive cooperativity in ATP hydrolysis. *J. Biol. Chem* (1996). 271(9): 4858-4863.
16. Bao H., Duong F. Discovery of an auto-regulation mechanism for the maltose ABC transporter $MalFGK_2$. *PloS One.* (2012). 7(4):34836.
17. Bao H., Dalal K., Wang V., Rouilleur I., Duong F. The maltose ABC transporter: Action of membrane lipids on the transporter stability, coupling and ATPase activity. *BBA-Biomembranes.* (2013). 1828(8): 1723-1730.
18. Zoghbi M.E., Altenberg G.A. Membrane protein reconstitution in nanodiscs for luminescence spectroscopy studies. *Nanotechnology Reviews.* 2017. 6:1.

Appendix

Detailed Instructions on Fluorescence Anisotropy Experiments

Materials

- 200 mM ATP (or close to)
- 10% DDM
- 2M or 5M NaCl
- 1M Tris
- Deionized H_2O
- MetQ Buff A (150 mM NaCl, 25 mM Tris pH 7.5, 5 mM BME)
- MetNI Buff A (250 mM NaCl, 50 mM TAPS pH 8.5, 0.05% DDM)
- MetNI protein
- Labeled MetQ protein
- Ultracentrifuge tubes
- Laptop (for calculations and setup)

Procedure (Before UCSF)

- Email johnny.rodriguez@ucsf.edu and emily.wong3@ucsf.edu ahead of time to reserve the ultracentrifuge and anisotropy plate reader
- Prepare buffers, ATP, EDTA, and DDM solutions a day before heading out to UCSF

Procedure (UCSF day) Preparing the proteins

- Turn on ultracentrifuge on 3rd floor, set to 4 C, 90,000 rpm. Get rotor and holder from cold room
- Turn on anisotropy plate reader (Agard Lab, 4th floor) so it can warm up for at least ~30 mins. Set the temperature to 37 C.

A difficult part about this experiment is knowing how much protein to centrifuge at the beginning of the day. Too many thawed aliquots and you waste precious protein, too little and you have to spend an additional hour to prepare and use the ultracentrifuge and also prepare the correct concentration of MetNI protein. To calculate the amount of protein needed it is crucial to predict the amount of non-aggregated protein that will be present after centrifugation. Expect the protein concentration to decrease by 25% after centrifugation. (For an estimate, 3 trials MetQ N229A – MetNI E166Q anisotropy assays required about 30 µL of 15 mg/mL MetNI and MetQ WT – MetNI E166Q assays required 90 µL of about 15 mg/mL MetNI.

- For each final concentration of MetNI in each trial, you need to make 5x concentrations for each. For example, if one well needs a final MetNI concentration of 10 µM, then we need to make 50 µM MetNI solutions. This is because the MetNI mix makes up 20% of the total volume of the final sample volume. An example table can be seen below.

Table 1: MetNI 5x serial dilution calculation. Concentration of stock MetNI was about 134 mM.

Final MetNI (nM)	MetNI 5x (nM)	Vol. previous (µL)	MetNI Buffer (µL)
10000	50000	18.63 stock	31.37
5000	25000	25.00 (50000 nM)	25.00
2500	12500	25.00	25.00
1000	5000	20.00	30.00
400	2000	20.00	30.00
200	1000	25.00	25.00
120	600	30.00	20.00
80	400	33.33	16.67
40	200	25.00	25.00
20	100	25.00	25.00
10	50	25.00	25.00
5	25	25.00	25.00
1	5	10.00	40.00
0.1	0.5	5.00	45.00

- Add up all the stock MetNI needed and use it to predict the amount of MetNI protein needed. Keep in mind, the bottom 20 µL of the centrifuged solution will be aggregated protein that will not be collected, so add 20 µL to your predicted volume.
- Pipette 20 µL of labeled MetQ (normally 20-30% labeled, curves may be noisier if less) and 80 µL MetQ Buff A into one centrifuge tube, find another tube and balance with 100 µL MetQ buff A. (This should be more than enough labeled MetQ (assuming 1 mg/mL, only 20 nM for each well's final concentration).
- Pipette the predicted necessary amount of stock MetNI into another centrifuge tube, balance with another tube of equal volume MetNI buff A
- Spin down in JLA-100 rotor for 20 minutes at 90k rpm
- Once completed, change the temperature of the centrifuge to 25 C and close the centrifuge lid. This helps with removing any condensation in the vacuum. Once the temperature reaches 25 C, open the lid of the centrifuge and turn it off.
- Pipette the centrifuged solutions into labeled eppendorf tubes. Leave 20 µL at the bottom of the tubes to be certain that you do not pipette any of the aggregated protein.
- Use the nanodrop located next to the fish tank to record Abs @ 280 nm and calculate concentrations of each protein. Use the single readout option and perform the readings on sensor A1. Ext. coeff. MetNI = 83365 $M^{-1}*cm^{-1}$, MW = 122034.85 g/mol ; Ext. Coeff. MetQ = 20400 $M^{-1}*cm^{-1}$, MW = 29431.65 g/mol
- Adjust the MetNI well calculations according to the true concentration of the stock.
- Create the 5x MetNI concentrations in labeled Eppendorf tubes and keep on ice.
- Prepare the Master Mix solution

Table 2: Anisotropy Master Mix Set-Up (60 reactions)

	MM (µL)
2M NaCl	41.25
1M Tris	75
10% DDM	7.5
100 mM MgCl2	45
193 mM ATP	23.32
ddH2O	557.93
66 nM MetQ mix	450
Total	1200

This table will give you 60 reactions worth of Master Mix with final well concentrations of 55 mM Tris pH 7.5, 5 mM TAPS pH 8.5, 0.055% DDM, 55 mM NaCl, 1 mM BME, 3 mM $MgCl_2$, and 3 mM ATP. This table may change based on the variables of the experiment. Double check your calculations before creating the master mix.

With the Master Mix and MetNI 5x solutions prepared, the procedure can begin. Make sure to complete each step on ice until the solutions are transferred to the 384-black clear bottom (opaque bottom may work too) well plate.

- Label eppendorf tubes for rxn mixtures with their final MetNI concentrations
- Pipette 20 µL of MM into each labeled eppendorf tube
- Pipette 5 µL of MetNI 5x stock into their respective tube
- Transfer 20 µL of each solution into their own respective well
- Place the well plate in the plate reader and allow it to warm up for 10 minutes. To use the plate reader, read the following instructions.
- Press "Drawer" button on instrument, insert plate. Close "Drawer."
- In Experiment window, check settings, Endpoint.
- Read mode: Fluorescence or Fluorescence Polarity
- Wavelength: default is 485 ex /538 em
- Sensitivity: choose "High" unless signal is too Sat. "Precise" default setting is ok.
- Assay Plate Type: 384 Grenier Blk/clr
- Wells to Read: select
- Press ok
- Click on "Read" icon.
- Save data under desktop > User > Laura > Janet. Taking a picture of the data is also a good idea.

Once all the assays have been performed, be sure to clean up your lab bench and turn off both the ultracentrifuge and anisotropy plate reader. Sign up for the anisotropy plate reader on the calendar in the

plate reader room if you know when you will return. If the next experiment day is unknown, email or text Emily Wong afterwards to reserve a time to use the reader.